Partial Synchronization in Coupled Systems with Repulsive and Attractive Interaction

---

Erik Teichmann

Univ.-Diss.
zur Erlangung des akademischen Grades
"doctor rerum naturalium"
(Dr. rer. nat.)
in der Wissenschaftsdisziplin
"Theoretische Physik"

eingereicht an der
Mathematisch-Naturwissenschaftlichen Fakultät
Institut für Physik und Astronomie
der Universität Potsdam

Ort und Tag der Disputation: Potsdam, 16.11.2021

Hauptbetreuer*in: apl. Prof. Dr. Michael Rosenblum
Betreuer*innen: PD Dr. Fred Feudel
Gutachter*innen: apl. Prof. Dr. Michael Rosenblum, Dr. habil. Michael Zaks,
Prof. Dr. Rene Medrano-T.

Published online on the
Publication Server of the University of Potsdam:
https://doi.org/10.25932/publishup-52894
https://nbn-resolving.org/urn:nbn:de:kobv:517-opus4-528943

Declaration of Authorship

I, Erik Teichmann, declare that this thesis titled, "Partial Synchronization in Coupled Systems with Repulsive and Attractive Interaction" and the work presented in it are my own. I confirm that:

- This work was done wholly or mainly while in candidature for a research degree at this University.
- Where any part of this thesis has previously been submitted for a degree or any other qualification at this University or any other institution, this has been clearly stated.
- Where I have consulted the published work of others, this is always clearly attributed.
- Where I have quoted from the work of others, the source is always given. With the exception of such quotations, this thesis is entirely my own work.
- I have acknowledged all main sources of help.

Signed:

Date:

UNIVERSITY OF POTSDAM

Abstract

Faculty of Science
Institute of Physics and Astronomy

Dr. rer. nat.

Partial Synchronization in Coupled Systems with Repulsive and Attractive Interaction

by Erik Teichmann

Partial synchronous states exist in systems of coupled oscillators between full synchrony and asynchrony. They are an important research topic because of their variety of different dynamical states. Frequently, they are studied using phase dynamics. This is a caveat, as phase dynamics are generally obtained in the weak coupling limit of a first-order approximation in the coupling strength. The generalization to higher orders in the coupling strength is an open problem. Of particular interest in the research of partial synchrony are systems containing both attractive and repulsive coupling between the units. Such a mix of coupling yields very specific dynamical states that may help understand the transition between full synchrony and asynchrony. This thesis investigates partial synchronous states in mixed-coupling systems. First, a method for higher-order phase reduction is introduced to observe interactions beyond the pairwise one in the first-order phase description, hoping that these may apply to mixed-coupling systems. This new method for coupled systems with known phase dynamics of the units gives correct results but, like most comparable methods, is computationally expensive. It is applied to three Stuart-Landau oscillators coupled in a line with a uniform coupling strength. A numerical method is derived to verify the analytical results. These results are interesting but give importance to simpler phase models that still exhibit exotic states. Such simple models that are rarely considered are Kuramoto oscillators with attractive and repulsive interactions. Depending on how the units are coupled and the frequency difference between the units, it is possible to achieve many different states. Rich synchronization dynamics, such as a Bellerophon state, are observed when considering a Kuramoto model with attractive interaction in two subpopulations (groups) and repulsive interactions between groups. In two groups, one attractive and one repulsive, of identical oscillators with a frequency difference, an interesting solitary state appears directly between full and partial synchrony. This system can be described very well analytically.

Acknowledgements

First of all, I want to thank my supervisor Prof. Michael Rosenblum. His help and guidance were paramount to the research presented here. Next, I want to thank the people that worked directly with me on the paper presented here, Prof. Arkady Pikovsky and my fellow Ph.D. student Erik Gengel. I want to thank the members of the Statistical Physics and Theory of Chaos group at the University of Potsdam, Chris Gong, Franziska Peter, Chunming Zheng, Rok Cestnik, Caroline Reid, and Ralf Tönjes for making my time there an enjoyable one. Last but not least, I want to thank the participants and organizers of the IRTG 1740 project of the DFG, David Hansmann, Prof. Rene Medrano-Torricos, and Prof. Elbert Macau for their support.

And finally, I want to thank my wife Anika and my parents for always being there and rooting for me.

Contents

Chapter 1

Introduction

Systems with complex rhythmical behavior can be modeled as networks of coupled self-sustained oscillators. This approach is not just restricted to physics [1, 2], but is also applicable to biology [3, 4] or sociology [5, 6]. Examples of such models are coupled Josephson junctions [7], power grids [8], neuronal populations [9], or the interaction of organs in the human body [10]. The widespread usability of networks of coupled oscillators makes them an exciting and worthwhile topic to study.

Especially interesting in such systems of multiple units is the appearance of a common mode. This phenomenon is called synchronization and was first observed in two pendulum clocks, fastened to the same beam, by Huygens [11]. He observed entrainment of both clocks, where they swung with the same frequency but in opposite directions. Nowadays, this is called synchronization in antiphase. In systems with more than two units, it is possible to observe more complex states that are not fully synchronized, i.e., do not have a common behavior like the pendulum clocks but do not have random dynamics (asynchrony). These states in between are called partial synchrony and usually fill the biggest part of the possible parameter space. The importance of studying such states is evident, yet they are harder to study than full and asynchrony. One famous example of this is the chimera [12] state. A system in this state exhibits both synchronous and asynchronous behavior simultaneously.

While there are many studies of partial synchrony, they are mostly restricted to an attractive coupling between the oscillators [12–16]. There are few investigations of repulsive coupling, even though it is undoubtedly observable in real-world systems, as the first observation of synchronization by Huygens shows, and has similarly interesting properties [17–19]. Even less research has been dedicated to mixed systems, where both, attractive and repulsive interactions, are present [20–26]. These systems show some interesting partial synchronous states that are not easily achieved in more regularized coupling schemes, such as the solitary state [24] or the Bellerophon state [26]. Studying these more closely may reveal underlying principles of synchronization that are not accessible by considering only one type of coupling. From a purely practical point of view, it is necessary to investigate such systems more closely as one of the most complex systems, the brain, contains just such a mix of different couplings between the single units [27–30], which yields the phenomenal ability of thought and consciousness as a result of synchronization.

To study partial synchronization, the networks of coupled oscillators have to be investigated. They are described as coupled differential equations, where the

number of equations scales with the number of units in the system N. In the simples case of 1-dimensional dynamics, the system is N-dimensional, but in the case of higher-dimensional units with dimension M, the number of equations increases to $M \times N$. Solving such a large number of coupled equations is no simple task. So, a way to decrease the dimensionality is needed. The phase reduction method [11, 13, 31, 32] is the most popular tool to achieve this. It reduces the system's dimensionality to the number of units N by introducing 1-dimensional phase variables. This phase is 2π-periodic and has, in the uncoupled units, a constant normalized frequency. This approach's difficulties lie in first finding the phase of the uncoupled oscillators and then the phase dynamics of the coupled system. Even the first step is nontrivial, as there are only a few oscillators with a known phase description.

The phase reduction of the whole system is mainly reduced to the weak coupling limit, where only terms in the first order of the coupling strength are considered. This yields systems, such as the seminal Kuramoto model [13, 33] which is widely used for its analytical solvability [34–37]. However, it is known that higher-order phase approximations are needed to explain some partial synchronous states [38]. The extension to higher-order is non-trivial. Some methods achieve this [38–42], but they cannot be applied in every case. The use of phase reduction is not just restricted to theoretical considerations but also applies to laboratory experiments, where the phase reduction is used for its simplicity [43–47] (having only N 2π-periodic variables is certainly preferable to having $M \times N$ possibly non-periodic variables). It is used to find, e.g., the links or connections between units. Even in this seemingly simple case of connection reconstruction, the weak coupling limit may yield erroneous results. While the first-order phase approximation only contains interactions that exist as physical connections, this is no longer the case in higher-order phase approximations [48–50], where also non-structural terms may appear that could influence the reconstruction. Considering all these points, it is crucial to study partial synchronization not only in the context of the weak coupling limit of the phase reduction, but also, beyond it.

This thesis is a cumulation of four papers [51–54] I was part of and is split into four parts (albeit one of those papers is a review and does not correspond to one of the chapters). The first chapter introduces the necessary tools and equations of dynamical system theory. It gives a short overview of the theory of phase dynamics and synchronization and concludes with the basic analytic properties of the Kuramoto model.

The second chapter investigates higher-order phase reductions and presents the results of Ref. [52]. First, a short literature review is given. Then, a new method, based on a perturbation Ansatz, is introduced and applied to a simple model of three Stuart-Landau oscillators coupled in a line. These oscillators have a known phase dynamic, which is essential for the method. The phase reduction up to the second-order contains interesting non-structural terms, coupling the two outer oscillators, and hypernetwork-like terms, containing the phases of all three oscillators. To verify the new analytical results, a numerical method based on a Fourier series representation is given. The analytical and numerical methods both agree very well, and the numerical results give

even higher-order phase reductions. A more general model of three van der Pol (without known phase dynamic) oscillators is investigated using the numerical method. The phase reduction describes the system very well, although it is worse than for the three Stuart-Landau oscillators. Despite these good results, the applicability is restricted, as these methods are computationally intensive. A phase model is still preferred for the study of partial synchronization in bigger systems.

The third chapter treats Ref. [54]. The chapter begins with a short description of the Bellerophon state [26], a non-stationary state with coherent clusters. This state is observed in a Kuramoto model of two groups with independent frequency distributions. Coupling between oscillators of the same group is attractive, and coupling between oscillators of different groups repulsive. Such a model is comparable to a Kuramoto model with a weaker coupling strength. For a small coupling strength, the agreement is very good. After an increase to moderate coupling strength, the attractive and repulsive system reaches the Bellerophon state and deviates from the Kuramoto model's synchronization behavior. A further increase in the coupling strength then transitions the behavior to resemble an equally strongly coupled Kuramoto model, and the Bellerophon state disappears. These observations show the richness of synchronization behavior in even comparably simple models with mixed couplings.

The final chapter contains the results of Ref. [51] and investigates a particular partial synchronous state, the solitary state. It is situated between full and partial synchrony. After a short overview of the current literature about the solitary state, a Kuramoto model with attractive and repulsive coupling of two groups of identical oscillators is considered. This system can be analyzed very well, and all important properties of the synchronous and the solitary state can be calculated analytically. The difference to the model in which the solitary state was discovered initially [24] lies in the difference of frequencies between the groups. It is shown that this frequency difference stabilizes the solitary state. Using the analytical solvability of the Kuramoto model, specifically the Watanabe-Strogatz theory [34, 35], it is even possible to find good analytical approximations of the common modes of the oscillators in the partial synchronous regime. There the average dynamics of the repulsive oscillators and their common mode differs, making it a self-consistent partial synchronous state [55].

Chapter 2

Dynamical Systems & Synchronization

2.1 Dynamical Systems

One way to describe dynamical systems is by the use of ordinary differential equation (ODE) for the state $\boldsymbol{y}$ as

$$\frac{d\boldsymbol{y}}{dt} = \boldsymbol{f}(t, \boldsymbol{y}) \ . \tag{2.1}$$

The time dependence of $\boldsymbol{f}$ can result from, e.g., a time-dependent external forcing or a stochastic noise. In the case of noise, the system loses its deterministic nature while keeping it for external forcing. From here on, the ODEs are considered to be always deterministic and even autonomous $\boldsymbol{f}(t, \boldsymbol{y}) = \boldsymbol{f}(\boldsymbol{y})$, unless explicitly specified. In general, using the same initial condition will always yield the same time evolution, and a small change in the initial conditions often leads to only a small change in the state after a long time. However, chaotic systems exist where such a small deviation of the initial conditions grows exponentially over time, leading to a vastly different trajectory. An example of such a chaotic system is the first strike of a Billiard game. A slight change in force or direction will lead to a vastly different position of the balls on the table. One famous dynamical system exhibiting chaotic dynamics is the Lorenz system [56] (see Fig. 2.1)

$$\begin{aligned} \dot{x} &= \sigma(y - x) \ , \\ \dot{y} &= x(\rho - z) - y \ , \\ \dot{z} &= xy - \beta z \ . \end{aligned} \tag{2.2}$$

This system exhibits a strange attractor, i.e., points outside of the attractor will move onto it. However, any perturbation, even a small one, outside or on the limit cycle, will change the trajectory dramatically [11, 57].

These types of systems are interesting to study but are not well suited for the description of synchronization. A neutrally stable, attractive manifold is more useful in this context. If this manifold Y is periodic with period T, i.e., $Y(t + T) = Y(t)$ in the phase space, then it is called a limit cycle. Systems with a limit cycle are dissipative, but they also include non-oscillatory sources. One popular oscillator exhibiting such behavior is the van der Pol oscillator [3]. It

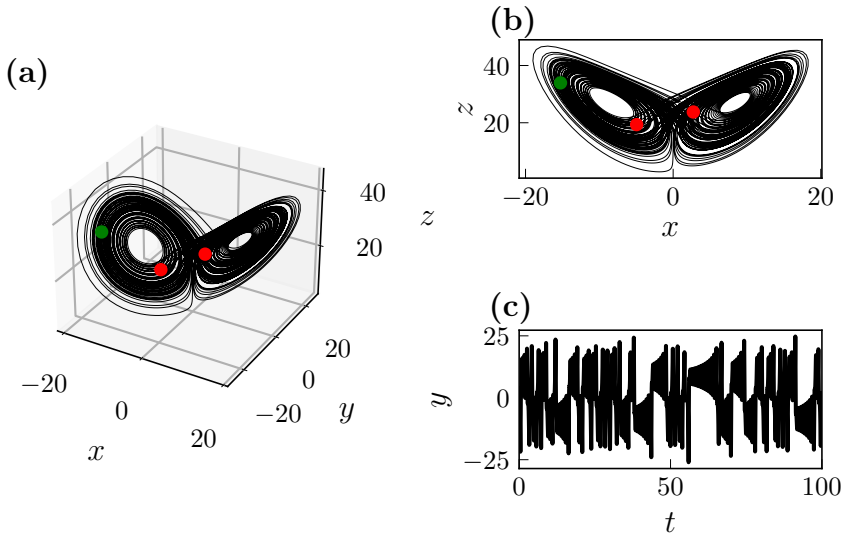

FIGURE 2.1: A trajectory of the Lorenz system from Eq. (2.2). The chosen parameters $\sigma = 10$, $\beta = 8/3$, and $\rho = 28$ were originally used by Lorenz. In (a) the phase space of all three variables x, y, and z are shown, and in (b) a projection on the x-z plane. A time series for y is plotted in (c). The green dot in (a) and (b) shows the state at the time of a small perturbation in the y-coordinate with $y' = y + 10^{-5}$; the unperturbed and perturbed state 50 time-units after the perturbation are shown as red dots.

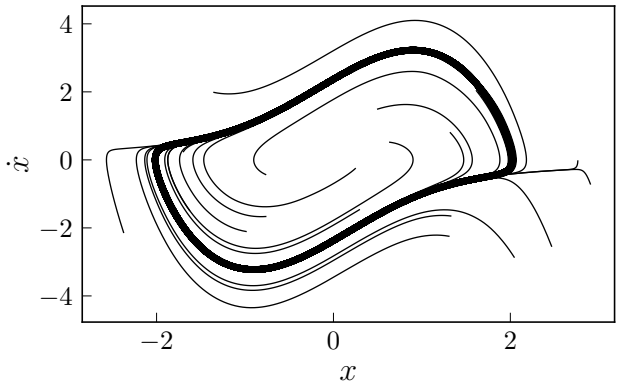

FIGURE 2.2: The limit cycle of the van der Pol oscillator from Eq. (2.3) with $\mu = 1.5$. The limit cycle is depicted as a thick black line and 20 different initial conditions as thin black lines. All initial conditions reach the limit cycle.

is given by a second-order differential equation as

$$\ddot{x} - \mu(1 - x^2)\dot{x} + x = 0 \; . \tag{2.3}$$

The limit cycle for $\mu = 1.5$ is shown in Fig. 2.2, as well as different initial conditions. It can be seen clearly that every initial condition relaxes onto the limit cycle, regardless of whether it starts inside or outside it.

One way to characterize the stability of the system of differential equations lies in the Lyapunov exponents λ. They are connected to the Jacobian $\boldsymbol{J}$ in the linearized evolution of a point of Eq. (2.1) in the phase space

$$\frac{d\boldsymbol{y}}{dt} = \boldsymbol{J}(t)\boldsymbol{y} \; . \tag{2.4}$$

The Jacobian $\boldsymbol{J}$ leads to N eigenvalues for an N-dimensional problem. In the simplest case of a fixed point, the real parts of the eigenvalues are the Lyapunov exponents λ_j. In more complex systems, the Lyapunov exponents are better represented by their effect on the evolution of a perturbation $\delta\boldsymbol{y}$

$$|\delta\boldsymbol{y}(t)| \approx e^{\lambda t} \, |\delta\boldsymbol{y}(0)| \; , \tag{2.5}$$

where λ is the biggest Lyapunov exponent. Reordered, this can also be written as

$$\lambda = \lim_{t\to\infty} \lim_{|\delta\boldsymbol{y}(0)|\to 0} \frac{1}{t} \ln \frac{|\delta\boldsymbol{y}(t)|}{|\delta\boldsymbol{y}(0)|} \; . \tag{2.6}$$

Equivalently, to find all Lyapunov exponents in this way, one considers perturbations in an N-dimensional hyper-sphere around the initial condition [58]. After some time, the sphere will be deformed into an ellipsoid, where each principal axis p_i's length corresponds to a Lyapunov exponent as

$$\lambda_j = \lim_{t\to\infty} \lim_{|\delta\boldsymbol{y}(0)|\to 0} \frac{1}{t} \ln \frac{p_j(t)}{p_j(0)} \; . \tag{2.7}$$

By convention, they are ordered by their value, so $\lambda_1 \geq \lambda_2 \geq \ldots$ [11]. Each Lyapunov exponent λ_j determines the stability in a direction. A negative exponent leads to a contraction in the phase space (or stability), a zero exponent to the conservation of volume (or neutral stability), and a positive exponent to expansion in the phase space (or chaos). The attractor in the Lorenz system shown in Fig. 2.1 is a strange attractor. It is chaotic in one direction, $\lambda_1 > 0$, while $\lambda_2 = 0$ and $\lambda_3 < 0$. For the strange attractor to be attractive, the phase space volume has to shrink, so $\sum_j \lambda_j < 0$. Limit cycles, on the other hand, are also dissipative, so $\sum_j \lambda_j < 0$, but not chaotic, i.e., $\lambda_1 = 0$.

The limit cycle is a closed trajectory inside a possibly high-dimensional phase space. This trajectory can be parameterized to reduce the dynamics to just one dimension. By convention, a 2π-periodic quantity, the protophase θ, is chosen for the parametrization. In the simplest case of a 2-dimensional phase space, this corresponds to the polar angle. To reduce the complexity even further, this protophase θ is normalized to the uniformly growing phase φ, such that the

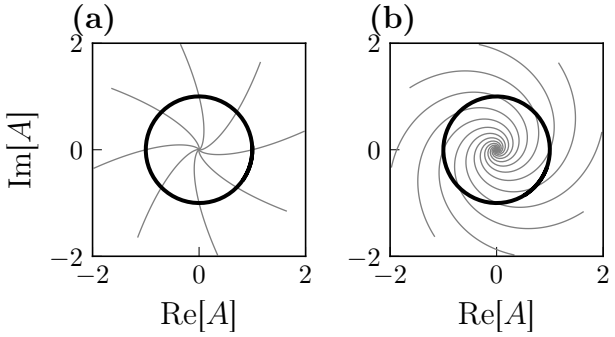

FIGURE 2.3: The Stuart-Landau oscillator's limit cycle from Eq. (2.10) is shown with a thick black line. The isochrones for $\alpha = 0.25$ in (a) and for $\alpha = 2.5$ in (b) are visualized with gray lines.

frequency is constant via

$$\varphi = \frac{2\pi}{T} \int_0^\theta \dot{\theta}^{-1} d\theta \; . \tag{2.8}$$

This phase rotates uniformly with the natural frequency $\omega = 2\pi/T$. The phase φ is only defined for a closed trajectory, i.e., a limit cycle in our case. With the help of isochrones, it can be extended outside the limit cycle into the basin of attraction. An isochrone describes the set of points that share the same phase in the limit of $t \to \infty$. The dynamical equation Eq. (2.1) can be written in terms of the isochrones $\varphi = \Phi(\boldsymbol{y})$ as

$$\dot{\varphi} = \omega = \frac{\partial \Phi}{\partial \boldsymbol{y}} \boldsymbol{f}(\boldsymbol{y}) \; . \tag{2.9}$$

The phase is neutrally stable on the limit cycle, as the limit cycle itself is the neutrally stable direction. Every perturbation of the phase will stay constant, i.e., if $\varphi'(t = 0) = \varphi(t = 0) + \Delta$, then $\varphi'(t) = \varphi(t) + \Delta$ for all $t \geq 0$.

A phase reduction is often only possible in a numerical way, but some oscillators exist where the phase is known analytically. One such an oscillator is the Stuart-Landau oscillator

$$\frac{dA}{dt} = (1 + i\omega)A - |A|^2 A - i\alpha A(|A|^2 - 1) \; . \tag{2.10}$$

Here A is a complex amplitude and rewriting the ODE in terms of the magnitude R and the polar phase θ yields

$$\begin{aligned} \dot{R} &= R - R^3 \; , \\ \dot{\theta} &= \omega - \alpha(R^2 - 1) \; . \end{aligned} \tag{2.11}$$

It is straightforward to check that the uniformly growing phase in this case is

$$\varphi = \theta - \alpha \ln R \; . \tag{2.12}$$

The limit cycle of the Stuart-Landau oscillator is a circle with radius $R = 1$, and some isochrones are shown in Fig. 2.3. For small α, the isochrones are nearly straight (Fig. 2.3(a)), while for a big α, they resemble a spiral (Fig. 2.3(b)). Because of this, α is called the non-isochronicity parameter.

2.2 Phase Response Curve

When describing phase dynamics, it is important to consider perturbations to the limit cycle. Such a perturbed system may be given by

$$\frac{d\boldsymbol{y}}{dt} = \boldsymbol{f}(\boldsymbol{y}) + \varepsilon \boldsymbol{G}(t) \ , \tag{2.13}$$

where $\boldsymbol{G}$ is a perturbation with strength ε. Then the dynamics can be written in the first order of ε as the Winfree equation [59]

$$\dot{\varphi} = \omega + \varepsilon P(\varphi) p(t) + \mathcal{O}(\varepsilon^2) \ . \tag{2.14}$$

Here $p(t)$ describes the form of the perturbation and $P(\varphi)$ the phase change of the oscillator as a reaction to the perturbation. The $P(\varphi)$ is called the phase response curve (PRC) and contains information about the system, such as the synchronization properties of the system [60,61] or the connectivity in a network of oscillators [62].

2.3 Coupled Oscillators

When N oscillatory units are coupled, the dynamics of Eq. (2.1) change to

$$\frac{d\boldsymbol{y}_k}{dt} = \boldsymbol{f}_k(\boldsymbol{y}_k) + \varepsilon \boldsymbol{G}_k(\boldsymbol{y}_1, \boldsymbol{y}_2, \ldots) \ , \tag{2.15}$$

where every oscillator may be described by a different dynamical equation $\boldsymbol{f}_k$ and is coupled with strength ε and function $\boldsymbol{G}_k$ to the other oscillators. The dimensionality of these coupled equations is the sum of the dimensionalities of all $\boldsymbol{f}_k$ and can be arbitrarily high, but again a reduction to phase dynamics and N dimensions (1 for every oscillatory unit) is possible if the isochrones $\varphi_k = \Phi_k(\boldsymbol{y}_k)$ are known. Then equivalently to Eq. (2.8)

$$\begin{aligned} \dot{\varphi}_k =& \frac{\partial \Phi_k}{\partial \boldsymbol{y}_k} \boldsymbol{f}_k(\boldsymbol{y}_k) + \varepsilon \frac{\partial \Phi_k}{\partial \boldsymbol{y}_k} \boldsymbol{G}_k(\boldsymbol{y}_1, \boldsymbol{y}_2, \ldots) \\ =& \omega_k + \varepsilon \frac{\partial \Phi_k}{\partial \boldsymbol{y}_k} \boldsymbol{G}_k(\boldsymbol{y}_1, \boldsymbol{y}_2, \ldots) \ . \end{aligned} \tag{2.16}$$

This is a hard problem to solve because the isochrones for the whole phase space have to be known. However, in a first-order approximation of ε, the dynamics stay close to the limit cycle, so $\boldsymbol{y}_k \approx \boldsymbol{Y}_k$. Assuming the phases are known on the limit cycles, this leads to the first-order phase reduction

$$\dot{\varphi}_k = \omega_k + \varepsilon G_k(\varphi_1, \varphi_2, \ldots) + \mathcal{O}(\varepsilon^2) \ . \tag{2.17}$$

2.3.1 Synchronization

Two oscillators

In its most general form, synchronization describes the appearance of collective dynamics. In the phase representation, this is the locking of frequencies. If we assume the simplest possible model of two coupled phase oscillators φ_1 and φ_2, with natural frequencies ω_1 and ω_2, then their mutual interactions are described by some coupling functions $G_1(\varphi_1, \varphi_2)$ and $G_2(\varphi_1, \varphi_2)$ and some coupling constant ε, as in Eq. (2.17), such that

$$\begin{aligned} \dot{\varphi_1} &= \omega_1 + \varepsilon G_1(\varphi_1, \varphi_2) \ , \\ \dot{\varphi_2} &= \omega_2 + \varepsilon G_2(\varphi_1, \varphi_2) \ . \end{aligned} \tag{2.18}$$

Reformulating the functions G as Fourier series yields

$$G_j(\varphi_1, \varphi_2) = \sum_{k,l \in \mathbb{Z}} \hat{g}_{j;k,l} e^{i(k\varphi_1 + l\varphi_2)} \ . \tag{2.19}$$

If both frequencies are close, i.e., $\omega_1 \approx \omega_2$, then these terms can now be split into fast oscillating terms, where $|k| > 1$ and $|l| > 1$, slow resonant terms with $|k| = 1$ and/or $|l| = 1$, and constant terms with $|k| = |l| = 0$. Averaging over the fast terms leaves only the slow and constant terms. Assuming a rotational invariance, the interaction depends only on the difference in phases, and using the simplest possible coupling term, $\sin(\cdot)$ then reduces Eqs. (2.18) to

$$\begin{aligned} \dot{\varphi_1} &= \omega_1 + \varepsilon \sin(\varphi_2 - \varphi_1) \ , \\ \dot{\varphi_2} &= \omega_2 + \varepsilon \sin(\varphi_1 - \varphi_2) \ . \end{aligned} \tag{2.20}$$

These equations should only be seen as a time average because of the averaging over the fast oscillations. Still, it becomes clear now that the dynamics only depend on the phase difference $\Delta\varphi$ and the difference in frequencies $\Delta\omega$

$$\frac{d\Delta\varphi}{dt} = \Delta\omega - \varepsilon \sin(\Delta\varphi) \ . \tag{2.21}$$

This equation is called the Adler equation [63] and is usually derived for a forced oscillator. This also shows the close connection between coupling and forcing. A coupled oscillator is forced from its coupled units, although in difference to an independent forcing, the oscillator now influences the force acting on it (in the case of pairwise or similar interactions).

Eq. (2.21) shows that there are can be no stationary states, i.e., $d\Delta\varphi/dt = 0$, for $|\Delta\omega| > \varepsilon$. The system thus synchronizes for $|\Delta\omega| \leq \varepsilon$. This region is called the Arnold tongue and is shown in Fig. 2.4. For the case of $\Delta\omega \neq 0$, synchronization is not achieved by equal phases but only by equal frequencies. Possible stationary states include anti-phase synchrony with $\varphi_2 = \varphi_1 + \pi$, while $\varphi_2 = \varphi_1$ is in-phase, and all other cases are called out-of-phase. These cases are for $\varepsilon > 0$. If instead $\varepsilon < 0$, then the oscillators will be in anti-phase.

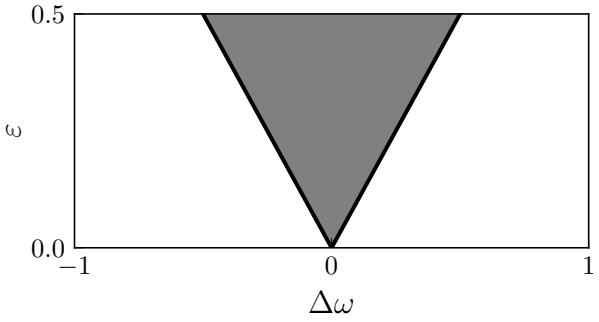

FIGURE 2.4: The Arnold tongue for the Adler equation in Eq. (2.21). The black lines show $\varepsilon = |\Delta\omega|$ and the gray region the parameters for which the system synchronizes, i.e., $d\Delta\varphi/dt = 0$.

N Oscillators

Richer dynamics can be observed by considering more than 2 oscillators. For a bigger ensemble of oscillators, it becomes viable to observe the macroscopic dynamics generated by the average of the oscillators' phases. The average behaves like one complex oscillator and can typically be observed easily in an experiment. It is convenient to define synchronization with reference to this macroscopic mean-field. Different states and their mean-fields are shown in Fig. 2.5.

The simplest state is the fully synchronized one, where all phases and frequencies are equal. Such a state can be seen in Fig. 2.5(a). A more complex state, and the focus of this thesis, is the partial synchronous state. There are different definitions of partial synchrony (cf. Fig. 2.5(b)), but the most common one is the difference in phases and in instantaneous frequencies. The average frequencies may coincide. Here we use a slightly different definition, in that also states with an equal instantaneous frequency, but different phases (of at least one oscillator) are also called partial synchronous. This then makes the difference between full and partial synchrony observable in the mean-field. Full synchrony then corresponds to a magnitude of the mean-field of 1, partial synchrony has a magnitude between 0 and 1. These are just general guidelines, as the symmetric 2-cluster state in Fig. 2.5(d) is a partial synchronous state, according to the definition, but has a vanishing magnitude in the first order. In the fully synchronous case, the macroscopic dynamics are phase dynamics themselves, while the dynamics of the partial synchronous dynamics also need to consider an amplitude.

The final macroscopic state is asynchrony, see Fig. 2.5(c). It does not have any macroscopic dynamics and is characterized by a uniform distribution of phases, the so-called splay state. It is important to discern between the splay state and different states without macroscopic dynamics, such as the synchronized 2-cluster state in Fig. 2.5(d). Any symmetric distribution of phases will lead to vanishing macroscopic dynamics but may indicate different synchronization phenomena.

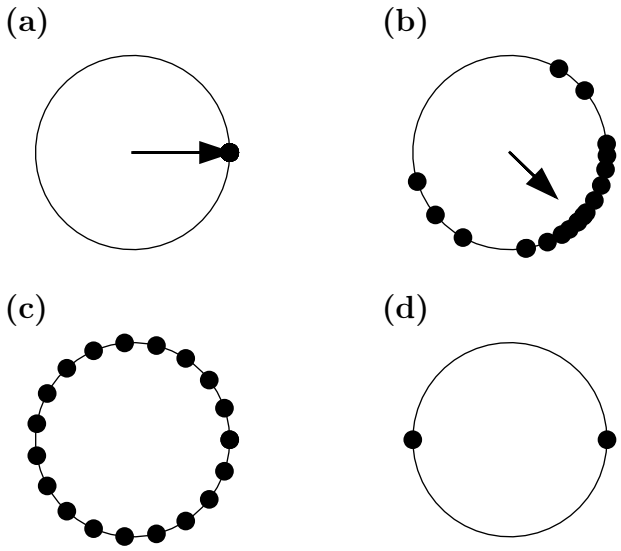

FIGURE 2.5: Different synchronization states for N phase oscillators. Arrows indicate the mean if its magnitude is not 0. In (a) all phases are equal — this is the fully synchronized state. Partial synchrony is shown in (b). The states in (c) (splay state) and (d) (symmetric 2-cluster state) have no first-order macroscopic dynamics.

Some interesting partial synchronous states include the chimera state [12], the Bellerophon state [26], the π state [26], or the traveling wave state [26].

2.3.2 Kuramoto Model

The Kuramoto model is a paradigmatical first-order phase model of coupled oscillators. It is used widely to study synchronization [64,65] and has been applied to study the motion of pedestrians on a bridge [5] or the human brain [66]. The model describes N coupled phase oscillators with coupling strength K using a first harmonic

$$\dot{\varphi}_j = \omega_j + \frac{K}{N} \sum_{k=1}^{N} \sin(\varphi_k - \varphi_j + \alpha_j) \; . \tag{2.22}$$

The natural frequency ω_j follows some distribution $g(\omega)$, and a phase shift parameter α_j modifies the interaction. This is the simplest solvable model of pairwise coupled phase oscillators and describes, e.g., the first-order approximation of diffusively coupled Stuart-Landau oscillators [38].

The model can be simplified with the introduction of a complex mean-field $Z = Re^{i\theta} = 1/N \sum_k e^{i\varphi_k}$ to

$$\dot{\varphi}_j = \omega_j + KR \sin(\theta - \varphi_j + \alpha_j) \; . \tag{2.23}$$

The magnitude of the mean-field R is called the order parameter and describes the coherence of the state. An order parameter of 1 shows full synchrony,

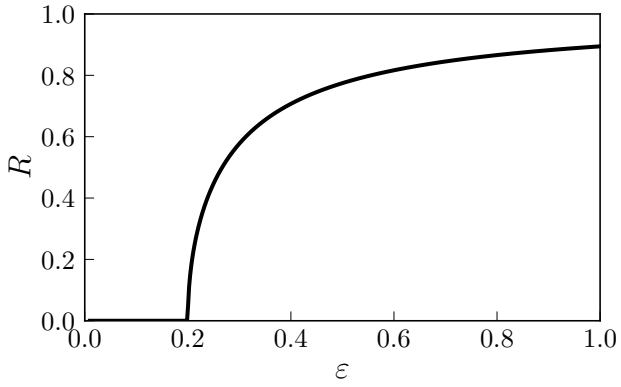

FIGURE 2.6: Synchronization transition in the Kuramoto model with a Lorentzian frequency distribution with scale $\gamma = 0.1$, according to Eqs. (2.24) and (2.27).

i.e., all oscillators have the same phase. A small order parameter indicates a uniform distribution of phases, although it also describes uniformly spaced clusters of oscillators. To discern between these states, it is necessary to use the Kuramoto-Daido [39] order parameters R_m from $Z_m = R_m e^{i\theta_m} = 1/N \sum_k e^{im\varphi_k}$. The disappearance of all R_m then indicates incoherence or asynchrony, while m-cluster states correspond to $R_m = 1$, as well as higher resonant terms.

The transition from asynchrony to synchrony in the thermodynamical limit for an unimodal symmetrical frequency distribution, and with $\alpha_j = 0$, happens at a critical coupling strength K_c, which is determined by the frequency distribution $g(\omega)$ [11] as

$$K_c = \frac{2}{\pi g(0)} \, . \tag{2.24}$$

For a Lorenzian distribution of the frequencies with center ω_0 and scale γ

$$g(\omega) = \frac{\gamma}{\pi \left[(\omega - \omega_0)^2 + \gamma^2\right]} \tag{2.25}$$

it is possible to calculate the order parameter R [11] and the critical coupling as

$$K_c = 2\gamma \, , \tag{2.26}$$

$$R = \sqrt{1 - \frac{K_c}{K}} \, . \tag{2.27}$$

Such a well-formed transition, as in Fig. 2.6, is only expected in the thermodynamic limit with $N \to \infty$. In a finite-size system, the order parameter depends strongly on the sampling of the natural frequencies. It is better to use the minimal order parameter as a measure of synchronization [67] in such circumstances.

Analytical Solvability

For systems with a common forcing H of the form,

$$\dot{\varphi}_j = \omega(t) + \mathrm{Im}\left[H(t)e^{-i\varphi_j}\right] \tag{2.28}$$

it is possible to reduce the dynamics of systems with dimensionality $N > 3$ to just three dimensions and $N-3$ constants of motion with the Watanabe-Strogatz (WS) theory [34, 35]. For this, H must not depend on the oscillator index j. This is the case for the Kuramoto model in Eq. (2.23) for $\alpha_j = \alpha$, with $H = KZe^{i\alpha}$. The reduction is based on the Möbius transformation [65] and requires the reformulation in terms of $e^{i\varphi_j}$ as

$$\frac{d}{dt}e^{i\varphi_j} = i\omega(t)e^{i\varphi_j} + \frac{1}{2}H(t) - \frac{e^{i2\varphi_j}}{2}H^*(t)\ , \tag{2.29}$$

where * denotes the complex conjugate. The Möbius transformation changes the N phases φ_j to N real variables ζ_j and a complex variable z with $|z| < 1$ with

$$e^{i\varphi_j} = \frac{z + e^{i\zeta_j}}{1 + z^* e^{i\zeta_j}}\ . \tag{2.30}$$

Since a degree of freedom was added by introducing z, an additional, arbitrary constraint of the average over the j being 0, $\left\langle e^{i\zeta_j}\right\rangle_j = 0$ (and hence also the average over the time derivative $\left\langle \dot{\zeta}_j e^{i\zeta_j}\right\rangle$) can be added

$$\begin{aligned} \frac{1}{N}\sum_k e^{i\zeta_k} &= 0\ , \\ \frac{1}{N}\sum_k \dot{\zeta}_k e^{i\zeta_k} &= 0\ . \end{aligned} \tag{2.31}$$

Taking the derivative of Eq. (2.30) with reference to the time yields

$$\begin{aligned} \frac{d}{dt}e^{i\varphi_j} &= \frac{\left(\dot{z} + i\dot{\zeta}_j e^{i\zeta_j}\right)\left(1 + z^* e^{i\zeta_j}\right) - \left(z + e^{i\zeta_j}\right)\left(\dot{z}^* e^{i\zeta_j} + iz^*\dot{\zeta}_j e^{i\zeta_j}\right)}{\left(1 + z^* e^{i\zeta_j}\right)^2} \\ &= \frac{\dot{z} + \left[\dot{z}z^* - z\dot{z}^* + i\dot{\zeta}_j\left(1 - i\left|z\right|^2\right)\right]e^{i\zeta_j} - \dot{z}^* e^{i2\zeta_j}}{\left(1 + z^* e^{i\zeta_j}\right)^2}\ . \end{aligned} \tag{2.32}$$

Substituting this and Eq. (2.30) in Eq. (2.29) and reordering leads to

$$\begin{aligned} &\dot{z} - i\omega z - \frac{H}{2} + \frac{H^*}{2}z^2 \\ &\quad = \left[-\dot{z}z^* + z\dot{z}^* - i\dot{\zeta}_j\left(1 - i\left|z\right|^2\right) + i\omega\left(1 + \left|z\right|^2\right) + \left(z^* H - zH^*\right)\right]e^{i\zeta_j} \\ &\qquad + \left[\dot{z}^* + i\omega z^* - \frac{H^*}{2} + \frac{H}{2}z^{*2}\right]e^{i2\zeta_j}\ . \end{aligned} \tag{2.33}$$

Averaging over j removes the first term on the right side because it only contains terms of the form $\left\langle e^{i\zeta_j} \right\rangle_j$ and $\left\langle \dot{\zeta}_j e^{i\zeta_j} \right\rangle_j$ and these disappear according to Eq. (2.31). This leaves the equation

$$\dot{z} - i\omega z - \frac{H}{2} + \frac{H^*}{2} z^2 = \left[\dot{z}^* + i\omega z^* - \frac{H^*}{2} + \frac{H}{2} z^{*2} \right] \left\langle e^{i2\zeta_j} \right\rangle_j \ , \tag{2.34}$$

which is trivially fulfilled for

$$\dot{z} = i\omega z + \frac{H}{2} - \frac{H^*}{2} z^2 \ , \tag{2.35}$$

yielding the ODE for the new quantity z. Inserting Eq. (2.35) into Eq. (2.33) then also gives the ODE for the ζ_j as

$$\dot{\zeta}_j = \omega + \frac{z^* H - z H^*}{2i} = \omega + \mathrm{Im}\left[z^* H \right] \ . \tag{2.36}$$

This solution does not depend on the index j, and hence the time evolution for all ζ_j is equal, and their values only differ by some constants. Introducing now the new variable χ and the constants ψ_j as $\zeta_j = \chi + \psi_j$ yields the final equations for the WS theory

$$\begin{aligned} \dot{z} &= i\omega z + \frac{H}{2} - \frac{H^*}{2} z^2 \ , \\ \dot{\chi} &= \omega + \mathrm{Im}\left[z^* H \right] \ . \end{aligned} \tag{2.37}$$

The new variable z can be interpreted to be closely related to the mean-field Z (but not equal). The more synchronized a state becomes, i.e., the bigger R is, the bigger $|z|$ will be. Moreover, the phase of z is close to the mean-field phase θ. Finding an equivalent representation for χ is harder. It can be seen as a description of the clustering, but this is not exact [68]. It is also important to note that the WS theory cannot describe fully synchronized systems, as then $z = 1$, and in the Möbius transformation $|z| < 1$.

While the WS theory describes some collective variables, it is possible to gain information about the single oscillators, more precisely their average frequencies ν_j [69]. The angle χ determines the shift between the oscillators and $\arg(z)$. A growing in the phase φ_j leads to a decrease in the shift, i.e., if φ_j rotates once, then χ decreases by 2π. From there, it follows that

$$\langle \nu \rangle = \langle \dot{\Theta} \rangle - \langle \dot{\chi} \rangle \ . \tag{2.38}$$

In the case of the thermodynamic limit, it is possible to further simplify the system. The mean-field and the local mean-field Y in this case are

$$Y(\omega, t) = \int_0^{2\pi} w(\varphi, t|\omega) e^{i\varphi} d\varphi \ , \tag{2.39}$$

$$Z(t) = \int_{-\infty}^{\infty} g(\omega) Y(\omega, t) d\omega \ , \tag{2.40}$$

where $w(\varphi, t|\omega)$ is the density of the oscillators with frequency ω at phase φ. In

the thermodynamic limit with a uniform distribution of the ψ_j, the mean-field directly follows the WS theory $z = Z$ [65,68]. If H is now independent of χ, as is the case in the Kuramoto model, then the second equation of Eqs. (2.37) can be dropped and

$$\frac{\partial Y(\omega,t)}{\partial t} = i\omega Y + \frac{H(\omega,t)}{2} - \frac{H^*(\omega,t)}{2} Y^2 \ . \tag{2.41}$$

Because of the continuity equation for the phases and the ODE in the thermodynamics limit

$$\frac{\partial w}{\partial t} + \frac{\partial w\dot{\varphi}}{\varphi} = 0 \tag{2.42}$$

the derivative of the Kuramoto-Daido local mean-field Y_m (compare Eq. (2.39)) can be written as

$$\frac{\partial Y_m}{\partial t} = \int_0^{2\pi} \frac{\partial w}{\partial t} e^{im\varphi} d\varphi = -\int_0^{2\pi} \frac{\partial w\dot{\varphi}}{\partial \varphi} e^{im\varphi} d\varphi \ . \tag{2.43}$$

With the dynamical equation in the thermodynamic limit

$$\dot{\varphi} = \omega + \mathrm{Im}\left[He^{-i\varphi}\right] \tag{2.44}$$

and integration by parts this is reducible to

$$\begin{aligned}
\frac{\partial Y_m}{\partial t} &= -\int_0^{2\pi} \frac{\partial w\dot{\varphi}}{\partial \varphi} e^{im\varphi} d\varphi && (2.45)\\
&= -\left[w\dot{\varphi}e^{im\varphi}\right]_0^{2\pi} + im\int_0^{2\pi} w\dot{\varphi}e^{im\varphi} d\varphi && (2.46)\\
&= -\left[w\dot{\varphi}e^{im\varphi}\right]_0^{2\pi} + im\int_0^{2\pi} w\left(\omega + \mathrm{Im}\left[He^{-i\varphi}\right]\right) e^{im\varphi} d\varphi && (2.47)\\
&= -\left[w\dot{\varphi}e^{im\varphi}\right]_0^{2\pi} + im\omega\int_0^{2\pi} we^{im\varphi} d\varphi + \frac{m}{2}H\int_0^{2\pi} we^{i(m-1)\varphi} d\varphi \\
&\quad - \frac{m}{2}H^*\int_0^{2\pi} we^{i(m+1)\varphi} d\varphi && (2.48)\\
&= -\left[w\dot{\varphi}e^{im\varphi}\right]_0^{2\pi} + im\omega Y_m + \frac{m}{2}\left(HY_{m-1} - H^*Y_{m+1}\right) \ . && (2.49)
\end{aligned}$$

In the case of $m = 1$, so Y, the first term disappears. A particular realization of this is called the Ott-Antonsen (OA) manifold, with the Ansatz $Y_m = Y_1^m = Y^m$ [36,37]. Then the infinite series of ODEs resulting from Eq. (2.49) reduces to just one equation. This manifold is the only attractor [36], although the relaxation onto it is not described by the OA Ansatz [70] and may be slow [71]. In the special case of a Lorentzian frequency distribution g with center ω_0 and scale γ, as in Eq. (2.25), the integration from the local mean-field Y to the mean-field Z can be solved analytically [37] and results in [37,72,73]

$$\dot{Z} = (i\omega_0 - \gamma)Z + \frac{1}{2}\left(H - H^*Z^2\right) \ . \tag{2.50}$$

M-Kuramoto Model

The Kuramoto model in Eq. (2.22) is generalized by splitting the system in M groups. Oscillators with phases φ_j^σ belonging to group σ are coupled with strength $K_{\sigma\sigma'}$ to group σ', according to

$$\dot{\varphi}_j^\sigma = \omega_{\sigma,j} + \sum_{\sigma'=1}^{M} \frac{K_{\sigma\sigma'}}{N} \sum_{k=1}^{N_{\sigma'}} \sin(\varphi_k^{\sigma'} - \varphi_j^\sigma + \alpha_{\sigma\sigma'}) \; . \tag{2.51}$$

Here N_σ is the number of oscillators in group σ and $\alpha_{\sigma\sigma'}$ the phase shift between the groups. Introducing a group mean-field, as in the Kuramoto model $Z_\sigma = R_\sigma e^{i\theta_\sigma} = 1/N_\sigma \sum_k e^{i\varphi_k^\sigma}$ allows for the reformulation

$$\dot{\varphi}_j^\sigma = \omega_{\sigma,j} + \mathrm{Im}\left[\sum_{\sigma'=1}^{M} K_{\sigma\sigma'} \frac{N_{\sigma'}}{N} Z_{\sigma'} e^{i\alpha_{\sigma\sigma'}} e^{-i\varphi_j^\sigma}\right] \; , \tag{2.52}$$

which yields the common forcing of group σ as

$$H_\sigma = \sum_{\sigma'=1}^{M} K_{\sigma\sigma'} \frac{N_{\sigma'}}{N} Z_{\sigma'} e^{i\alpha_{\sigma\sigma'}} \; . \tag{2.53}$$

This form does not allow for a direct application of the WS theory, as there is not the same forcing acting on all oscillators at the same time. But since the forcing applies group-wise, it is possible to apply the WS theory to each group separately [68], such that the dimensionality of the problem reduces from $N > 3M$ to $3M$ and $N-3M$ constants of motion. The dynamics of every group are then determined according to the WS equations Eq. (2.37).

2.3.3 Partial Synchronous States

The Kuramoto model is used widely for its analytical solvability, but by changing the coupling scheme, such as in the M-Kuramoto model, it is possible for a plethora of different partial synchronous states to exist. The chimera state [12] has gathered much attention in recent time [15, 74–76]. This state was first observed in a system with nonlocal coupling and is characterized by the existence of two subpopulations, one phase-locked and one phase-randomized. Both subgroups are coherent in their natural order, e.g., their spatial position in the nonlocal coupling or their natural frequency.

Another similar, albeit different, state is the Bellerophon state [26]. It appears in a system with two populations of nonidentical oscillators. Oscillators in each group act attractively on all other oscillators in the same group and repulsively on oscillators belonging to the other group. The average frequencies of this state exhibit clusters. Between the clusters exists a regime of incoherent frequencies, leading to a step-like picture.

The M-Kuramoto model with two groups, one acting attractive and one repulsive on all oscillators, yields the solitary state [24]. Here all attractive, as well as all repulsive oscillators, except for one, cluster at the same phase,

and a single solitary oscillator is phase-shifted by π. In the same system, a Mercedes state appears [24], where all but two repulsive oscillators cluster at the same approximate phase, and the remaining two oscillators are phase-shifted by $\pm\pi/2$.

Chapter 3

Higher-Order Phase Dynamics

This chapter contains the results from the paper "Higher-Order Phase Reduction for Coupled Oscillators" by Gengel, Teichmann, Rosenblum, and Pikovsky. It was published 2021 in J. Phys. Complex. 2 015005 [52].

As described earlier, phase dynamics are generally only applied in the weak coupling limit, where the dynamics stay close to the limit cycle, as in Eq. (2.17). However, this is not the case in all real-world systems; their coupling may very well be strong. It has been shown that the weak coupling limit does not explain all dynamical states in even rather relatively simple models of coupled Stuart-Landau oscillators [38]. These shortcomings makes the description of higher-order coupling an essential tool in studying synchronization.

3.1 State of the Literature

In the following, a short overview of the literature about higher-order coupling will be given.

3.1.1 Kuramoto-Daido Model

One of the historically first ways to extend the weak coupling limit past the Kuramoto model, was the generalization of it (Eq. (2.22)) by Daido [39]. The Kuramoto-Daido model is averaged over fast oscillations, comparable to the derivation Eq. (2.20) for the Adler equation, to only consider phase differences and still only in the first-order in ε. The resulting coupling is pairwise

$$\dot{\varphi}_j = \omega_j + \frac{\varepsilon}{N} \sum_{k=1}^{N} h(\varphi_k - \varphi_j) \; . \tag{3.1}$$

The coupling function h is assumed to be 2π-periodic. All the other quantities are the same as in the Kuramoto model. For the simplest case of $h(\varphi) = \sin(\varphi)$ the Kuramoto-Daido model reduces to the Kuramoto model. Higher-order coupling is realized by considering an arbitrarily complex function h instead of a

simple trigonometric one, although higher-order coupling terms of the form of non-pairwise connections are disregarded.

Since h is a real valued, 2π-periodic function, it can be written as a Fourier series with coefficients $\hat{h}_k = A_k/2 + iB_k/2$

$$h(\varphi) = \sum_{k\in\mathbb{Z}} \hat{h}_k e^{ik\varphi} = \sum_{k=1}^{\infty} \left(A_k \cos(k\varphi) - B_k \sin(k\varphi)\right) \ . \tag{3.2}$$

By changing the reference frame to an appropriate frequency, the term $\hat{h}_0$ disappears. Using this and the Kuramoto-Daido mean-field $Z_m = X_m + iY_m = 1/N \sum_k e^{im\varphi_k}$, which are the Fourier coefficients of the phases, results in

$$\dot{\varphi}_j = \omega_j + \varepsilon \sum_{k=1}^{N} \frac{1}{N} \sum_{l\in\mathbb{Z}} \hat{h}_l e^{il(\varphi_k - \varphi_j)} \tag{3.3}$$

$$= \omega_j + \varepsilon \sum_{l\in\mathbb{Z}} \hat{h}_l e^{-il\varphi_j} \frac{1}{N} \sum_{k=1}^{N} e^{il\varphi_k} \tag{3.4}$$

$$= \omega_j + \varepsilon \sum_{l\in\mathbb{Z}} \hat{h}_l Z_l e^{-il\varphi_j} \tag{3.5}$$

$$= \omega_j + \varepsilon \sum_{l=1}^{\infty} \left([A_l X_l - B_l Y_l] \cos(l\varphi_j) + [A_l Y_l + B_l X_l] \sin(l\varphi_j)\right) \tag{3.6}$$

$$= \omega_j + \varepsilon H(\varphi_j, t) \ . \tag{3.7}$$

The time dependence of H stems from the Kuramoto-Daido mean-field. Daido called H the order function and hypothesized that in the thermodynamic limit, this function will lose its time dependence, yielding a system of the form

$$\dot{\varphi}_j = \omega_j + \varepsilon H(\varphi_j) = F(\varphi_j) \tag{3.8}$$

for asymptotically large times. Then constraining the form of the function H to only one maximum and one minimum separates the oscillators into two populations, a phase-locked one and a freely rotating one. Considering then the order parameters as a result of the phase distributions yields

$$H(\varphi) = \int_0^{2\pi} w(\theta) h(\theta - \varphi) d\theta \ , \tag{3.9}$$

with $w(\theta)$ being the phase distribution. This form can be used for the analytical treatment of a system.

The Kuramoto-Daido model was later picked up by Rosenblum and Pikovsky [77] and generalized further to consider a nonlinear coupling function, i.e.,

$$\dot{\varphi}_j = \omega_j + \sum_{k\in\mathbb{Z}} \hat{h}^{(1)}_k Z_k e^{-ik\varphi_j} + \sum_{k,l\in\mathbb{Z}} \hat{h}^{(2)}_{kl} Z_k Z_l e^{-i(k+l)\varphi_j} + \dots \ , \tag{3.10}$$

thus increasing the possible solution space.

3.1.2 Decomposition of External Forcing

A different approach to higher-order coupling is investigated in the context of control theory. Here an external forcing acts on the system to achieve the desired state. The phase description in such a case uses a PRC, which quantifies the change of phase after a perturbation. This is, again, only valid in the weak coupling limit. Kurebayashi et al. [40] extend this by using a decomposable force. Consider a dynamical system similar to Eq. (2.1) with

$$\frac{d\boldsymbol{y}}{dt} = \boldsymbol{f}(\boldsymbol{y}(t), \boldsymbol{I}(t)) \,, \tag{3.11}$$

where $\boldsymbol{I}$ the time-varying parameter, i.e., the forcing. For a constant $\boldsymbol{I}(t)$, there has to exist a limit cycle with a corresponding phase φ. Using the set P of all possible perturbations $\boldsymbol{I} \in A$, where A is some subset of $\mathbb{R}^m$, the limit cycle is embedded in the space $\mathbb{R}^n \times A$, forming a cylinder (under the assumption that the state $\boldsymbol{y}(t, \boldsymbol{I})$ is differentiable in this space). This then introduces isochrons in this new space for each possible perturbation $\boldsymbol{I}$.

Now the $\boldsymbol{I}$ becomes time dependent, but can be decomposed in a slowly varying component $\boldsymbol{q} \in A$ and a weak fluctuation $\boldsymbol{p} \in \mathbb{R}^m$ as

$$\boldsymbol{I}(t) = \boldsymbol{q}(\mu t) + \sigma \boldsymbol{p}(t) \,. \tag{3.12}$$

The parameters μ and σ are small, such that $\boldsymbol{q}(\mu t)$ varies slowly in comparison to the relaxation onto the limit cycle. So the oscillator stays close to its limit cycle. The phase is then a function of the state and the slowly varying component

$$\varphi(t) = \Theta(\boldsymbol{y}(t), \boldsymbol{q}(\mu t)) \,. \tag{3.13}$$

The resulting phase reduction in the first order in μ and σ is

$$\dot{\varphi}(t) = \omega(\boldsymbol{q}(\mu t)) + \sigma \boldsymbol{P}_1(\varphi, \boldsymbol{q}(\mu t))\boldsymbol{q}(t) + \mu \boldsymbol{P}_2(\varphi, \boldsymbol{q}(\mu t)) \frac{d\boldsymbol{q}(\mu t)}{dt} \,. \tag{3.14}$$

The new phase response curves $\boldsymbol{P}_1$ and $\boldsymbol{P}_2$ describe the response to the weak fluctuation of $\boldsymbol{p}$ and the deformation of the limit cycle along the set A, respectively. It is important to note that the frequency depends on the form of the limit cycle along the space of the perturbations. As can be seen in Eq. (3.14), all terms depend on the slowly varying component, which may be arbitrarily big and not the weak fluctuation. This extends the phase description far beyond the weak perturbation (or, in our case, coupling) limit.

Pyragas and Novičenko [41] consider, based on the results by Kurebayashi et al., a different kind of strong amplitude-modulated high-frequency (AMHF) forcing. One example of such forcing is a function of the form $\sin(\Omega_0 t)\sin(\Omega_1 t)$, where the envelope frequency Ω_0 is comparable to the natural frequency ω and the carrier frequency $\Omega_1 \gg \omega$. Additionally, it is assumed that $\Omega_1/\Omega_0 \in \mathbb{N}$, so that the forcing term is periodic with frequency Ω_0. To accommodate the application to neurostimulations, where no net charge can be inserted into the tissue, the high-frequency term has to average to zero.

The ODE for the AMHF perturbation has the form

$$\frac{d\boldsymbol{x}}{dt} = \boldsymbol{f}(\boldsymbol{x}) + \boldsymbol{K}\boldsymbol{\psi}(\Omega_0 t)\theta(\Omega_1 t) \,, \tag{3.15}$$

where $\boldsymbol{\psi}$ is the envelope vector and θ the scalar high-frequency carrier signal. By replacing the high-frequency term with an antiderivative

$$\Theta(s) = \int_0^s \theta(s')ds' - \left\langle \int_0^{2\pi} ds \int_0^s \theta(s')ds' \right\rangle \tag{3.16}$$

and changing the coordinates to $\boldsymbol{y}(t) = \boldsymbol{x}(t) - \Theta(\omega t)\boldsymbol{A}\boldsymbol{\psi}(\Omega_0 t)$ yields

$$\frac{d\boldsymbol{y}}{dt} = \boldsymbol{f}(\boldsymbol{y} + \Theta(\Omega_1 t)\boldsymbol{A}\boldsymbol{\psi}(\Omega_0 t)) - \Theta(\Omega_1 t)\boldsymbol{A}\frac{d\boldsymbol{\psi}(\Omega_0 t)}{dt} \,, \tag{3.17}$$

where $\boldsymbol{A} = \boldsymbol{K}/\Omega_1$. There, it is possible to use the method of averaging. This results in a decomposition of a slow envelope phase variable $\alpha = \Omega_0 t$ and the new coordinates. The envelope phase variable has a constant frequency and the ODE for the new coordinates consist only of the average over the autonomous equation $\boldsymbol{f}$

$$\begin{aligned} \frac{d\left\langle \boldsymbol{y} \right\rangle}{dt} &= \boldsymbol{f}(\left\langle \boldsymbol{y} \right\rangle + \Theta(\Omega_1 t)\boldsymbol{A}\boldsymbol{\psi}(\alpha)) - \Theta(\Omega_1 t)\boldsymbol{A}\Omega_0\frac{d\boldsymbol{p}(\alpha)}{d\alpha} \,, \\ \dot{\alpha} &= \Omega_0 \,. \end{aligned} \tag{3.18}$$

The averaged derivative is now entirely described by the originally autonomous function $\boldsymbol{f}$. If the components of $\boldsymbol{A}$ are small, then the right-hand side of Eq. (3.18) can be written as the first few terms of a Taylor series. This yields, in up to the second-order in the components of $\boldsymbol{A}$,

$$\frac{d\left\langle \boldsymbol{y} \right\rangle}{dt} = \boldsymbol{f}(\left\langle \boldsymbol{y} \right\rangle) + \frac{\left\langle \Theta^2 \right\rangle}{2} \sum_{i,j} \frac{\partial^2 \boldsymbol{f}(\left\langle \boldsymbol{y} \right\rangle)}{\partial \left\langle y \right\rangle_i \partial \left\langle y \right\rangle_j} A_i A_j \psi_i(\Omega_0 t)\psi_j(\Omega_0 t) \,. \tag{3.19}$$

The first order term in A_i disappears, as it is compensated by the second term on the right hand side of Eq. (3.18). Because the right hand side is small, this can be solved using the traditional phase reduction methods.

3.1.3 Isostable Coordinates

The range for which the first-order phase approximation is correct depends heavily on the system. For a limit cycle with a slow rotation but fast relaxation, bigger coupling strength will yield more acceptable results than a system where the time scales are switched. This is described by the Floquet multipliers, which are the complex eigenvalues of the linearized system of a Poincaré section, similar to Eq. (2.4). If the Floquet multipliers are close to 1, then even small perturbations will significantly affect the dynamics. Wilson and Moehlis [42] introduce a method to apply the phase approximation to these types of systems by adding one additional isostable coordinate, which describes the distance to the limit cycle. They consider a perturbed autonomous system with the

perturbation function $\boldsymbol{G}(\boldsymbol{y}, t)$

$$\frac{d\boldsymbol{y}}{dt} = \boldsymbol{f}(\boldsymbol{y}) + \boldsymbol{G}(\boldsymbol{y}, t) \ . \tag{3.20}$$

Isostable coordinates ψ_i are defined as

$$\psi_k(\boldsymbol{y}) = \boldsymbol{e}_k^T \boldsymbol{V}^{-1}(\boldsymbol{y}_\Gamma - \boldsymbol{y}_0) e^{-\log \lambda_k t_\Gamma / T} \ . \tag{3.21}$$

The limit cycle quantities are marked by Γ, where $\boldsymbol{y}_\Gamma$ and t_Γ are the location and time when the trajectory first returns to the isochron of phase 0. $\boldsymbol{V}$ is a matrix containing the eigenvectors of the linearized equation around the limit cycle as columns, and the λ are the corresponding eigenvalues. Finally, $\boldsymbol{e}_k$ is a unit vector in the k-dimensions direction and $\boldsymbol{y}_0$ the coordinates of the $\varphi = 0$ on the limit cycle.

These new isostable coordinates ψ_k can be seen as an expansion of the limit cycle tangentially to the neutral direction. Level sets of ψ_k indicate the distance to the limit cycle, which decreases exponentially, determined by the corresponding Floquet multiplier λ_k. Because the isostable coordinates result from the linearized ODE, they are not universally valid but only relatively close to the limit cycle. The level sets can be shown further by considering the isostable coordinates in the first order of the distance to the limit cycle by

$$\psi_k(\boldsymbol{y}(t+T)) = \lambda_k \psi_k(\boldsymbol{y}(t)) \ . \tag{3.22}$$

Considering the isostable coordinates together with the phase leads to the equations

$$\begin{aligned} \dot{\varphi} =& \omega + P(\varphi) G(t) \ , \\ \dot{\psi}_k =& \frac{\log(\lambda_k)}{T} \psi_k + \hat{P}_k(\varphi) G(t) \ . \end{aligned} \tag{3.23}$$

Here P is the PRC of the autonomous system, and $\hat{P}_k$ a corresponding isostable response curve (IRC). They are both the gradients of their respective coordinates on the limit cycle. This system has one more dimension than the original one, but coordinates with $|\lambda_k| \approx 0$ are dampened by the first term on the right-hand side and can be disregarded, effectively reducing the dimensionality of the dynamics. This method itself does not directly extend the validity of the weak coupling limit but expands the possible systems on which to apply this method.

3.1.4 Perturbation Method

León and Pazó [38] applied the higher-order phase reduction to a specific system. They consider a mean-field complex Ginzburg-Landau model, which consists of Stuart-Landau oscillators (see Eq. (2.10) with $\omega = \alpha$) diffusively coupled to their mean-field $\bar{A} = 1/N \sum_k A_k$ via a cross-coupling term c

$$\dot{A}_j = A_j - (1 + i\alpha) |A_j|^2 A_j + \varepsilon(1 + ic)(\bar{A} - A_j) \ . \tag{3.24}$$

This system is special, as the phase dynamics of the uncoupled oscillators are known analytically. Furthermore, it was already known that the first-order

phase reduction leads to the Kuramoto Model in Eq. (2.22). To extend this to higher-orders, León and Pazó first rewrite it in terms of magnitude r_j and phase φ cf. Eqs. (2.11) and (2.12), as

$$\begin{aligned}
\dot{r}_j =& r_j(1-\varepsilon-r_j^2) \\
&+ \frac{\varepsilon}{N}\sum_k r_k\left[\cos\left(\varphi_k-\varphi_j+\alpha\ln\frac{r_k}{r_j}\right)-c\sin\left(\varphi_k-\varphi_j+\alpha\ln\frac{r_k}{r_j}\right)\right] \\
=& f(r_j)+\varepsilon g_j(\boldsymbol{r},\boldsymbol{\varphi}) \\
\dot{\varphi}_j =& \varepsilon(\alpha-c) \\
&+ \frac{\varepsilon}{Nr_j}\sum_k r_k\left[(c-\alpha)\cos\left(\varphi_k-\varphi_j+\alpha\ln\frac{r_k}{r_j}\right)+(1+\alpha c)\sin\left(\varphi_k-\varphi_j+\alpha\ln\frac{r_k}{r_j}\right)\right] \\
=& \varepsilon h_j(\boldsymbol{r},\boldsymbol{\varphi})\ .
\end{aligned} \tag{3.25}$$

Because of the numerical observation that the ordering of the oscillators does not change, they assume that r_j is fully determined by the phases, i.e., $r_j = r_j(\varphi_1,\varphi_2,\ldots)$ and further that the r_j can be expanded in a power series as $r_j = r_j^{(0)} + \varepsilon r_j^{(1)} + \varepsilon^2 r_j^{(2)} + \ldots$. Now, $\dot{\varphi}_j$ is also expanded in powers of ε as a Taylor series around $\boldsymbol{r}^{(0)}$. In the 0th order, this yields the Kuramoto Sakaguchi model and at order ε

$$r_j^{(1)} = \frac{g_j(\boldsymbol{r}^0,\boldsymbol{\varphi})}{2}\ . \tag{3.26}$$

This can then be inserted into the Taylor expansion again, to get the ε^2-term and so on. Up to the second order this yields then the phase dynamics

$$\begin{aligned}
\dot{\varphi}_j =& \Omega+\varepsilon\nu R\sin(\Theta-\varphi_j+\beta) \\
&+ \frac{\varepsilon^2\nu^2}{4}\left[RR_2\sin(\Theta_2-\Theta-\varphi_j)-\sum_{m=1}^{2}(-R)^m\sin(m(\Theta_2-\varphi_j)+\gamma)\right]\ .
\end{aligned} \tag{3.27}$$

Here R and Θ denote the mean-field values, and R_2 and Θ_2 the values of the second Kuramoto-Daido mean-field. The first three terms on the right-hand side are the Kuramoto model with $\nu = \sqrt{(1+\alpha^2)(1+c^2)}$ and $\beta = \arg[1+\alpha c+i(c-\alpha)]$ and a coupling strength-depended frequency $\Omega = -\alpha+\varepsilon(\alpha-c)$. A new phase shift is introduced in the second-order as $\gamma = \arg[1-c^2+2ic]$. It is interesting to note here the appearance of the second Kuramoto-Daido mean-field, i.e., Z_2, when written out in the last two terms, yields non-pairwise coupling terms. This means that already in the second-order hypernetwork-like terms appear. Later on, León and Pazó derive the cubic order in ε and show that the higher-order terms are necessary to explain any states beyond full synchrony and incoherence in this system.

Shortly before León and Pazó [38], Matheny et al. [48] designed an experiment using eight nanoelectromechanical oscillators coupled in a ring. The model of the oscillators resembles that of the Stuart-Landau oscillator from Eq. (2.10)

and reads

$$\dot{A}_j = -\frac{A_j}{2} + \frac{A_j}{2\,|A_j|} + i\left(\omega_j A_j + \alpha\,|A_j|^2\,A_j\right) - i\varepsilon A_j + i\frac{\varepsilon}{2}(A_{j-1} + A_{j+1}) \quad (3.28)$$

with $A_j = A_{j+N}$ as a periodic boundary condition. Rewriting this equation in polar coordinates yields

$$\begin{aligned} \dot{r}_j &= \frac{1-r_j}{2} - \frac{\varepsilon}{2}\left[r_{j+1}\sin(\theta_{j+1}-\theta_j) + r_{j-1}\sin(\theta_{j-1}-\theta_j)\right] \\ \dot{\theta}_j &= \omega_j + \alpha r_j^2 - \varepsilon + \frac{\varepsilon}{2r_j}\left[r_{j+1}\cos(\theta_{j+1}-\theta_j) + r_{j-1}\cos(\theta_{j-1}-\theta_j)\right]\ . \end{aligned} \quad (3.29)$$

The solution of $r_j = 1$ is stable, as in the Stuart-Landau oscillator and by using a similar Ansatz as León and Pazó the perturbation in r_j can be written in the first order of the coupling strength ε as

$$r_j = 1 - \varepsilon\left[\sin(\theta_{j+1}-\theta_j) + \sin(\theta_{j-1}-\theta_j)\right]\ . \quad (3.30)$$

By inserting this relation for r_j into the polar phase equation of Eq. (3.29), the phase equation up to the second order in ε can be found. The phase equation then reads

$$\begin{aligned} \dot{\varphi}_j =& \omega_j + \alpha - \varepsilon \\ & - 2\alpha\varepsilon\left[\sin(\varphi_{j+1}-\varphi_j) + \sin(\varphi_{j-1}-\varphi_j)\right] \\ & + \frac{\varepsilon}{2}\left[\cos(\varphi_{j+1}-\varphi_j) + \cos(\varphi_{j-1}-\varphi_j)\right] \\ & + \frac{\varepsilon^2}{4}\left[\sin(\varphi_{j+2}-\varphi_j) + \sin(\varphi_{j-2}-\varphi_j)\right] \\ & - \frac{\varepsilon^2}{2}\left[\sin(2(\varphi_{j+1}-\varphi_j)) + \sin(2(\varphi_{j-1}-\varphi_j))\right] \\ & - \frac{\varepsilon^2}{4}\left[\sin(\varphi_{j+2}-2\varphi_{j+1}+\varphi_j) + \sin(\varphi_{j-2}-2\varphi_{j-1}+\varphi_j)\right] \\ & + \frac{\varepsilon^2}{2}\sin(\varphi_{j+1}-2\varphi_j+\varphi_{j-1})\ . \end{aligned} \quad (3.31)$$

The first three lines in Eq. (3.31) describe the first-order phase reduction, which resembles the Kuramoto model with a phase-shift parameter. In the second order phase reduction unexpected terms appear. Even though the system has only coupling terms between neighbors, there appear non-structural coupling terms between next-nearest neighbors in line four and triadic terms involving the nearest neighbors and next-nearest neighbors in lines six and seven. The triadic terms are unexpected, as they connect the phases of three oscillators instead of the pairwise coupling. In line five, higher harmonics appear. Experimentally they find many interesting dynamical states, which are verified by numerical simulations. All observed states could be found using the phase model, but only using the first order yields the wrong stability for, e.g., the splay state. This work shows the importance of higher-order phase reduction in describing more complex dynamical states.

3.2 Higher-Order Phase Reduction for Coupled Oscillators

Based on the observations by Matheny et al. in Ref. [48], we have investigated a simple model of three Stuart-Landau oscillators coupled in a line [52]. In difference to León and Pazó [38], the oscillators are not coupled to a global mean-field but only to their nearest neighbors. This system exhibits non-structural terms in the higher orders of the phase dynamics, meaning connections that are not present in the coupling scheme, such as the triadic or next-nearest neighbor interactions in Eq. (3.31). The method for the phase reduction is based on a perturbation Ansatz, similar to León and Pazó's [38], but it is better suited to networks and non-identical oscillators. To verify the analytical results, we also introduced a numerical method to reconstruct the phase dynamics. Finally, we have applied the numerical method to coupled van-der-Pol oscillators, for which there exists no analytical phase description.

3.2.1 Model

The model describes nonidentical, coupled Stuart-Landau-oscillators (cf. Eq. (2.10)) with the coupling function G_j of the form

$$\dot{A}_j = (1 + i\omega_j)A_j - |A_j|\,A_j - i\alpha A_j(|A_j|^2 - 1) + \varepsilon G_j(A_1, A_2, \ldots)\ . \tag{3.32}$$

The natural frequencies of the single oscillators may differ, but they share the same non-isochronicity parameter α, so the form of the isochrones is identical across all oscillators. Reformulating this in terms of the amplitude R_j and phase φ_j, as in Eqs. (2.11) and (2.12) yields

$$\dot{R}_j = R_j - R_j^3 + \varepsilon \mathrm{Re}\left[e^{-i(\varphi_j + \alpha \ln R_j)} G_j(R_1, \varphi_1, R_2, \varphi_2, \ldots)\right]\ , \tag{3.33}$$

$$\begin{aligned}\dot{\varphi}_j =& \omega_j + \frac{\varepsilon}{R_j}\left\{\mathrm{Im}\left[e^{-i(\varphi_j + \alpha \ln R_j)} G_j(R_1, \varphi_1, R_2, \varphi_2, \ldots)\right]\right. \\ &\left. -\alpha \mathrm{Re}\left[e^{-i(\varphi_j + \alpha \ln R_j)} G_j(R_1, \varphi_1, R_2, \varphi_2, \ldots)\right]\right\}\ .\end{aligned} \tag{3.34}$$

3.2.2 Perturbation Method

We assume that both R_j and $\dot{\varphi}_j$ can be expressed as a power series in ε of the phases (from a Taylor series)

$$R_j = 1 + \varepsilon r_j^{(1)}(\varphi_1, \varphi_2, \ldots) + \varepsilon^2 r_j^{(2)}(\varphi_1, \varphi_2, \ldots) + \ldots\ , \tag{3.35}$$

$$\dot{\varphi}_j = \omega_j + \varepsilon \Psi_j^{(1)}(\varphi_1, \varphi_2, \ldots) + \varepsilon^2 \Psi_j^{(2)}(\varphi_1, \varphi_2, \ldots) + \ldots\ . \tag{3.36}$$

The constant values correspond to the quantities on the limit cycle. Finding the unknown functions $r^{(1)}$, $r^{(2)}$, $\Psi^{(1)}$, $\Psi^{(2)}$, and so on, is achieved by inserting the power series into Eqs. (3.33) and (3.34) and comparing the powers of ε.

In the leading order of ε this yields

$$\Psi_j^{(1)} = \mathrm{Im}\left[e^{-i\varphi_j} G_j(1, \varphi_1, 1, \varphi_2, \ldots)\right] - \alpha \mathrm{Re}\left[e^{-i\varphi_j} G_j(1, \varphi_1, 1, \varphi_2, \ldots)\right]\ , \tag{3.37}$$

where only the 0th-order of R_j has to be considered. And equivalently for the amplitude dynamics

$$\dot{r}_j^{(1)} = -2r_j^{(1)} + \mathrm{Re}\left[e^{-i\varphi_j} G_j(1, \varphi_1, 1, \varphi_2, \ldots)\right] \ . \tag{3.38}$$

To then find the coefficient $r_j^{(1)}(\varphi_1, \varphi_2, \ldots)$, Eq. (3.38) can be expressed via the partial derivatives, where only the 0th-order expansion of the phases has to be accounted for. This yields

$$\begin{aligned} \dot{r}_j^{(1)} &= \frac{\partial r_j^{(1)}}{\partial \varphi_1}\dot{\varphi}_1 + \frac{\partial r_j^{(1)}}{\partial \varphi_2}\dot{\varphi}_2 + \ldots \\ &= \frac{\partial r_j^{(1)}}{\partial \varphi_1}\omega_1 + \frac{\partial r_j^{(1)}}{\partial \varphi_2}\omega_2 + \ldots + \mathcal{O}(\varepsilon) \ . \end{aligned} \tag{3.39}$$

Equating Eqs. (3.38) and (3.39) and reordering

$$\begin{aligned} 2r_j^{(1)} + \frac{\partial r_j^{(1)}}{\partial \varphi_1}\omega_1 + \frac{\partial r_j^{(1)}}{\partial \varphi_2}\omega_2 + \ldots &= \mathrm{Re}\left[e^{-i\varphi_j} G_j(1, \varphi_1, 1, \varphi_2, \ldots)\right] \\ &= \sum_{m_1, m_2, \ldots} g_{j;m_1,m_2,\ldots} e^{i(m_1\varphi_1 + m_2\varphi_2 + \ldots)} \ . \end{aligned} \tag{3.40}$$

The right side is 2π-periodic in all the phases and can be rewritten as Fourier series with coefficients $g_{j;m_1,m_2,\ldots}$. Likewise, $r_j^{(1)}$ is also 2π-periodic and is representable as a Fourier series

$$r_j^{(1)} = \sum_{m_1, m_2, \ldots} \varrho_{j;m_1,m_2,\ldots} e^{i(m_1\varphi_1 + m_2\varphi_2 + \ldots)} \ . \tag{3.41}$$

Inserting Eq. (3.41) into Eq. (3.40) and comparing the terms finally gives the Fourier coefficients of $r_j^{(1)}$ as

$$\varrho_{j;m_1,m_2,\ldots} = \frac{g_{j;m_1,m_2,\ldots}}{2 + im_1\omega_1 + im_2\omega_2 + \ldots} \ . \tag{3.42}$$

Finding $r_j^{(1)}$ is thus reduced to calculating the Fourier coefficients of the right hand side of Eq. (3.40). Inserting this then into Eq. (3.34) yields the phase dynamics up to $\mathcal{O}(\varepsilon^2)$. To find the $r_j^{(2)}$, in a similar way to $r_j^{(1)}$, the terms $\psi_j^{(1)}$ and $r_j^{(1)}$ are needed and so on.

3.2.3 Example: Three Stuart-Landau Oscillators in a Line

As the simplest possible model, we apply the perturbation method to three Stuart-Landau oscillators coupled in a line. The oscillators j and k are coupled with a modified strength $\varepsilon c_{k,j}$ and a phase shift $\beta_{k,j}$ in their complex amplitudes. This coupling scheme preserves the rotational invariance of the system.

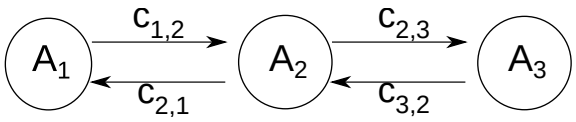

FIGURE 3.1: A schematic representation of three Stuart-Landau oscillators, coupled in a line, as described by Eq. (3.43). Reproduced from Ref. [53].

A visualization of the scheme is given in Fig. 3.1. The three ODEs are as follows

$$\begin{aligned}
\dot{A}_1 &= (1+i\omega_1)A_1 - |A_1|^2 A_1 - i\alpha A_1(|A_1|^2 - 1) + \varepsilon c_{2,1} e^{i\beta_{2,1}} A_2 \ , \\
\dot{A}_2 &= (1+i\omega_2)A_2 - |A_2|^2 A_2 - i\alpha A_2(|A_2|^2 - 1) + \varepsilon \left(c_{1,2} e^{i\beta_{1,2}} A_1 + c_{3,2} e^{i\beta_{3,2}} A_3 \right) \ , \\
\dot{A}_3 &= (1+i\omega_3)A_3 - |A_3|^2 A_3 - i\alpha A_3(|A_3|^2 - 1) + \varepsilon c_{2,3} e^{i\beta_{2,3}} A_2 \ .
\end{aligned} \tag{3.43}$$

The corresponding amplitude and phase equations are

$$\begin{aligned}
\dot{R}_1 =& R_1 - R_1^3 + \varepsilon c_{2,1} R_2 \cos(\theta_2 - \theta_1 + \beta_{2,1}) \ , \\
\dot{R}_2 =& R_2 - R_2^3 + \varepsilon c_{1,2} R_1 \cos(\theta_1 - \theta_2 + \beta_{1,2}) \\
&+ \varepsilon c_{3,2} R_3 \cos(\theta_3 - \theta_2 + \beta_{3,2}) \ , \\
\dot{R}_3 =& R_3 - R_3^3 + \varepsilon c_{2,3} R_2 \cos(\theta_2 - \theta_3 + \beta_{2,3}) \ , \\
\dot{\varphi}_1 =& \omega_1 + \varepsilon c_{2,1} \frac{R_2}{R_1} \left[\sin(\theta_2 - \theta_1 + \beta_{2,1}) - \alpha \cos(\theta_2 - \theta_1 + \beta_{2,1}) \right] \ , \\
\dot{\varphi}_2 =& \omega_2 + \varepsilon c_{1,2} \frac{R_1}{R_2} \left[\sin(\theta_1 - \theta_2 + \beta_{1,2}) - \alpha \cos(\theta_1 - \theta_2 + \beta_{1,2}) \right] \\
&+ \varepsilon c_{3,2} \frac{R_3}{R_2} \left[\sin(\theta_3 - \theta_2 + \beta_{3,2}) - \alpha \cos(\theta_3 - \theta_2 + \beta_{3,2}) \right] \ , \\
\dot{\varphi}_3 =& \omega_3 + \varepsilon c_{2,3} \frac{R_2}{R_3} \left[\sin(\theta_2 - \theta_3 + \beta_{2,3}) - \alpha \cos(\theta_2 - \theta_3 + \beta_{2,3}) \right] \ .
\end{aligned} \tag{3.44}$$

It is important to note that the right-hand side does not contain the phases φ, but the polar phases θ. If this was not the case, then the phase dynamics would be fully known. This means that the relation between θ_j and φ_j has to be solved up to some order of ε. Here it is shown up to the second-order

$$\begin{aligned}
\varphi_j &= \theta_j - \alpha \ln(R_j) \\
&= \theta_j - \alpha \ln(1 + \varepsilon r_j^{(1)} + \varepsilon^2 r_j^{(2)} + \ldots) \\
&= \theta_j - \alpha \left[\varepsilon r_j^{(1)} + \varepsilon^2 r_j^{(2)} - \frac{(\varepsilon r_j^{(1)} + \varepsilon^2 r_j^{(2)})^2}{2} \right] + \mathcal{O}(\varepsilon^3) \\
&= \theta_j - \alpha \left[\varepsilon r_j^{(1)} + \varepsilon^2 r_j^{(2)} - \frac{\varepsilon^2}{2} {r_j^{(1)}}^2 \right] + \mathcal{O}(\varepsilon^3) \ .
\end{aligned} \tag{3.45}$$

This yields the relation between the polar phase and phase

$$\theta_j = \varphi_j + \alpha \left[\varepsilon r_j^{(1)} + \varepsilon^2 r_j^{(2)} - \frac{\varepsilon^2}{2} {r_j^{(1)}}^2 \right] + \mathcal{O}(\varepsilon^3) \ . \tag{3.46}$$

Specifically, the cosine and sine terms of the phase differences have to be known. For simplicity's sake, let $h_j = \varepsilon r_j^{(1)} + \varepsilon^2 r_j^{(2)} - \frac{\varepsilon^2}{2} {r_j^{(1)}}^2$. Writing out the sine term up to the second-order

$$\begin{aligned}
\sin(\theta_k - \theta_j + \beta_{k,j}) =& \sin(\varphi_k - \varphi_j + \beta_{k,j} + \alpha[h_k - h_j]) + \mathcal{O}(\varepsilon^3) \\
=& \sin(\varphi_k - \varphi_j + \beta_{k,j}) \cos(\alpha[h_k - h_j]) \\
&+ \cos(\varphi_k - \varphi_j + \beta_{k,j}) \sin(\alpha[h_k - h_j]) + \mathcal{O}(\varepsilon^3) \\
=& \sin(\varphi_k - \varphi_j + \beta_{k,j}) \left[1 - \frac{\alpha^2}{2}(h_k - h_j)^2\right] \\
&+ \cos(\varphi_k - \varphi_j + \beta_{k,j}) \alpha (h_k - h_j) + \mathcal{O}(\varepsilon^3) \\
=& \sin(\varphi_k - \varphi_j + \beta_{k,j}) \left[1 - \frac{\alpha^2}{2}\varepsilon^2 (r_k^{(1)} - r_j^{(1)})^2\right] \\
&+ \alpha \cos(\varphi_k - \varphi_j + \beta_{k,j}) \\
&\left[\varepsilon(r_k^{(1)} - r_j^{(1)}) + \varepsilon^2 \left(r_k^{(2)} - r_j^{(2)} + \frac{{r_j^{(1)}}^2 - {r_k^{(2)}}^2}{2}\right)\right] \\
&+ \mathcal{O}(\varepsilon^3) \,. \qquad (3.47)
\end{aligned}$$

And similarly for the cosine

$$\begin{aligned}
\cos(\theta_k - \theta_j + \beta_{k,j}) =& \cos(\varphi_k - \varphi_j + \beta_{k,j}) \left[1 - \frac{\alpha^2}{2}\varepsilon^2 (r_k^{(1)} - r_j^{(1)})^2\right] \\
&- \alpha \sin(\varphi_k - \varphi_j + \beta_{k,j}) \\
&\left[\varepsilon(r_k^{(1)} - r_j^{(1)}) + \varepsilon^2 \left(r_k^{(2)} - r_j^{(2)} + \frac{{r_j^{(1)}}^2 - {r_k^{(2)}}^2}{2}\right)\right] \\
&+ \mathcal{O}(\varepsilon^3) \,. \qquad (3.48)
\end{aligned}$$

Also the terms of the form R_m/R_j in Eq. (3.44) have to be calculated up to some order in ε. For $1/R_j$ the second-order approximation is

$$\begin{aligned}
\frac{1}{R_j} &= \frac{1}{1 + \varepsilon r_j^{(1)} + \varepsilon^2 r_j^{(2)} + \ldots} \\
&= 1 - \varepsilon r_j^{(1)} - \varepsilon^2 r_j^{(2)} + \varepsilon^2 {r_j^{(1)}}^2 + \mathcal{O}(\varepsilon^3) \,. \qquad (3.49)
\end{aligned}$$

From this follows

$$\frac{R_m}{R_j} = 1 + \varepsilon \left[r_m^{(1)} - r_j^{(1)}\right] + \varepsilon^2 \left[r_m^{(2)} - r_j^{(2)} - r_m^{(1)} r_j^{(1)} + {r_j^{(1)}}^2\right] + \mathcal{O}(\varepsilon^3) \,. \qquad (3.50)$$

Substituting the second-order approximations Eqs. (3.47), (3.48), and (3.50) into the dynamics Eq. (3.44) gives the phase dynamics up to the third order in

ε in terms of the amplitude expansion Eq. (3.35)

$$
\begin{aligned}
\dot{\varphi}_1 &= \omega_1 + \varepsilon c_{2,1}[\sin(\varphi_2 - \varphi_1 + \beta_{2,1}) - \alpha\cos(\varphi_2 - \varphi_1 + \beta_{2,1})] \\
&\quad + \varepsilon^2 c_{2,1}(1+\alpha^2)\sin(\varphi_2 - \varphi_1 + \beta_{2,1})(r_2^{(1)} - r_1^{(1)}) \\
&\quad + \varepsilon^3 c_{2,1}(1+\alpha^2)\Big[\left(r_2^{(2)} - r_1^{(2)} - r_2^{(1)}r_1^{(1)} + {r_1^{(1)}}^2\right)\sin(\varphi_2 - \varphi_1 + \beta_{2,1}) \\
&\quad + \alpha\left(0.5{r_1^{(1)}}^2 + 0.5{r_2^{(1)}}^2 - r_2^{(1)}r_1^{(1)}\right)\cos(\varphi_2 - \varphi_1 + \beta_{2,1})\Big] + \mathcal{O}(\varepsilon^4)\,, \\
\dot{\varphi}_2 &= \omega_2 + \varepsilon c_{1,2}[\sin(\varphi_1 - \varphi_2 + \beta_{1,2}) - \alpha\cos(\varphi_1 - \varphi_2 + \beta_{1,2})] \\
&\quad + \varepsilon c_{3,2}[\sin(\varphi_3 - \varphi_2 + \beta_{3,2}) - \alpha\cos(\varphi_3 - \varphi_2 + \beta_{3,2})] \\
&\quad + \varepsilon^2 c_{1,2}(1+\alpha^2)\sin(\varphi_1 - \varphi_2 + \beta_{1,2})(r_1^{(1)} - r_2^{(1)}) \\
&\quad + \varepsilon^2 c_{3,2}(1+\alpha^2)\sin(\varphi_3 - \varphi_2 + \beta_{3,2})(r_3^{(1)} - r_2^{(1)}) \\
&\quad + \varepsilon^3 c_{1,2}(1+\alpha^2)\Big[\left(r_1^{(2)} - r_2^{(2)} - r_1^{(1)}r_2^{(1)} + {r_2^{(1)}}^2\right)\sin(\varphi_1 - \varphi_2 + \beta_{1,2}) \\
&\quad + \alpha\left(0.5{r_2^{(1)}}^2 + 0.5{r_1^{(1)}}^2 - r_1^{(1)}r_2^{(1)}\right)\cos(\varphi_1 - \varphi_2 + \beta_{1,2})\Big] \\
&\quad + \varepsilon^3 c_{3,2}(1+\alpha^2)\Big[\left(r_3^{(2)} - r_2^{(2)} - r_3^{(1)}r_2^{(1)} + {r_2^{(1)}}^2\right)\sin(\varphi_3 - \varphi_2 + \beta_{3,2}) \\
&\quad + \alpha\left(0.5{r_2^{(1)}}^2 + 0.5{r_3^{(1)}}^2 - r_3^{(1)}r_2^{(1)}\right)\cos(\varphi_3 - \varphi_2 + \beta_{3,2})\Big] + \mathcal{O}(\varepsilon^4)\,, \\
\dot{\varphi}_3 &= \omega_3 + \varepsilon c_{2,3}[\sin(\varphi_2 - \varphi_3 + \beta_{2,3}) - \alpha\cos(\varphi_2 - \varphi_3 + \beta_{2,3})] \\
&\quad + \varepsilon^2 c_{2,3}(1+\alpha^2)\sin(\varphi_2 - \varphi_3 + \beta_{2,3})(r_2^{(1)} - r_3^{(1)}) \\
&\quad + \varepsilon^3 c_{2,3}(1+\alpha^2)\Big[\left(r_2^{(2)} - r_3^{(2)} - r_2^{(1)}r_3^{(1)} + {r_3^{(1)}}^2\right)\sin(\varphi_2 - \varphi_3 + \beta_{2,3}) \\
&\quad + \alpha\left(0.5{r_3^{(1)}}^2 + 0.5{r_2^{(1)}}^2 - r_2^{(1)}r_3^{(1)}\right)\cos(\varphi_2 - \varphi_3 + \beta_{2,3})\Big] + \mathcal{O}(\varepsilon^4)\,.
\end{aligned}
\tag{3.51}
$$

To evaluate Eq. (3.51) the coefficients $r_j^{(1)}$ and $r_j^{(2)}$ have to be known. This is achieved by finding the Fourier coefficients from Eq. (3.41) via Eq. (3.42) for the first order and in a similar way for all higher-orders. For the first oscillator

the first and second order terms are given in the 0th-order by

$$\frac{\partial r_1^{(1)}}{\partial \varphi_1}\omega_1 + \frac{\partial r_1^{(1)}}{\partial \varphi_2}\omega_2 + \frac{\partial r_1^{(1)}}{\partial \varphi_3}\omega_3 + 2r_1^{(1)} = c_{2,1}\cos(\varphi_2 - \varphi_1 + \beta_{2,1}) \,, \tag{3.52}$$

$$\begin{aligned}
\frac{\partial r_1^{(2)}}{\partial \varphi_1}\omega_1 + \frac{\partial r_1^{(2)}}{\partial \varphi_2}\omega_2 + \frac{\partial r_1^{(2)}}{\partial \varphi_3}\omega_3 + 2r_1^{(2)} &= -3{r_1^{(1)}}^2 \\
&- \alpha c_{2,1}\left(r_2^{(1)} - r_1^{(1)}\right)\sin(\varphi_2 - \varphi_1 + \beta_{2,1}) + c_{2,1}r_2^1\cos(\varphi_2 - \varphi_1 + \beta_{2,1}) \\
&+ c_{2,1}\left[\sin(\varphi_2 - \varphi_1 + \beta_{2,1}) - \alpha\cos(\varphi_2 - \varphi_1 + \beta_{2,1})\right]\frac{\partial r_1^{(1)}}{\partial \varphi_1} \\
&+ \Big[c_{1,2}\left[\sin(\varphi_1 - \varphi_2 + \beta_{1,2}) - \alpha\cos(\varphi_1 - \varphi_2 + \beta_{1,2})\right] \\
&+ c_{3,2}\left[\sin(\varphi_3 - \varphi_2 + \beta_{3,2}) - \alpha\cos(\varphi_3 - \varphi_2 + \beta_{3,2})\right]\Big]\frac{\partial r_1^{(1)}}{\partial \varphi_2} \\
&+ c_{2,3}\left[\sin(\varphi_2 - \varphi_3 + \beta_{2,3}) - \alpha\cos(\varphi_2 - \varphi_3 + \beta_{2,3})\right]\frac{\partial r_1^{(1)}}{\partial \varphi_3} \,.
\end{aligned} \tag{3.53}$$

Similar calculations for $r_2^{(1)}$ and $r_3^{(1)}$ yield the first-order terms as a Fourier series, similar to Eq. (3.42), as

$$r_1^{(1)} = \frac{2c_{2,1}}{4 + (\omega_2 - \omega_1)^2}\cos(\varphi_2 - \varphi_1 + \beta_{2,1}) + \frac{(\omega_2 - \omega_1)c_{2,1}}{4 + (\omega_2 - \omega_1)^2}\sin(\varphi_2 - \varphi_1 + \beta_{2,1}) \,, \tag{3.54}$$

$$\begin{aligned}
r_2^{(1)} =& \frac{2c_{1,2}}{4 + (\omega_1 - \omega_2)^2}\cos(\varphi_1 - \varphi_2 + \beta_{1,2}) + \frac{(\omega_1 - \omega_2)c_{1,2}}{4 + (\omega_1 - \omega_2)^2}\sin(\varphi_1 - \varphi_2 + \beta_{1,2}) \\
&+ \frac{2c_{3,2}}{4 + (\omega_3 - \omega_2)^2}\cos(\varphi_3 - \varphi_2 + \beta_{3,2}) + \frac{(\omega_3 - \omega_2)c_{3,2}}{4 + (\omega_3 - \omega_2)^2}\sin(\varphi_3 - \varphi_2 + \beta_{3,2}) \,,
\end{aligned} \tag{3.55}$$

$$r_3^{(1)} = \frac{2c_{2,3}}{4 + (\omega_2 - \omega_3)^2}\cos(\varphi_2 - \varphi_3 + \beta_{2,3}) + \frac{(\omega_2 - \omega_3)c_{2,3}}{4 + (\omega_2 - \omega_3)^2}\sin(\varphi_2 - \varphi_3 + \beta_{2,3}) \,. \tag{3.56}$$

The second order phase dynamics are then given in a closed form by inserting Eqs. (3.54) - (3.56) into Eq. (3.51)

$$\begin{aligned}
\dot{\varphi}_1 =&\omega_1 + \varepsilon c_{2,1}[\sin(\varphi_2 - \varphi_1 + \beta_{2,1}) - \alpha\cos(\varphi_2 - \varphi_1 + \beta_{2,1})] \\
&+ \varepsilon^2\Big[a^{(2)}_{1;0} + a^{(2)}_{1;-2,2,0}\cos(2\varphi_2 - 2\varphi_1) + b^{(2)}_{1;-2,2,0}\sin(2\varphi_2 - 2\varphi_1) \\
&+ a^{(2)}_{1;-1,2,-1}\cos(2\varphi_2 - \varphi_1 - \varphi_3) + b^{(2)}_{1;-1,2,-1}\sin(2\varphi_2 - \varphi_1 - \varphi_3) \\
&+ a^{(2)}_{1;-1,0,1}\cos(\varphi_3 - \varphi_1) + b^{(2)}_{1;-1,0,1}\sin(\varphi_3 - \varphi_1)\Big] , \\
\dot{\varphi}_2 =&\omega_2 + \varepsilon c_{1,2}[\sin(\varphi_1 - \varphi_2 + \beta_{1,2}) - \alpha\cos(\varphi_1 - \varphi_2 + \beta_{1,2})] \\
&+ \varepsilon c_{3,2}[\sin(\varphi_3 - \varphi_2 + \beta_{3,2}) - \alpha\cos(\varphi_3 - \varphi_2 + \beta_{3,2})] \\
&+ \varepsilon^2\Big[a^{(2)}_{2;0} + a^{(2)}_{2;2,-2,0}\cos(2\varphi_1 - 2\varphi_2) + b^{(2)}_{2;2,-2,0}\sin(2\varphi_1 - 2\varphi_2) \\
&+ a^{(2)}_{2;0,-2,2}\cos(2\varphi_3 - 2\varphi_2) + b^{(2)}_{2;0,-2,2}\sin(2\varphi_3 - 2\varphi_2) \\
&+ a^{(2)}_{2;-1,2,-1}\cos(2\varphi_2 - \varphi_1 - \varphi_3) + b^{(2)}_{2;-1,2,-1}\sin(2\varphi_2 - \varphi_1 - \varphi_3) \\
&+ a^{(2)}_{2;1,0,-1}\cos(\varphi_1 - \varphi_3) + b^{(2)}_{2;1,0,-1}\sin(\varphi_1 - \varphi_3)\Big] , \\
\dot{\varphi}_3 =&\omega_3 + \varepsilon c_{2,3}[\sin(\varphi_2 - \varphi_3 + \beta_{2,3}) - \alpha\cos(\varphi_2 - \varphi_3 + \beta_{2,3})] \\
&+ \varepsilon^2\Big[a^{(2)}_{3;0} + a^{(2)}_{3;-2,2,0}\cos(2\varphi_2 - 2\varphi_3) + b^{(2)}_{3;-2,2,0}\sin(2\varphi_2 - 2\varphi_3) \\
&+ a^{(2)}_{3;-1,2,-1}\cos(2\varphi_2 - \varphi_3 - \varphi_1) + b^{(2)}_{3;-1,2,-1}\sin(2\varphi_2 - \varphi_3 - \varphi_1) \\
&+ a^{(2)}_{3;-1,0,1}\cos(\varphi_1 - \varphi_3) + b^{(2)}_{3;-1,0,1}\sin(\varphi_1 - \varphi_3)\Big] .
\end{aligned} \tag{3.57}$$

The coefficients $a^{(k)}_{j;\boldsymbol{l}}$, and $b^{(k)}_{j;\boldsymbol{l}}$ denote the coefficients of the sine and cosine terms in the kth order, respectively, and the vector $\boldsymbol{l} = (l_1, l_2, l_3)$ signifies the coefficients before the corresponding phases in the trigonometric functions via $l_1\varphi_1 + l_2\varphi_2 + l_3\varphi_3$. The concrete values of the coefficients are given in the Appendix in Tabs. A.1 and A.2. It can be seen that the first order coupling terms correspond to simple pairwise coupling, as expected. However, new terms arise in the second-order, while no corrections to the terms of the first order are made. The newly appearing terms can be described as follows.

1. As the simplest expansion of the pairwise coupling, we find higher harmonics, i.e., couplings of the form $\sin(2\varphi_2 - 2\varphi_1)$. These can be seen as the squares of the first-order terms and are still pairwise.

2. New non-structural pairwise terms appear that are not present in the coupling scheme. These have the form $\sin(\varphi_3 - \varphi_1)$. It is interesting to note that the interaction has to be mediated by the middle oscillator φ_2, but the phase does not appear here. Such terms are often reconstructed numerically but are seen as spurious. The result above provides justification for the observations.

3. Non-pairwise connections appear. These combine the phases of all three oscillators, like $\sin(2\varphi_2 - \varphi_1 - \varphi_3)$. These resemble hypernetworks and can appear with different coefficients to the phases. Because of the rotational

symmetry of the coupling function and oscillators, the coefficients will always have to sum to zero, i.e., $\sum_j l_j = 0$.

4. The first-order terms are independent of the natural frequencies. This is no longer the case in the second order. Here the coefficients $a_{j;\boldsymbol{l}}$ and $b_{j;\boldsymbol{l}}$ depend explicitly on the frequency differences.

An overview of modes that appear up to the 5th-order is given in Tables A.3 and A.4.

3.2.4 Numerical Method for the Phase Reduction

To verify the results for the three coupled Stuart-Landau oscillators, we develop a numerical algorithm for the phase reduction. This can also be applied to more general models where the phase of the uncoupled oscillators may not be known analytically.

Numerical Calculation of the Phase and Instantaneous Frequency

Consider an oscillator with the state $\boldsymbol{u} = \boldsymbol{y}(t)$ and $\boldsymbol{v} = d\boldsymbol{y}(t)/dt$. To find the phase, we need to consider an uncoupled and autonomous copy of the oscillator as

$$\frac{d\boldsymbol{w}}{dt} = \boldsymbol{f}(\boldsymbol{w}) \ . \tag{3.58}$$

This copy has the initial condition of $\boldsymbol{w}(0) = \boldsymbol{u}$. Then, to find the phase, this copy is evolved for a time nT, where n is a sufficiently big integer to reach the limit cycle. This guarantees that the phase of the state $\boldsymbol{w}$ is the same as that of $\boldsymbol{u}$. To find the derivative of the phase, the evolution of the same copy with the initial condition $\boldsymbol{u} + \boldsymbol{v}dt$ has to be considered. Because of the infinitesimal time step dt, this can be achieved by using the linearized equation with the Jacobian $\boldsymbol{J}$. This then yields two points on the limit cycle, $\bar{\boldsymbol{w}}$ and $\bar{\boldsymbol{w}} + \bar{\boldsymbol{v}}dt$ with the phases φ and $\varphi + d\varphi$. Now comes the main point, evolution of the autonomous system on the limit cycle also leads to the same phase shift $d\varphi$, but in a generally different time interval $\bar{dt}$. This interval is determined by

$$\bar{\boldsymbol{w}} + \bar{\boldsymbol{v}}dt = \bar{\boldsymbol{w}} + \boldsymbol{f}(\bar{\boldsymbol{w}})\bar{dt} \ . \tag{3.59}$$

From there follows the relation between the two time intervals as

$$\bar{dt} = \frac{\bar{\boldsymbol{v}} \cdot \boldsymbol{f}(\bar{\boldsymbol{w}})}{|\boldsymbol{f}(\bar{\boldsymbol{w}})|^2} dt \ . \tag{3.60}$$

The phase grows uniformly with $d\varphi = \omega\bar{dt}$, so the instantaneous frequency follows as

$$\frac{d\varphi}{dt} = \omega \frac{\bar{\boldsymbol{v}} \cdot \boldsymbol{f}(\bar{\boldsymbol{w}})}{|\boldsymbol{f}(\bar{\boldsymbol{w}})|^2} \ . \tag{3.61}$$

This algorithm can be applied numerically, with an error of $\mathcal{O}(dt^2)$ because of the linearization, and, applied to every unit in the network, yields the phase and instantaneous frequency of the whole system.

Numerical Phase Reduction

Having calculated the phase and instantaneous frequency as described in the previous section, we still lack a method for finding the phase dynamics of the coupled system. The phase dynamics in Eq. (3.36) are 2π-periodic in all phases, and accordingly, they can be written as a real-valued Fourier series

$$\dot{\varphi}_j = a_{j;\mathbf{0}} + \sum_{\boldsymbol{l}\neq\mathbf{0}} \left[a_{j;\boldsymbol{l}} \cos(\boldsymbol{\varphi}\cdot\boldsymbol{l}) + b_{j;\boldsymbol{l}} \sin(\boldsymbol{\varphi}\cdot\boldsymbol{l})\right] \ , \tag{3.62}$$

where $\boldsymbol{\varphi} = (\varphi_1, \varphi_2, \ldots)$ and the rest as in Eq. (3.57). The $\boldsymbol{l}$ can be further restricted by considering the property of the real-valued Fourier coefficients $a_{j;-\boldsymbol{l}} = a^*_{j;\boldsymbol{l}}$, where * denotes the complex conjugate. So it is enough to consider only one of the $\boldsymbol{l}$ and $-\boldsymbol{l}$ terms in the sum when fitting. The resemblance to the phase dynamics can be seen already. By writing the coefficients as a power series in ε as

$$\begin{aligned} a_{j;\boldsymbol{l}} =& a^{(0)}_{j;\boldsymbol{l}} + \varepsilon a^{(1)}_{j;\boldsymbol{l}} + \varepsilon^2 a^{(2)}_{j;\boldsymbol{l}} + \ldots \\ b_{j;\boldsymbol{l}} =& b^{(0)}_{j;\boldsymbol{l}} + \varepsilon b^{(1)}_{j;\boldsymbol{l}} + \varepsilon^2 b^{(2)}_{j;\boldsymbol{l}} + \ldots \end{aligned} \tag{3.63}$$

the resemblance becomes perfect. Fitting the coefficients in Eq. (3.62) on L datapoints yields L linear equations. Fitting these L equations restricts the Fourier series to L terms, although in general only Fourier series with $M \ll L$ terms are needed. We have chosen to restrict the modes to $l_j \leq m$, which leaves

$$M = \sum_{k=1}^{N} m(2m+1)^{k-1} + 1 \tag{3.64}$$

terms to be considered. The resulting complexity is $\mathcal{O}(m^N)$, meaning this method is better suited for small systems. The fitting itself can be done by any method suited for linear systems; we chose singular value decomposition (SVD). To differentiate between the analytical results and the numerical fits, we call the approximated coefficients of the truncated Fourier series $A_{j;\boldsymbol{l}}$ and $B_{j,\boldsymbol{l}}$.

The success of the fit depends on the filling surface of the N-dimensional torus of the phases $\boldsymbol{\varphi}$. If only some small subset of the manifold is observed, then it is not possible to fit the dynamics farther away from it. This is the case in a synchronized system or in a short time series. Also, some initial transient has to be integrated over to reach the invariant manifold. Choosing random initial conditions may not start on the invariant torus, and fitting over these values will yield the wrong coefficients. The chosen transient time has to be longer than the relaxation time of the amplitude but shorter than the synchronization time (should the system synchronize). Depending on the synchronization of the system, different methods have to be applied to fill the torus.

Asynchronous Case. In the case of asynchronous dynamics, the torus will be filled by one long trajectory. It is sufficient to integrate over some initial transient and observe one long time series.

	Asynchronous	Synchronous
ω_1	$-\sqrt{5}/2$	-0.055
ω_2	$(\sqrt{2}-1)/10$	0
ω_3	0.8	0.33

TABLE 3.1: Natural frequencies for the asynchronous and synchronous dynamics.

Synchronous Case. Synchronous dynamics yield only one single periodic trajectory on the torus, i.e., they do not yield enough data to fit the coefficients. Instead, many random initial conditions should be chosen. After some transient, they will settle on the invariant torus. Then a short time series is observed until the phases fully synchronize. This can be done by simply stopping the integration when the differences between all three phases become very small. All the short trajectories together fill the torus, and fitting onto them yields the desired Fourier coefficients.

Example: Three Stuart-Landau Oscillators in a Line

A numerical analysis of the Stuart-Landau system in Eq. (3.44) is performed to verify the analytical results using the numerical method. Both types of dynamics, asynchronous and synchronous ones, are analyzed. All systems share the same parameters, except for the natural frequencies. The chosen parameters are $\alpha = 0.1$, $\beta_{1,2} = 0.32$, $\beta_{2,1} = 0.44$, $\beta_{2,3} = 0.43$, $\beta_{3,2} = 0.18$, and $c_{j,k} = 1$ for all present connections. The frequencies for both dynamics are given in Table 3.1. The phase lags β are chosen randomly and do not represent any specific values.

For the simulation, a transient of $\Delta t = 20$ time units is integrated over after choosing random phases as initial conditions on the unit circle. Integration is done with a time step of $dt = 0.01$, and, in the case of synchronous dynamics, every 100 steps, a new system is generated to prevent synchronization. In total, about 10^6 data points are generated for the synchronous and asynchronous dynamics. Then the modes up to $m = 4$ are fitted onto the data. In Ref. [52] the same method is also applied but only modes fulfilling rotational invariance of $\sum_k l_k = 0$ up to $m = 8$ are considered. This increases the precision and gives the possibility to extend the numerical phase reduction to even higher-orders than the method presented here. The more general method is considered here to show its applicability, even without knowledge of the symmetries of the system. Only the first and second oscillator dynamics are discussed and shown, as the third oscillator shares the same dynamics as the first one. The results for the third oscillator are of the same quality as for the two presented here.

In Fig. 3.2, it can be seen that the reconstructed modes behave as expected. The analytically predicted modes are the biggest, while coefficients with $\sum_k l_k = 0$ follow closely. Modes not fulfilling this condition are comparably small. This verifies the numerical simulation for the studied system and the reconstruction of its symmetries.

Based on the analytical second-order phase reduction in Eq. (3.57), there are no second-order corrections to the first-order terms. So any corrections should

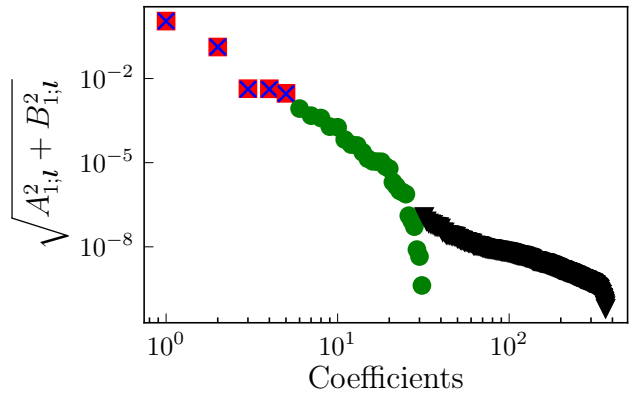

FIGURE 3.2: An overview of the first oscillator's coefficients, reconstructed by the numerical method in the asynchronous case of the Stuart-Landau model with $\varepsilon = 0.13281$. The coefficients are ordered as follows. First, the red squares are modes predicted by the analytical solution. Second, the green dots show modes with $\sum_k l_k = 0$, and finally all other modes as black triangles. Blue crosses mark the coefficients from Table A.1. The coefficients in each group are ordered by their magnitude.

be of third-order or higher. This is also found when comparing the analytical coefficients with the numerically reconstructed ones for the asynchronous and synchronous dynamics in Figs. 3.3(a) and 3.4(a). Deviations from a scaling of ε^3 starts slowly at around $\varepsilon = 0.3$ in the asynchronous case. In the synchronous case, the deviation is bigger and starts earlier at around $\varepsilon = 0.1$. This may be caused by the faster convergence to the synchronous solution. With a stronger coupling, there is a stronger convergence to the synchronous solution, leading to a sparser covering of the hypertorus far away from the synchronous trajectory and hence a worse fit. A similar observation can be made for the second-order corrections in Figs. 3.3(b) and 3.4(b). Here the corrections are in the fourth-order. All in all, the differences between analytical and numerical coefficients is very small.

Higher-order phase terms beyond the second-order are fitted numerically in Figs. 3.5 and 3.6. The appropriate scaling is determined by fitting the coefficients on a log-log scale to a linear function. The slope of this function is then the exponent of the coupling. A coefficient is determined to be scaling with a specific coefficient if the slope is within ± 0.1 of an integer and has a standard error of less than 0.01. A complete overview of all of the modes and the analytical prediction can be found in Tables A.3 and A.4 in the Appendix. In general, the modes are predicted correctly, although some are missing in the synchronous dynamics. The single missing mode in the asynchronous dynamics is the mode $\boldsymbol{l} = (3, -3, 0)$. When interpreting the figures, it has to be considered that in the fifth-order phase approximation, modes start appearing with $m = 5$ which are not part of the fitted coefficients, as they are restricted to $m = 4$. In general, there is a good agreement between the fitted order and the analytical order; modes may be missing but are never attributed to the wrong order. The

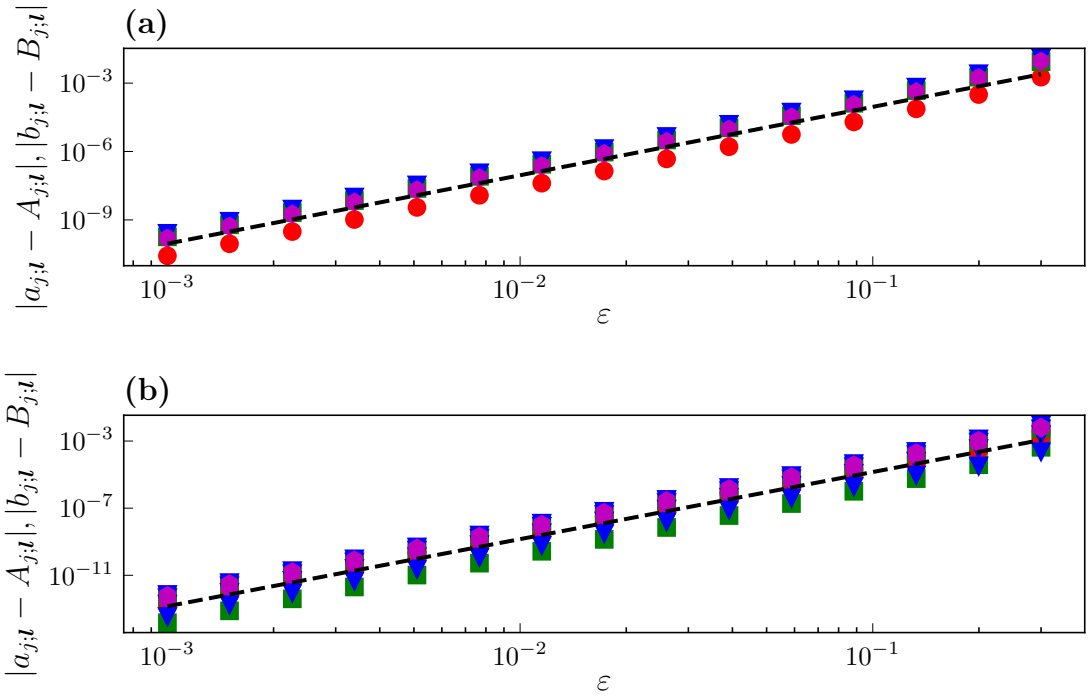

FIGURE 3.3: The difference between the second-order phase reduction for the Stuart-Landau system in Eq. (3.57) and the numerically fitted coefficients in Eq. (3.62) for the asynchronous dynamics. In (a) the first-order modes are shown, where the red circles (blue triangles) depict the cosine-coefficients and the green squares (magenta hexagons) the sine-coefficients of the first (second) oscillator. The third oscillator is not shown, as its dynamics resemble that of the first oscillator. The dashed line gives a scaling of ε^3. In (b) the same is shown for the second-order modes with the dashed line being a ε^4 function.

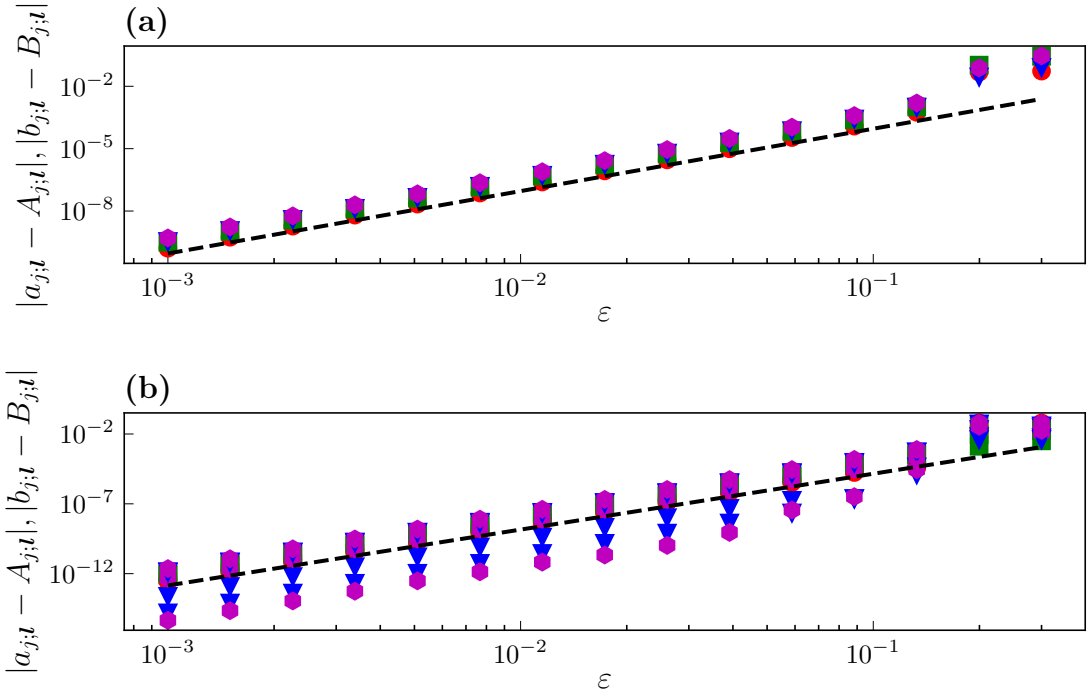

FIGURE 3.4: The same as Fig. 3.3 but for the synchronous dynamics.

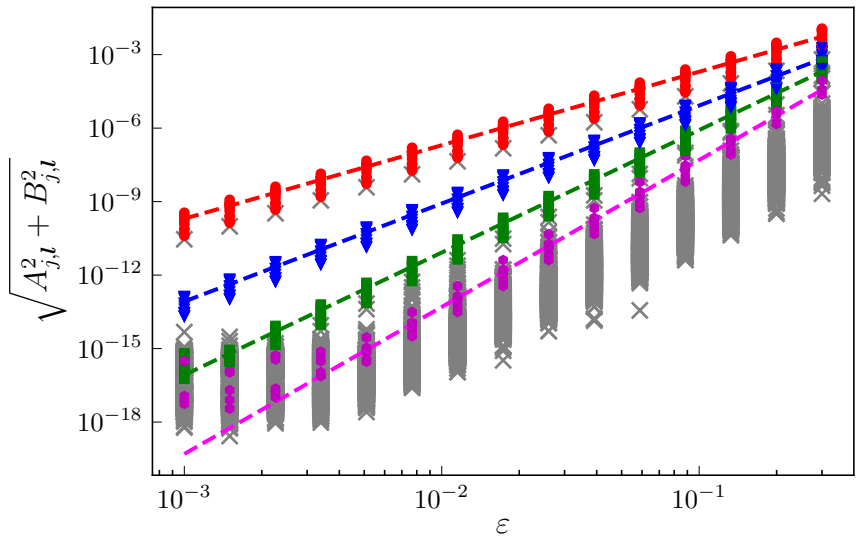

FIGURE 3.5: Scaling of the fitted modes' magnitudes that do not appear in the second order-phase approximation. The coefficients of both the first and second oscillator are shown for the asynchronous dynamics. The colors correspond to third-order (red dots), fourth-order (blue triangles), fifth-order (green squares) and sixth-order (magenta pentagon). The dashed lines of the same color show a function of the form ε^n. Gray crosses mark all other coefficients.

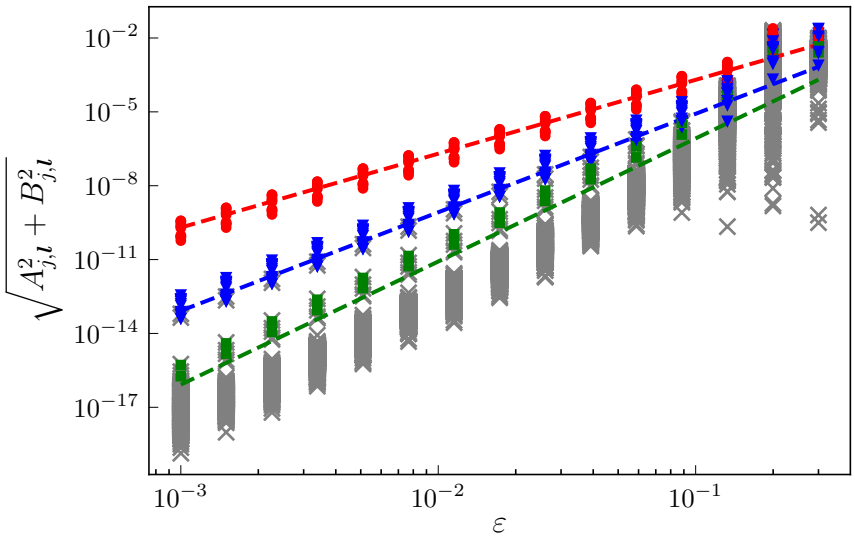

FIGURE 3.6: The same as in Fig. 3.5 but for the synchronous dynamics. In this case no mode of sixth- or higher-order has been found numerically.

missing modes may be influenced by a higher-order correction that shifts the slope further than ± 0.1 from an integer. This correction will have a bigger effect the higher-order the modes are. The fit for the synchronous dynamics starts to break down at around $\varepsilon = 0.1$ again, as in the figures before.

The quality of the fit can be determined by reconstructing the data points with Eq. (3.62) and measuring the difference ζ_j between the numerical and reconstructed $\dot{\varphi}_j$. This is shown in Figs. 3.7 and 3.8. As expected from the missing modes with $m = 5$ that appear in the fifth-order, the error scales as ε^5. In the synchronous case, the scaling starts to break down at about $\varepsilon = 0.07$ and, interestingly, the difference falls instead of rises. This is the result of a contraction of all observed trajectories close to the synchronized one, as predicted earlier. The coefficients then only need to describe the states close to the synchronization manifold, but not the points far away. This explains the difference between the analytical and numerical modes in the earlier figures and the falling reconstruction error. Mitigation strategies, in this case, could be the reduction of the initial transient or taking shorter time series for each system by, e.g., stopping even when moderately close to the synchronized trajectory.

All of the observed quantities fit the analytical predictions, especially when considering smaller and moderate coupling strength. In the asynchronous case, even bigger ε may be used, but in the case of synchronous dynamics, great care has to be taken to find all relevant coupling terms and their coefficients.

Example: Three van der Pol Oscillators in a Line

To test the numerical method on a system of oscillators without an analytical phase dynamic, we apply it to three nonidentical van der Pol oscillators (

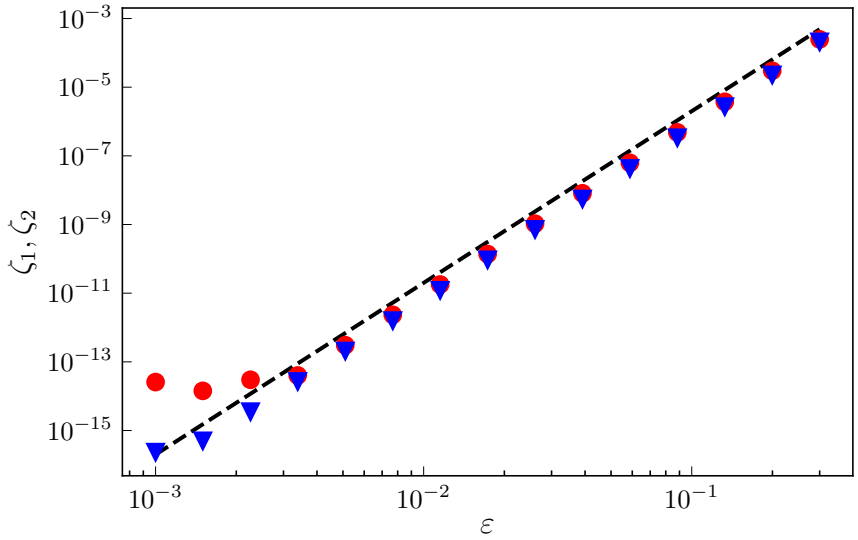

FIGURE 3.7: The mean reconstruction error ζ_j for the first and second oscillator with asynchronous dynamics. It is determined by reconstructing all data points from the fitted coefficients in Eq. (3.62), and measuring the difference to the original phase derivative. The red dots (blue triangles) show the differences for the first (second) oscillator. The dashed line is a ε^5 function.

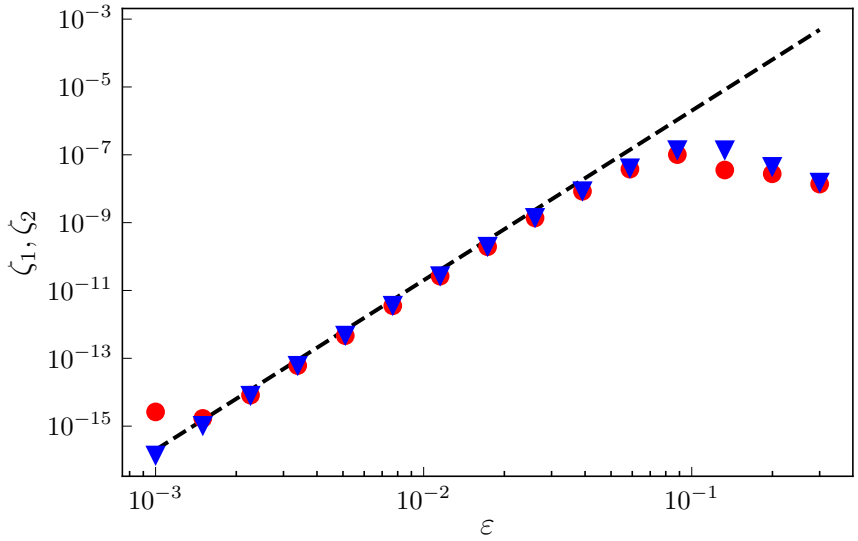

FIGURE 3.8: The same as Fig. 3.7 but for synchronous dynamics.

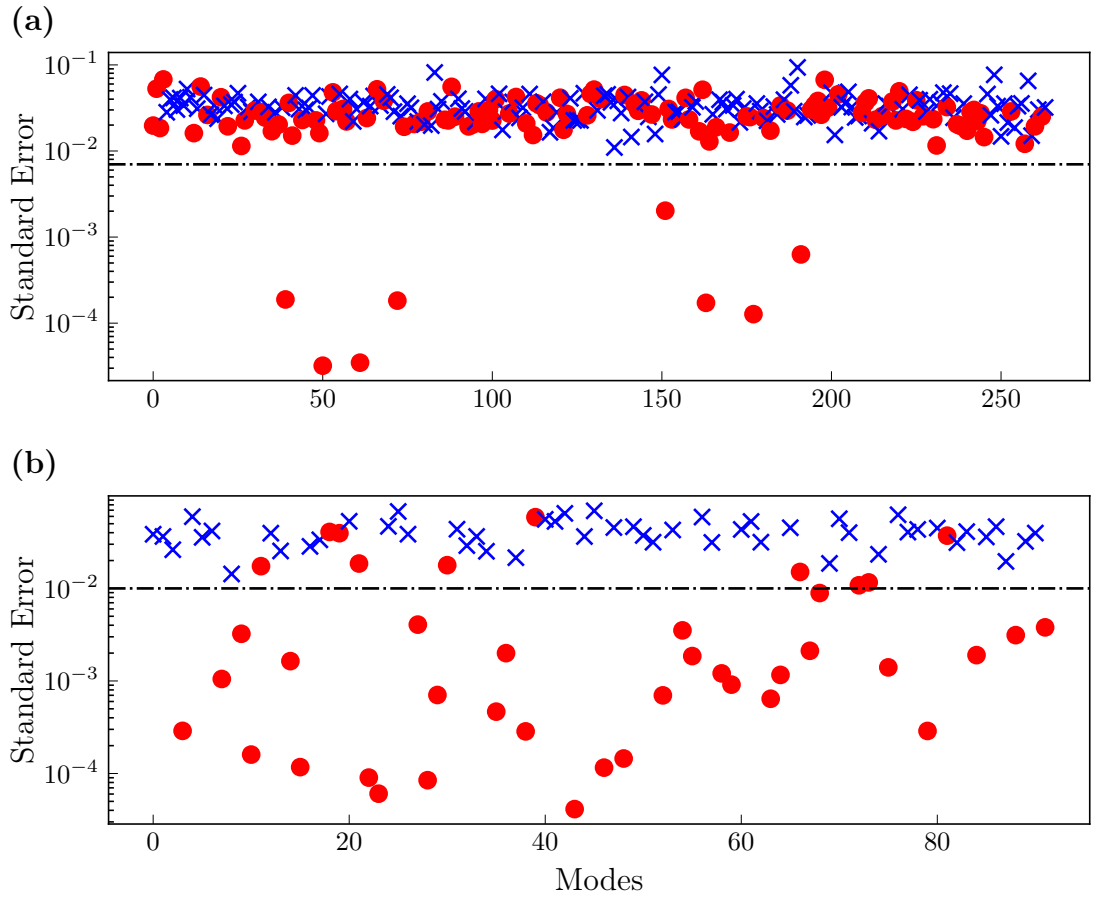

FIGURE 3.9: Standard error of the fitted scaling exponent for the first oscillator in the van der Pol system Eq. (3.65). The modes are sorted randomly. Red dots mark modes fitted to within 0.1 of an integer, and blue crosses the other modes. In (a) the modes that have a fitted scaling of between 0.5 and 1.5 are plotted and in (b) between 1.5 and 2.5. The dotted line marks the cutoff point to consider the scaling as an integer value.

Eq. (2.3)) coupled in a line

$$\begin{aligned} \ddot{x}_1 - \mu(1-x_1^2)\dot{x}_1 + \omega_1^2 x_1 &= \varepsilon x_2 \,, \\ \ddot{x}_2 - \mu(1-x_2^2)\dot{x}_2 + \omega_2^2 x_2 &= \varepsilon(x_1 + x_3) \,, \\ \ddot{x}_3 - \mu(1-x_3^2)\dot{x}_3 + \omega_3^2 x_3 &= \varepsilon x_2 \,. \end{aligned} \tag{3.65}$$

The coupling in this system is not rotationally invariant, such that the condition $\sum_k l_k = 0$ no longer holds. The parameters are fixed at $\mu = 1$, $\omega_1 = 1$, $\omega_2 = 1.324715957$ and $\omega_3 = \omega_2^2$ as a solution to $\omega_3^2 - \omega_2 - 1 = 0$. The system is asynchronous for these values up to at least $\varepsilon = 0.3$. For the numerical fit, similar parameters were used as for the Stuart-Landau system, i.e., a time step of $dt = 0.01$, $m = 4$, and a total of 10^6 data points after a transient of $\Delta t = 20$. Here, there are no analytical solutions, but the phase dynamics can be partially reconstructed from fitting the scaling of the modes.

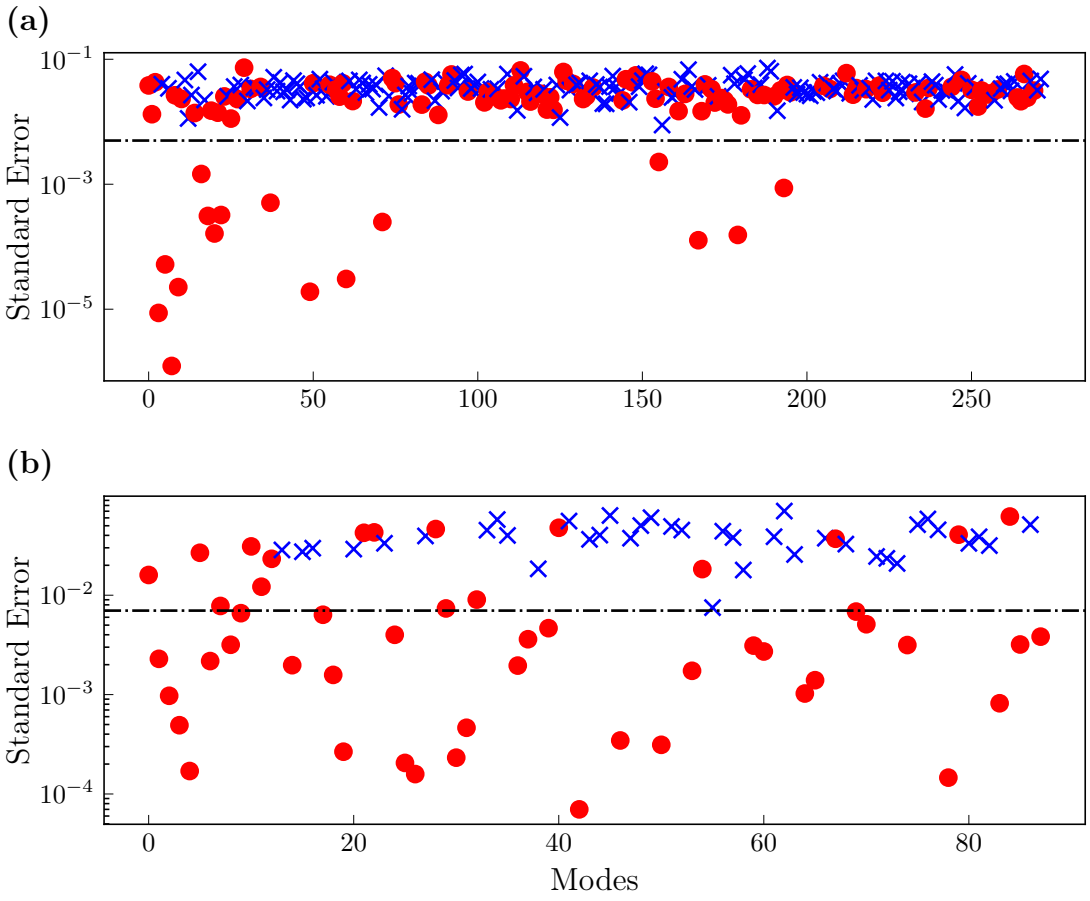

FIGURE 3.10: The same in Fig. 3.10 but for the second oscillator.

To determine which modes belong to a certain order, the modes were fitted onto the data in a log-log representation as before. The standard error for the slope is plotted in Figs. 3.9 and 3.10. The cutoff for determining the integer slope to be the leading order and not numerical noise has been determined by eye to split the population into two. This is easily done in the first-order in Fig. 3.9(a) and 3.10(a). In the second-order, this becomes harder, and the cutoff has been set to exclude all slopes that are not in the range $[1.9, 2.1]$. The resulting modes and their leading order, beyond the constant $\boldsymbol{l} = (0, 0, 0)$, can be found in the Appendix in Tab. A.5. The fitted modes and their scaling are plotted in Fig. 3.11. Only values below $\varepsilon = 0.13281$ were considered for the fit, as they start to diverge from the observed fitting behavior after that. A good agreement between the fitting and the modes can be observed in the plot. Any difference in the fitted modes to Ref. [52] results from a different cutoff point for the modes or the range of slopes that are considered. For the third-order fit, only $\varepsilon \in [0.02603, 0.13281]$ were considered, as the numerical error was too big for smaller values.

The reconstruction error plotted in Fig. 3.12 is not as nice as for the Stuart-Landau system. The error seems to scale as ε, and not as ε^2 or even better. Two reasons for this come to mind: first, the differential equation's linearization to find the phase derivative. This already introduces an error that scales with ε, as the distance to the limit cycle increases. The more plausible explanation is the number of considered modes. While $m = 4$ was sufficient for the Stuart-Landau system, there now appear terms up to $m = 3$ already in the first order of the van der Pol system. It is possible that modes with $m = 5$ and higher are already present in the first-order phase approximation, leading to the reconstruction error. It should still be noted that the error is comparably small to the phase derivative, which is of the order of 10^0. Even for a strong coupling, the reconstruction error is about two orders of magnitude smaller than the phase derivative.

In this system, not only phase differences appear, like in the Stuart-Landau system, but also phase sums. In the first-order in ε, they have very close amplitudes, i.e., the amplitude of $\boldsymbol{l} = (1, 1, 0)$ is very close to the amplitude of $\boldsymbol{l} = (1, -1, 0)$ for the first oscillator. This is reminiscent of the Winfree model Eq. (2.14), where the dynamics are determined by the product of the oscillator's phase and of the driving for (in this case, the phase of the coupled oscillator). This then agrees with the first-order phase approximation, which was not the case for the Stuart-Landau system with only phase differences.

The variable x in the uncoupled van der Pol equation contains not only even harmonics but also odd harmonics. This leads to the third harmonics with $m = 3$ in the first-order in ε.

While the detected modes here are only up to the third-order, modes up to the fourth-order could be detected in Ref. [52] with the same system and integration parameters. This depends on the chosen parameter for the fit, which have been set to a more conservative value here. This can already be seen in the unexpected modes that were detected in the first-order in Ref. [52], but not here. Still, there is a need for a longer data series or more modes that should be fitted.

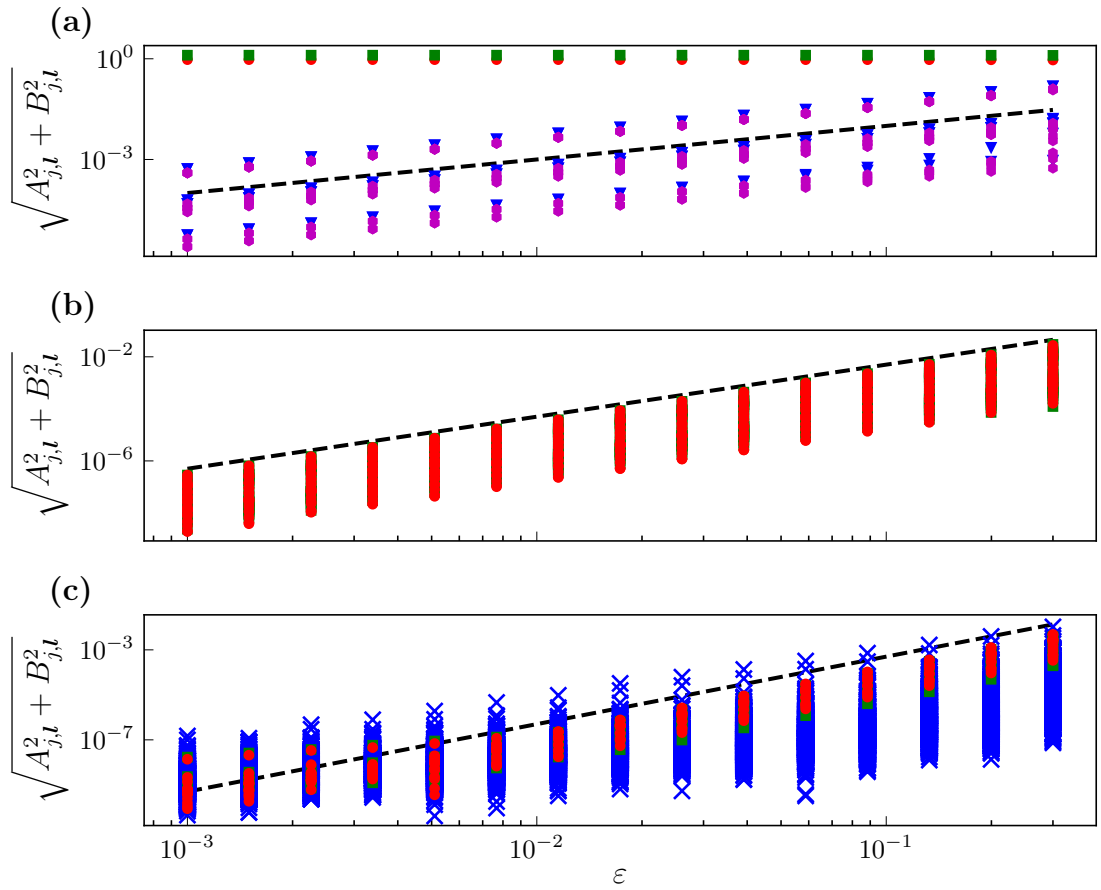

FIGURE 3.11: The scaling of the magnitude of the coefficients of the van der Pol system Eq.(3.65). In (a), the zeroth-order for the first oscillator (red circle) and the second oscillator (green square), as well as the first-order for the first (blue triangle) and the second (magenta hexagon) oscillator are shown. The dashed black line is a linear function in ε. In (b), the same is shown, but for the second-order (red circles for the first and green squares for the second oscillator). The dashed line is a quadratic function in ε. The third-order is plotted in (c), with the same symbols as in the second-order. All other modes are shown as blue crosses. The black dashed line is a ε^3 function.

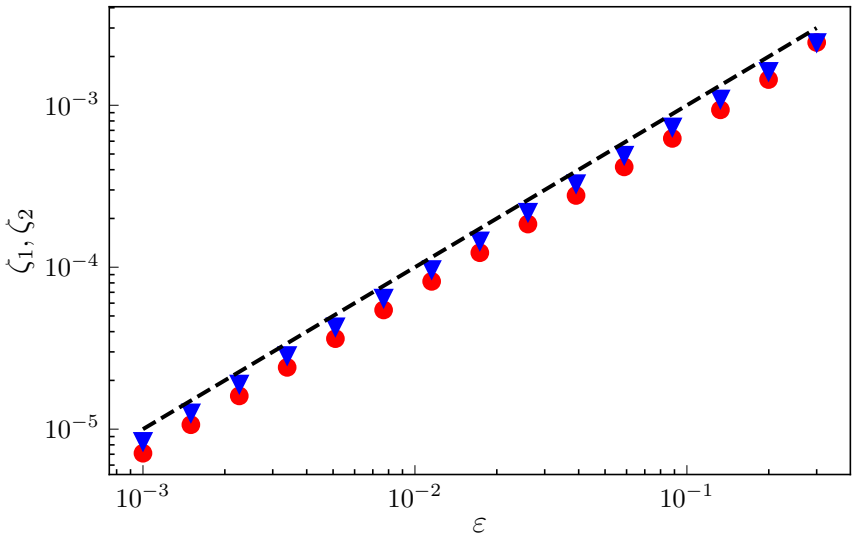

FIGURE 3.12: The mean reconstruction error ζ_1 and ζ_2 for the first (red circles) and second oscillator (blue triangles), respectively. The dashed line is a linear function in ε

.

3.3 Summary & Conclusion

The phase reduction of dynamical systems is a difficult problem and is usually only possible in a first-order approximation of the coupling strength. There are different methods to generalize the phase dynamics to higher-order, although every method has some caveats, like only working for very specific systems. We have developed a general method that can be applied to any system of oscillators with known phase dynamics. The method is based on the expansion of the phase derivative and amplitude as a power series in the coupling strength. The phase dynamics can then be solved iteratively by comparing powers in the coupling strength using a Fourier series.

This method has been applied to a system of the Stuart-Landau oscillators coupled in a line. Using the described method, it is possible to find the second-order phase approximation. Even higher-order can be calculated, but the number of terms increases sharply. In the second-order phase approximation, we already find some unexpected terms, such as hypernetworks terms, connecting all three oscillators, or nonstructural terms, connecting oscillators without a physical connection.

To verify the analytical results, we introduced a numerical method to find the phase derivatives by comparing the time intervals on the limit cycle of the uncoupled units and the coupled system. These phase derivatives can be fitted using a Fourier series of the phases. As in the analytical method, this approach is better suited to small systems, with Fourier coefficients that are not too big, as the number of coefficients that need to be fitted, scale as the highest order of the coefficients to the power of the number of oscillators.

Applied to the Stuart-Landau system, there was a very good agreement

between the numerical and analytical results. The fitted coefficients behaved as expected, and even with a limited number of modes, it was already possible to find good agreement in the modes up to the fifth-order in the coupling strength. The method yielded the best results for asynchronous dynamics, although it could also be applied to the synchronous case with a slight decrease in accuracy.

When applying the same method to a system without 'simple' phase dynamics, such as the van der Pol system, the obtained results still yielded the correct phase dynamics up to the third order in the coupling strength. The reconstruction error indicates that some important modes are missing, but an increase in computational resources by increasing the time series or the considered modes should be sufficient to reach a higher accuracy. Even with the currently chosen parameters, there is already a very good agreement between the actual phase dynamics and the reconstructed one.

Although it is possible, using the introduced methods, to find higher-order phase approximations with a high degree of confidence, they are still computationally expensive, even for small systems. To study systems beyond such small sizes, it is still favorable to use simple phase models, such as the Kuramoto model, even if they are only crude approximations.

Chapter 4

Kuramoto with Attractive and Repulsive Interactions

This chapter contains the results from the paper "Partial synchronization in the Kuramoto model with attractive and repulsive interactions via the Bellerophon state" by Teichmann and Medrano-T. It is submitted [54].

4.1 The Bellerophon State

4.1.1 Conformists-Contrarian Model

The term Bellerophon state was first coined by Qiu et al. in Ref. [26]. They consider a conformists-contrarians system, i.e., two groups of oscillators, where one group acts attractively and one repulsively. The governing ODE resembles the Kuramoto model in Eq. 2.22 and reads

$$\dot{\varphi}_j = \omega_j + \frac{K_j}{N} \sum_{k=1}^{N} \sin(\varphi_k - \varphi_j) \; . \tag{4.1}$$

The coupling strength K_j depends on the oscillator and can take one of two values, $K_+ > 0$ for the conformists and $K_- < 0$ for the contrarians. The frequencies ω_j are chosen from the Lorenzian distribution in Eq. (2.25) with vanishing center $\omega_0 = 0$. They investigate the change in dynamics, depending on the ratio between conformists and contrarians.

For certain ratios and $|K_-| \geq |K_+|$, there exists an interesting partial synchronous state. Multiple coherent clusters exist in a non-coherent state. Oscillators in the same cluster share the same average frequency but have different instantaneous frequencies and phases. They call this state the Bellerophon state. The clusters have average frequencies equal to odd multiples of some fundamental frequency, as shown in Fig. 4.1. Oscillators between the clusters behave quasiperiodically. Qui et al. interpret this state as a weak form of coherence.

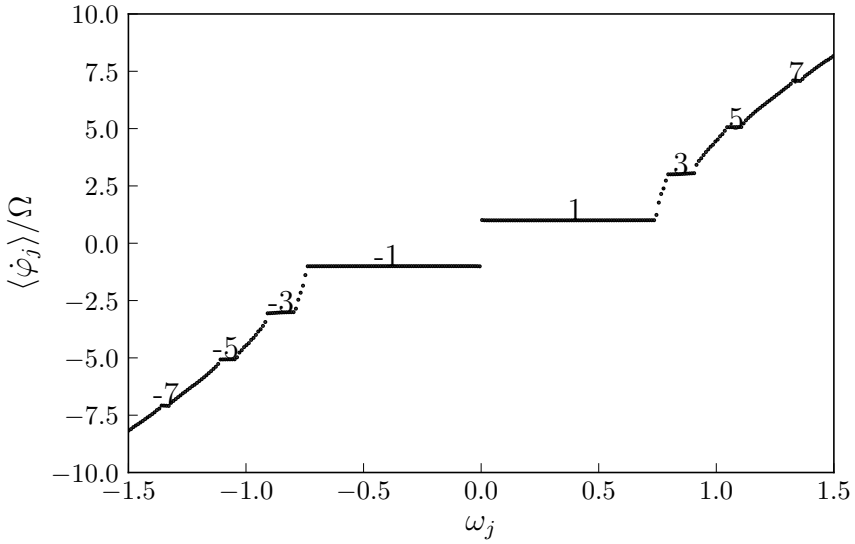

FIGURE 4.1: The Bellerophon state, as observed by Qiu et al. The numbers indicate cluster with odd multiples of the fundamental frequency Ω_1.

4.1.2 Model with Attractive and Repulsive Interactions

A similar state is also observed by Montbrió et al. in Ref. [14]. They investigate an M-Kuramoto model, as in Eq. (2.51), with two groups, where the coupling between groups has a different strength than the coupling in a group. Their model reads

$$\dot{\varphi}_j^\sigma = \omega_j^\sigma + K_p R_\sigma \sin(\Theta_\sigma - \varphi_j^\sigma - \alpha) + K R_{\sigma'} \sin(\Theta_{\sigma'} - \varphi_j^\sigma - \alpha) \,, \tag{4.2}$$

with the mean-fields $Z_\sigma = R_\sigma e^{i\Theta_\sigma}$ and phase shift α. The internal coupling strength in a group is K_p, and the coupling strength between groups is K. The frequencies ω_j^σ are distributed according to unimodal densities with equal widths γ but different means $\bar{\omega}_1$ and $\bar{\omega}_2$. Their chosen coupling scheme allows both attractive and repulsive interactions, but they restrict themselves to positive coupling strengths.

They observe such a step-like Bellerophon state for different α, but the average frequencies differ between both groups. They understand the appearance to be the result of the forcing of two mean-fields at the same time. The clusters themselves are the main contributors to their group's order parameter.

More general systems with a similar equation to Eq. (4.2) have been considered with both attractive and repulsive interactions [22, 78–86]. Some of the results include the comparability of the critical coupling strength in such systems to the Kuramoto model [22] and the reducibility of a two-group system with two different frequency distributions to a Kuramoto model with a bimodal frequency distribution and one additional bifurcation parameter [83].

4.2 Partial Synchronization in the Kuramoto Model with Attractive and Repulsive Interactions via the Bellerophon State

4.2.1 The Model

Consider the M-Kuramoto model in Eq. (2.51). In a simple model with attractive and repulsive interactions, there are only two groups. To further simplify this, we consider a system without phase shift α, equal intra- and inter-coupling $K_{\sigma\sigma'} = 2K$ if $\sigma = \sigma'$ and $K_{\sigma\sigma'} = -2K$ else, respectively, and equally sized groups $N_1 = N_2$. For the sake of analytical tractability, the oscillators' natural frequencies are chosen from a Lorentzian distribution $g(\omega)$, as in Eq. (2.25), where both groups have different centers $\bar{\omega} = \omega_0$ and widths γ. By rotating the reference frame, the first group can be centered at $\bar{\omega}_1 = 0$, and by scaling of the time, the width of the first group can be set to $\gamma_1 = 0.1$. Without loss of generality, the first group is always chosen to be the narrower one, i.e., $\gamma_2 \geq 0.1$.

Introducing the mean field for each group $Z_\sigma = R_\sigma e^{i\Theta_\sigma} = (1/N_\sigma)\sum_k e^{i\theta_k^\sigma}$ and renaming $\theta_j^1 = \varphi_j$ and $\theta_j^2 = \psi_j$ yields the system

$$\begin{aligned} \dot{\varphi}_j =& \omega_{1,j} + KR_1\sin(\Theta_1 - \varphi_j) - KR_2\sin(\Theta_2 - \varphi_j) \,, \\ \dot{\psi}_j =& \omega_{2,j} - KR_1\sin(\Theta_1 - \psi_j) + KR_2\sin(\Theta_2 - \psi_j) \,. \end{aligned} \tag{4.3}$$

Note that $K = K_{\sigma\sigma'}/2$, so the coupling strength of each group is halved compared to the M-Kuramoto model. From there, the forcing H for each group can be determined to be

$$H_\sigma = h_\sigma e^{i\Psi_\sigma} = K(Z_\sigma - Z_{\sigma'}) \,, \tag{4.4}$$

where σ' denotes the other group. Both forcings are connected via $H_2 = -H_1$, so their magnitudes are identical, $h_1 = h_2 = h$, and they are just shifted by a phase $\Psi_1 = \Psi = \Psi_2 - \pi$. The forced equations for the oscillators are then

$$\begin{aligned} \dot{\varphi}_j =& \omega_{1,j} + \mathrm{Im}\left[H_1 e^{-i\varphi_j}\right] = \omega_{1,j} + h\sin(\Psi - \varphi_j) \,, \\ \dot{\psi}_j =& \omega_{2,j} + \mathrm{Im}\left[H_2 e^{-i\psi_j}\right] = \omega_{2,j} + h\sin(\Psi - \psi_j + \pi) \,. \end{aligned} \tag{4.5}$$

Thermodynamic Limit

The OA Ansatz is usable here, by applying it to each group separately. By using the definition of the forcing in Eq. (4.4) and the OA Ansatz in Eq. (2.50) this becomes

$$\dot{Z}_\sigma = (-\gamma_\sigma + i\bar{\omega}_\sigma)Z_\sigma + \frac{K}{2}(Z_\sigma(1 - R_\sigma^2 + Z_{\sigma'}^* Z_\sigma) - Z_{\sigma'}) \,. \tag{4.6}$$

Calculating the derivative of the mean-field $\dot{Z}_\sigma = \dot{R}_\sigma e^{i\Theta_\sigma} + iR_\sigma\dot{\Theta}_\sigma e^{i\Theta_\sigma}$, multiplying Eq. (4.6) by $e^{-i\Theta_\sigma}$ and splitting the real and imaginary part yields the

dynamics of the order parameter and the phase of the mean-field as

$$\begin{aligned}\dot{R}_\sigma =& -\gamma_\sigma R_\sigma + \frac{K}{2}(1-R_\sigma^2)(R_\sigma - R_{\sigma'}\cos(\Theta_\sigma - \Theta_{\sigma'}))\ ,\\ \dot{\Theta}_\sigma =& \bar{\omega}_\sigma + \frac{K}{2}\frac{R_{\sigma'}}{R_\sigma}(1+R_\sigma^2)\sin(\Theta_\sigma - \Theta_{\sigma'})\ .\end{aligned} \tag{4.7}$$

Both equations only depend on the difference between the mean-field phases, as expected in a rotational invariant system. The 4-dimensional system (order parameter and mean-field phase of each group) can then be reduced to a 3-dimensional system of the order parameters and the phase difference $\Theta = \Theta_1 - \Theta_2$ to

$$\begin{aligned}\dot{R}_1 =& -\gamma_1 R_1 + \frac{K}{2}(1-R_1^2)(R_1 - R_2\cos\Theta)\ ,\\ \dot{R}_2 =& -\gamma_2 R_2 + \frac{K}{2}(1-R_2^2)(R_2 - R_1\cos\Theta)\ ,\\ \dot{\Theta} =& -\bar{\omega}_2 + \frac{K}{2}\sin\Theta\frac{R_1^2(R_2^2+1)+R_2^2(R_1^2+1)}{R_1R_2}\ .\end{aligned} \tag{4.8}$$

Indicator oscillators can be used to study the system in the thermodynamic limit. They are coupled to the OA mean-fields from Eqs. (4.7) but do not create a mean-field themselves. From Eqs. (4.5), the same forcing acts on both groups, so their dynamics will be equal for the same ω_j up to the phase shift. The dynamics of a single indicator oscillator depends only on the oscillator's frequency, not on the group it belongs to. To discern the phases of indicator oscillators, they are marked as θ'_j with their natural frequencies ω'_j. They follow the equations (we choose to consider them as part of group 2)

$$\dot{\theta}'_j = \omega'_j - KR_1\sin(\Theta_1 - \theta'_j) + KR_2\sin(\Theta_2 - \theta'_j)\ . \tag{4.9}$$

The $R_{1,2}$ and $\Theta_{1,2}$ are calculated from Eq. (4.7), and the ω' are chosen uniformly. This method makes it possible to calculate the observed frequencies $\dot{\theta}'$ and the phase distribution in the thermodynamic limit numerically.

4.2.2 Small Coupling Strength

In the Kuramoto model, i.e., Eq. (2.51) with $M = 1$, the critical coupling K_c for the emergence of a nonzero order parameter and the function $\hat{R}(\hat{K})$ in the case of a Lorentzian distribution of the phases are Eqs. (2.26) and (2.27). The hat notation ,$\hat{K}$, marks the quantities of the Kuramoto model.

In the considered model with $M = 2$, if both groups are identical, then the critical coupling strength of each group corresponds to the Kuramoto model's one [22]. To compare the nontrivial order parameter between the Kuramoto model in Eq. (2.27) and the model with attractive and repulsive interactions in Eq. (4.6), the coupling constants have to be scaled, as $K_{\sigma\sigma'} = 2K$ was chosen and in the case of the Kuramoto model $K_{\sigma\sigma'} = \hat{K}$, so $\hat{K} = 2K$. A comparable critical coupling K_c for the $M = 2$ model would then correspond to $K_c = 2\gamma = 4\hat{\gamma}$, i.e., $\gamma = 2\hat{\gamma}$. The order parameter will have the same form, as K_c/K from Eq. (2.27) only depends on K_c.

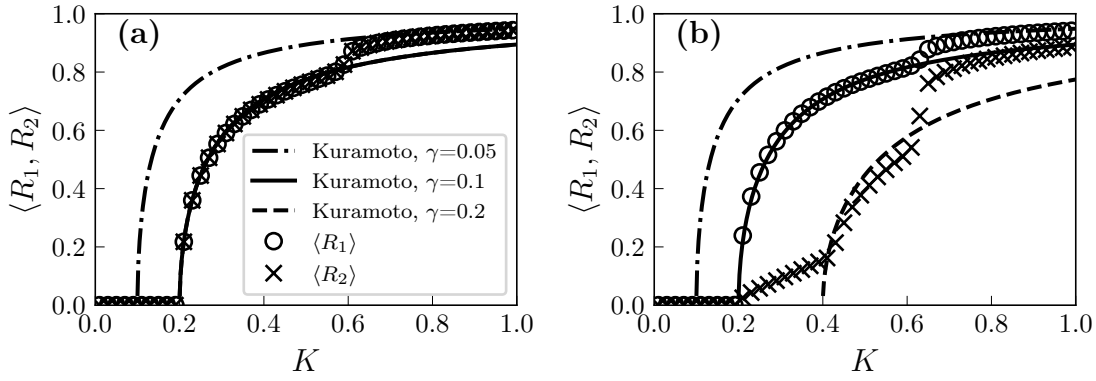

FIGURE 4.2: Average order parameters of group 1 $\langle R_1 \rangle$ as circles and group 2 $\langle R_2 \rangle$ as crosses. The solid (dashed, dash-dotted) black line shows the average order parameter in a Kuramoto model with $\gamma = 0.1$ ($\gamma = 0.2$, $\gamma = 0.05$). In (a) $\gamma_2 = 0.1$, so both distributions have the same width but different centers, and in (b) $\gamma_2 = 0.2$. The width is $\bar{\omega}_2 = 1$ in both cases.

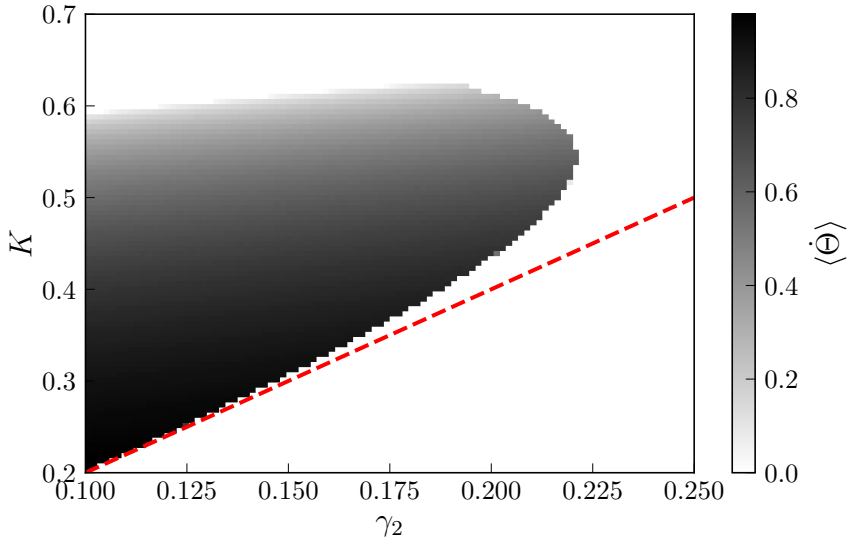

FIGURE 4.3: The difference in average frequencies of the mean fields $\langle \dot{\Theta} \rangle$ for $\bar{\omega}_2 = 1$. The red dashed line is the critical coupling of a Kuramoto model with the same width of the frequency distribution $\hat{\gamma} = \gamma$ as the second group in Eq. (2.26). The critical coupling for group 1 is $K = 0.2$, below this the system is incoherent ($R_1 = R_2 = 0$). For any scaling of $\bar{\omega}_2$, this image looks identical, if K and γ_2 scaled with the same factor (only the absolute values of the frequency difference change).

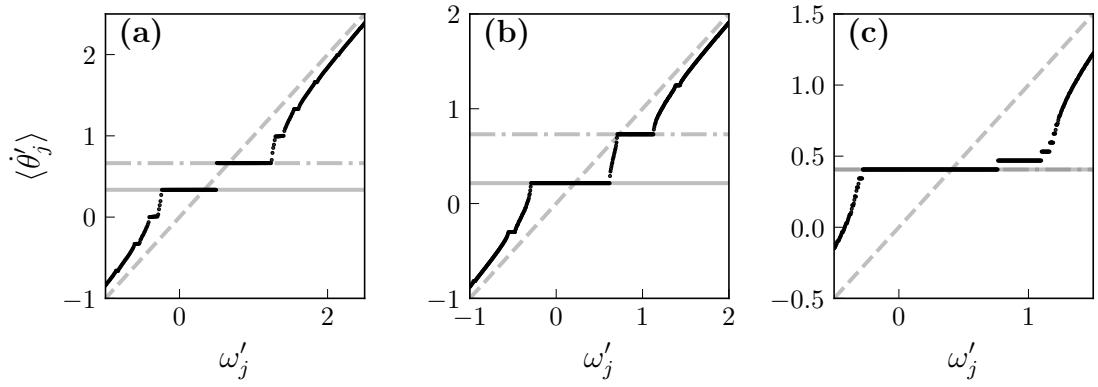

FIGURE 4.4: The average observed frequencies of indicator oscillators from Eqs. (4.7) and (4.9). The solid (dash-dotted) gray line marks the average mean field frequency $\langle\dot{\Theta}_1\rangle$ ($\langle\dot{\Theta}_2\rangle$) and the dashed gray line the identity function $\langle\dot{\theta}'_j\rangle = \omega'_j$. For all three subfigures $\bar{\omega}_2 = 1$. In (a) $\gamma_2 = 0.1$, $K = 0.56$ and identical order parameters $R_1 = R_2$, in (b) $\gamma_2 = 0.2$, $K = 0.56$ and $R_1 \neq R_2$, and in (c) $\gamma = 0.2$, $K = 0.63$ and $R_1 \neq R_2$ but the mean field frequencies are entrained.

For small coupling strength, both groups are incoherent. In Fig. 4.2, it is shown that the critical coupling strength for the first group corresponds to $K_{c,1} = 0.2$, the same as in a Kuramoto model with $\hat{\gamma}_1 = \gamma_1 = 0.1$, not the expected $\hat{\gamma}_1 = \gamma_1/2$. The effective coupling strength is only half as strong as in the Kuramoto model. For $K \lessapprox 0.6$, the first group follows the relation in Eq. (2.27) with $K_{c,1} = 0.2$ very well, regardless of γ_2, as can be observed from Fig. 4.2(a) and (b), when γ_2 changes from 0.1 to 0.2. The second group behaves somewhat differently. Its critical coupling follows a perturbed form of $K_{c,2} = 2\gamma_2$, half as strong as in the Kuramoto model. For $K_{c,1} < K \lessapprox K_{c,2}$ this group is not incoherent but becomes forced by group 1, as shown in Fig. 4.2(b).

Similar to the Kuramoto model, there exists a cluster of averagely entrained oscillators, centered around $\omega_j = 0$ [1] with a small shift in the direction of $\bar{\omega}_2$. They are entrained to the mean-field of group 1, and, as before, the observed frequency only depends on the oscillator's natural frequency ω_j, not on the group it belongs to [2]. The difference in the groups' mean-field frequencies can be seen in Fig. 4.3. The mean-fields are entrained in their average and instantaneous frequency since group 1 forces the, not yet self-synchronized, group 2.

4.2.3 Moderate Coupling Strength

With the increase of the coupling strength to $K > K_{c,2}$, new clusters begin to form. These new clusters lead to a stronger synchronization of group 2, and its order parameter better follows the relation Eq. (2.27) but is smaller than expected, as group 1 perturbs it. The clusters are coherent regions in ω with

[1] The center of group 1.

[2] Oscillators of group 2 are shifted by π in reference to oscillators of group 1 in this case.

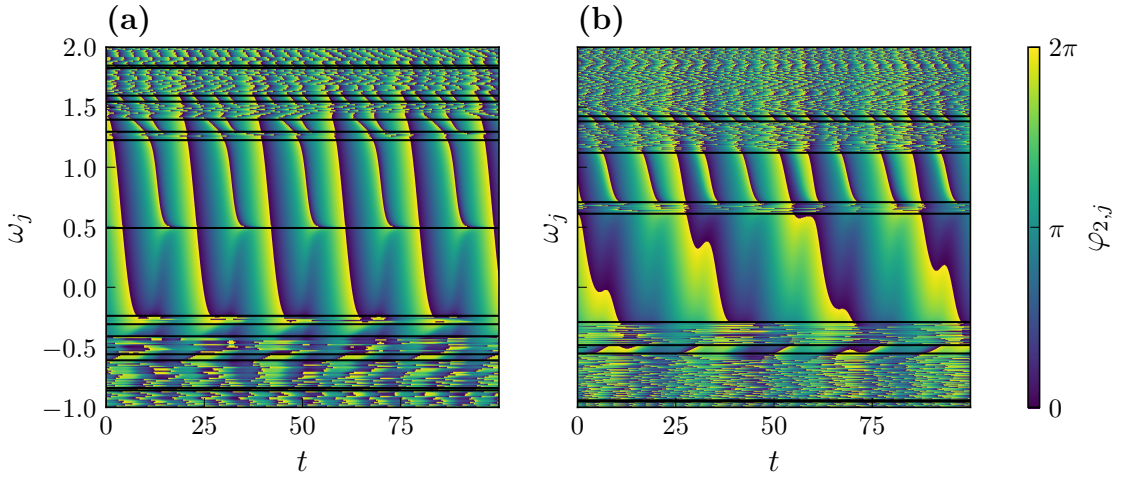

FIGURE 4.5: The phases of the indicator oscillators. Approximate cluster borders are marked with black lines. The parameters of (a) and (b) are the same as in Fig. 4.4 (a) and (b).

a common average frequency, as shown in Fig. 4.4. Oscillators between the clusters behave quasiperiodically. The entrained clusters decrease in size the further they are from the mean of the two distributions $\bar{\omega}_2/2$ [3], and the two biggest clusters lock to the average frequency of the mean fields (if they are non-entrained). In the case of non-entrainment of the mean-fields, the clusters have an average frequency of uneven multiples of the difference in average mean-field frequencies $\Delta\Omega = \langle\dot{\Theta}\rangle/2$ centered around their average mean $\Omega_0 = (\langle\Theta_1\rangle + \langle\Theta_2\rangle)/2$, i.e., the frequencies of the clusters Ω_j are

$$\Omega_{\pm(2n+1)} = \Omega_0 \pm (2n+1)\Delta\Omega \,. \tag{4.10}$$

The center frequency Ω_0 is not constant but changes with the coupling strength K and γ_2.

The transition between the clusters with Ω_{-1} and Ω_1 depends on γ_2. If both widths $\gamma_1 = \gamma_2$ are identical, then there is a sudden transition between the states (Fig. 4.4(a)) while for $\gamma_1 \neq \gamma_2$ the transition is smooth(Fig. 4.4(b)). A similar state has also been observed in Ref. [14] for a system of attractive and repulsive oscillators with frequency distributions of common width but different means. The dynamics observed here differ from both, as Ref. [26] only considers a conformists-contrarian model and finds only a case similar to the one depicted in Fig.4.4(a). The difference to Ref. [14] lies in the perfect overlap of the average frequencies of oscillators with the same ω_j, regardless of their group and the different width of the frequency distributions.

The clusters are stable in time, as seen in Fig. 4.5. While the clusters are fully entrained, they do not share a common phase. The difference in frequency can be seen very well by the additional rotation in the cluster with Ω_1 in reference to Ω_{-1}. Again, there is a difference in the case of $\gamma_1 \neq \gamma_2$, where the dynamics have a more complicated phase dynamic.

[3] Note that $\bar{\omega}_1$ has been chosen to be 0.

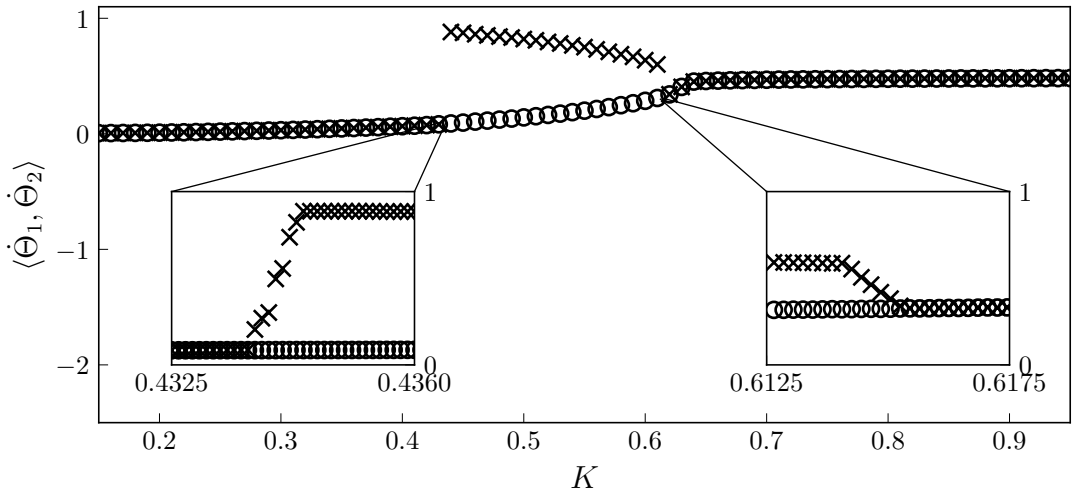

FIGURE 4.6: The average frequencies of the mean fields $\langle\dot{\Theta}_1\rangle$ (circles) and $\langle\dot{\Theta}_2\rangle$ (crosses) for $\bar{\omega}_2 = 1$ and $\gamma_2 = 0.2$. The inset figures show the transition from entrainment to non-entrainment and vice versa. Because the frequency has some very big peaks during the transition, all numerical values with $\left|\dot{\Theta}_2\right| > 100$ were removed to smoothen the transition.

The Bellerophon state comes into existence before the mean fields lose their entrainment, but after $K_{c,2}$. The clusters lead to the fast transition between entrainment and non-entrainment of the mean-fields in Fig. 4.6. In the case of $\gamma_1 = \gamma_2$, the forcing H has a unique role. Its average frequency $\langle\dot{\Psi}\rangle$ lies precisely between the clusters at Ω_0. For $\gamma_1 \neq \gamma_2$ this is not the case, as $\langle\dot{\Psi}\rangle = \langle\dot{\Theta}_1\rangle = \Omega_0 - \Delta\Omega$. The increase of the difference in K and $K_{c,2}$ for non-entrainment with γ_2 is shown in Fig. 4.3.

4.2.4 Strong Coupling Strength

For strong coupling strength of $K \approx 0.6$, the mean-fields entrain again. The clusters from the Bellerophon state persist but begin to shrink and approach a single big cluster, as shown in Fig. 4.4(c). The mean-fields are perfectly entrained, not just in their average frequency, and shifted by about π. As soon as both mean-fields entrain, the mean-field of group 2 adds a constant repulsive forcing to the oscillators of group 1, which increases their coherence and leads to a higher order parameter. In the case of a phase shift of π, both terms in the forcing in Eq. (4.4) would be identical, and the oscillators are forced by $2K$, and resemble a Kuramoto model with $\hat{K} = 2K$ (or a Kuramoto model with $\hat{K} = K$ and $\gamma_1 = 2\hat{\gamma}_1$), as expected. The same effect also happens for group 2. The phase shift between the two mean-fields is not π, so repulsion of the two groups is not perfect, and the average order parameter only approaches the Kuramoto model order parameter asymptotically. The closeness to the Kuramoto model's order parameter depends on the difference in the width γ_1 and γ_2. The closer

they are (as in Fig. 4.2(a)), the better the approximation will be, and the closer the phase shift will be to π for an equal K.

During the transition from non-entrainment to entrainment, the average mean-field frequency of group 2 quickly drops, while the cluster with Ω_1 persists and changes its position only slightly. This is a rather remarkable observation as there no longer exists a second-mean field frequency to entrain to. Instead, it shows that the middle-frequency Ω_0 and the step-like clusters are an intrinsic property of the system that is not simply generated from the interaction of the mean fields. Ω_0 is also different from the middle of the two frequency distributions and depends explicitly on the coupling strength. After a further increase in K, the distance between the clusters reduces even further in Fig. 4.4(c). With an increase in K, the distance in ω_j between the clusters decreases, and the jump between Ω_1 and Ω_3 becomes discontinuous. A further increase in the coupling strength finally asymptotically yields one entrained subpopulation, like expected in the Kuramoto model for nonidentical oscillators. This again verifies the connection between the M-Kuramoto model and the Kuramoto model already seen in the order parameters.

4.2.5 Numerical Realization

The Bellerophon state can be observed numerically for moderately big systems of the size of, e.g., 800 or 1000 oscillators. Their mean-field dynamics and their average frequencies fit very well to the predictions of the OA theory. In a few cases, a significant difference can be observed for non-entrained mean-fields[4]. One such case is shown in Fig. 4.7. While the initial phase distribution is of not much importance, the sampling of the frequencies is. In the shown case, the frequencies of group 2 were oversampled close to Ω_3, and group 1 was undersampled in Ω_1. This undersampling leads to a weaker order parameter R_1 [5], which disturbs the oscillators that would normally form the cluster Ω_3 in Fig. 4.7(b). This, in turn, leads to a significantly weaker order parameter $R_2 \approx 0.22$ compared to the OA solution with $R_2 \approx 0.36$.

4.3 Summary & Conclusion

The Bellerophon state is an interesting state in systems with multiple coupling strengths. Oscillators cluster in their average frequencies to odd multiples of a fundamental frequency. Between the clusters exist quasiperiodicity. Oscillators in each cluster only share their average frequency, not their instantaneous one. In a very simple model of two groups of Kuramoto oscillators with independent frequency distributions, attractive coupling between oscillators of the same group, and repulsive coupling between oscillator of different groups, the Bellerophon state plays an important part in the synchronization.

For small coupling strength, the dynamics resemble a Kuramoto model with a wider frequency distribution. With an increase in the coupling strength, the

[4] 1 case of about 100 observed systems with non-entrained frequencies

[5] The clusters are the main contributor to the order parameter

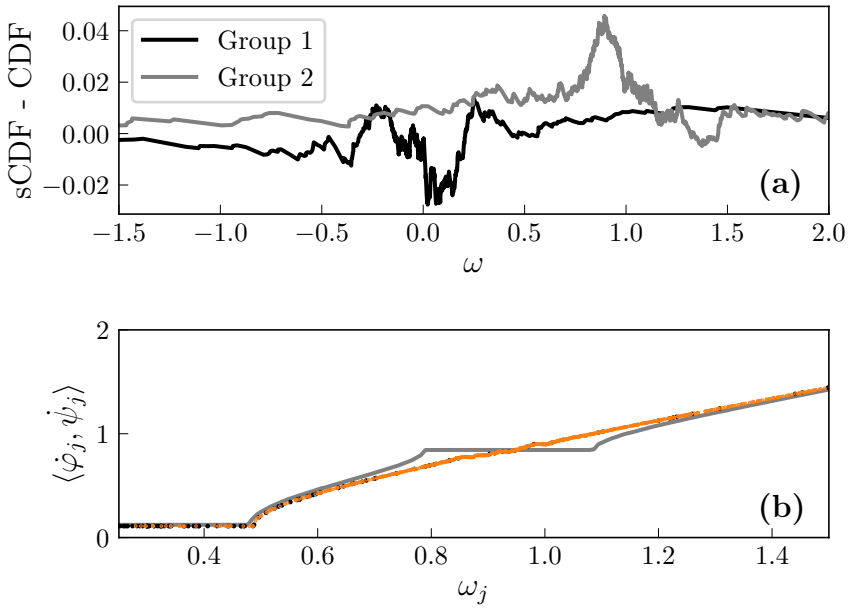

FIGURE 4.7: Numerical sampling leads to instabilities of the frequency distribution. This system uses the same parameters $\bar{\omega}_2 = 1$, $\gamma_2 = 0.2$ and a similar coupling of $K = 0.48$ to Fig. 4.4(b) and Fig. 4.6 with $N_1 = N_2 = 1000$. In (a), the difference between the sampled cumulative distribution function (sCDF) of ω_1 and ω_2 and the cumulative distribution function (CDF) of the corresponding Lorentz distribution in Eq. (2.25) is shown. In (b), the average frequencies are compared to the OA solution (gray line). Group 1 is shown as black circles, and group 2 as orange dots.

system transitions into the Bellerophon state. There the dynamics start to deviate from the Kuramoto model and are sensitive to noise in the frequency distribution. A further increase of the coupling strength leads to a strong increase in the synchronization. The synchronization is better described by a Kuramoto model with an equal frequency distribution, although the solution converges only asymptotically. These are not analytical results, but finding these may be an interesting topic research.

The results show how the consideration of both attractive and repulsive coupling in such a simple system as the Kuramoto model already yields rich dynamics.

Chapter 5

The Solitary State

This chapter contains the results from the paper "Solitary States and Partial Synchrony in Oscillatory Ensembles with Attractive and Repulsive Interactions" by Teichmann and Rosenblum. It was published 2019 in Chaos 29, 093124 [51] and has been chosen as a Featured Article.

5.1 Identical M-Kuramoto Model

Consider a simple model of oscillators, where there are two populations, one repulsive and one attractive. In the weak coupling limit, they are reduced to a two group Kuramoto model like in Eq. (2.51). Maistrenko et al. considered such a system in Ref. [24], where they made some simplifications. First of all, all oscillators are identical, i.e., they have equal natural frequencies $\omega_{\sigma,j} = \omega$, which disappears in a corotating reference frame. Further, they only considered forces, where the coupling and phase shift depend on the oscillators they are acting on, in other words, $K_{\sigma\sigma'} = K_{\sigma'}$ and $\alpha_{\sigma\sigma'} = \alpha_{\sigma'}$. With an appropriate time scale, the attractive interaction can be set to one, $K_1 = 1$, and then a new quantity e, the excess of repulsive coupling, is defined via $K_2 = -(1+\varepsilon)$. After these transformations, the ODEs for the oscillators of the attractive group φ and the repulsive group ψ are

$$\begin{aligned}\dot{\varphi}_j =& \frac{1}{N}\sum_{k=1}^{N_a}\sin(\varphi_k - \varphi_j + \alpha) - \frac{1+\varepsilon}{N}\sum_{k=1}^{N_r}\sin(\psi_k - \varphi_j + \beta)\ ,\\ \dot{\psi}_j =& \frac{1}{N}\sum_{k=1}^{N_a}\sin(\varphi_k - \psi_j + \alpha) - \frac{1+\varepsilon}{N}\sum_{k=1}^{N_r}\sin(\psi_k - \psi_j + \beta)\ ,\end{aligned} \tag{5.1}$$

here the phase shifts were renamed to $\alpha_1 = \alpha$, and $\alpha_2 = \beta$, as well as the number of oscillators in each group $N_1 = N_a$, and $N_2 = N_r$.

The forcing from Eq. (2.53) can be used, which yields

$$H = he^{i\Phi} = \frac{N_a}{N}e^{i\alpha}Z_a - \frac{N_r}{N}(1+\varepsilon)e^{i\beta}Z_r\ , \tag{5.2}$$

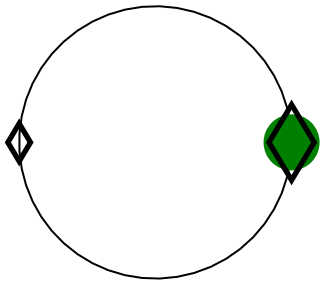

FIGURE 5.1: The solitary state, as found in Ref. [24]. The big diamond represents the $N_r - 1$ repulsive cluster, the circle the N_a attractive cluster and the small diamond the solitary repulsive oscillator.

where Z_a and Z_r are the mean-fields of the attractive and repulsive group. This reduces the dynamics to

$$\begin{aligned} \dot{\varphi}_j &= \mathrm{Im}\left[He^{-i\varphi_j}\right] = h\sin(\Phi - \varphi_j)\ , \\ \dot{\psi}_j &= \mathrm{Im}\left[He^{-i\psi_j}\right] = h\sin(\Phi - \psi_j)\ . \end{aligned} \tag{5.3}$$

All stationary states necessarily fulfill $h = 0$ and from Eq. (5.2) it follows that

$$R_1 = R_2(1 + \varepsilon)\ . \tag{5.4}$$

In this system, Maitrenko et al. found multiple partial synchronous states, including the solitary state. The solitary state is a two cluster state, as shown in Fig. 5.1. The first cluster consists of all attractive oscillators and all but one repulsive oscillators. The leftover repulsive oscillator is phase shifted to the cluster by π, hence solitary. This state is a realization of the Watanabe-Strogatz theory in Eq. (2.37), where $|z| = 1$, but with one single oscillator having $\lambda_j - \chi = \pi$ (the λ_j is here the constant of motion from the WS theory). They also note that this is the only allowed cluster state, except for the fully synchronous state.

The solitary state can exist for

$$\varepsilon > \frac{N_a\cos(\alpha)}{N_r\cos(\beta)} - 1\ , \tag{5.5}$$

although the exact region of existence is determined by the total number of oscillators. In the case of $N_a = N_r$ and without phase shifts, $\alpha = \beta = 0$, the existence is given by

$$0 < \varepsilon < \frac{4}{N-4}\ . \tag{5.6}$$

It turns out that even in this region, the solitary state does not have full measure. The further away from $\varepsilon = 0$, the more probable it becomes that the forcing disappears, $h = 0$, which yields only fuzzy clusters. The region of existence scales as N^{-1}, i.e., it exists even in the thermodynamics limit, although the

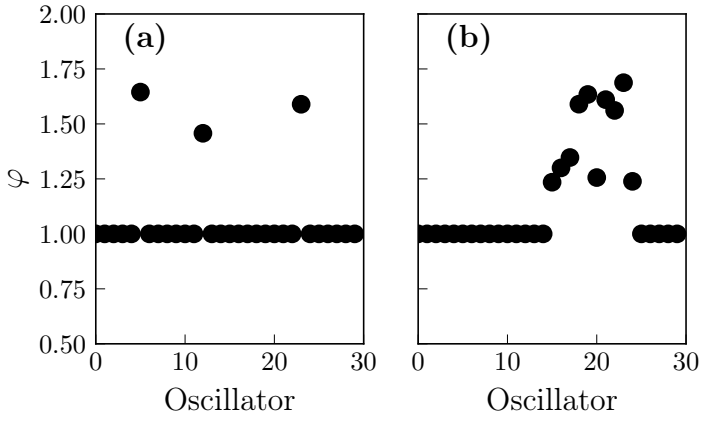

FIGURE 5.2: The difference between a solitary state (a) and a chimera state (b).

region of existence becomes very small.

While in the case of vanishing phase shifts, there exists a solitary state for all $N \geq 4$, in the more general case of nonvanishing phase shifts $\alpha, \beta \neq 0$, there is an upper limit for the number of oscillators to reach a solitary state. It becomes a low-dimensional phenomenon.

5.2 Solitary States in Other Systems

The solitary state is a rather newly observed phenomenon, so there are different definitions of the state. The strictest one is where one single oscillator exhibits different dynamics than all other oscillators. A more general, and more often observed, form resembles a chimera state. In a chimera state, there are some coherent subpopulations in the natural order of the system. For nonidentical oscillators, the order is determined by, e.g., their natural frequencies, while for identical ones, it would be the order in the phases. The solitary state exhibits different behavior for single oscillators, distributed over the whole population. The difference between the two is visualized in Fig. 5.2. In the following paragraphs about solitary states, the more general definition is used.

While most occurrences of the solitary state were found in numerical simulations, some physical experiments have resulted in the solitary state. In Ref. [87], 20 metronomes were coupled in a ring to their nearest and next-nearest neighbors. Depending on the initial conditions, the phases of the oscillator could be in a chimera state or a chimera state with some solitary oscillators. Using a one-dimensional array of magnetically coupled superconducting quantum interference devices in Ref. [75] also yielded a solitary state. Here the state was also dependent on the initial condition, and some yielded a solitary state for the phases. Because of the magnetic coupling, the interactions between oscillators were non-local, but they fell off quickly with the inverse cube of the distance.

The solitary state has been numerically found in multiple systems, such as nonlocally coupled Lorenz oscillators in Ref. [88]. While the Lorenz oscillator

has a strange attractor, there are also limit cycle oscillators that exhibit solitary states, such as a ring of coupled Stuart-Landau oscillators with symmetry breaking long-range attractive and repulsive coupling in Ref. [89]. Even in neurologically inspired multiplex networks of FitzHugh-Nagumo oscillators, there exists a solitary state — in Ref. [90], two coupled rings with a small mismatch in their intra-layer coupling solitary oscillators were observed.

There are only a few results about the emergence and stability of the solitary state, despite its multiple numerical observations. In another generalization of the Kuramoto model, a model with inertia has been investigated in Ref. [91]. There the solitary state appears in homoclinic bifurcation of a synchronized state. In comparison to the solitary state in the M-Kuramoto model, the region of existence becomes bigger with an increase in the system size. All of the considered systems are time continuous, but there are solitary states to be found even in coupled maps. Multiplex networks of nonlocally coupled maps with a singular hyperbolic attractor, such as the Lozi map, transition from coherence to incoherence via a solitary state [92,93]. The transition is characterized by more and more solitary oscillators appearing. The number of oscillators grows nearly linear with the decrease in the coupling strength, which is caused by the increase of the basin of attraction's size of the solitary set (of single oscillators). With increased size, it becomes more probable that initial conditions will lie inside it [94]. There is no solitary state in noiseless nonhyperbolic maps, although the addition of multiplicative noise of the coupling constant will lead to them [95].

5.3 M-Kuramoto Model with Identical Groups

In Ref. [51], we investigate an extended version of the original solitary state model Eq. (5.1) by Maistrenko et al. They assume the same dynamics for both populations, i.e., no frequency difference between the two groups. Motivated by a neurological model, we consider two groups with different dynamics [96]. In the brain, there are not only neurons, which interact electrically, but also glial cells. They influence surrounding neurons not by an electrical input but by changing the concentration of ions in the surrounding medium. Their interaction is purely chemical and some order of magnitude slower than the neurons' interactions. Adding this consideration leads to the model

$$\begin{aligned}\dot{\varphi}_j =& \frac{1}{N}\sum_{k=1}^{N_a}\sin(\varphi_k-\varphi_j+\alpha)-\frac{1+\varepsilon}{N}\sum_{k=1}^{N_r}\sin(\psi_k-\varphi_j+\beta)\,,\\ \dot{\psi}_j =& \omega+\frac{1}{N}\sum_{k=1}^{N_a}\sin(\varphi_k-\psi_j+\alpha)-\frac{1+\varepsilon}{N}\sum_{k=1}^{N_r}\sin(\psi_k-\psi_j+\beta)\,.\end{aligned} \tag{5.7}$$

Here ω is the frequency difference between the two, in themselves identical, groups. The reference frame is chosen so that the attractive group has no natural frequency. This additional parameter leaves the forcing in Eq. (5.2)

untouched, but changes the reduced form to

$$\begin{aligned}\dot{\varphi}_j =& \mathrm{Im}\left[He^{-i\varphi_j}\right] = h\sin(\Phi-\varphi_j)\ ,\\ \dot{\psi}_j =& \omega + \mathrm{Im}\left[He^{-i\psi_j}\right] = \omega + h\sin(\Phi-\psi_j)\ .\end{aligned} \tag{5.8}$$

The main interest of this investigation lies mainly in the solitary state, which is only a low-dimensional phenomenon in the system with a phase shift (as shown by Maistrenko et al.), so no phase shift is considered $\alpha = \beta = 0$ here, and $N_a = N_r = N/2$. These constraints simplify the forcing H to

$$H = he^{i\Phi} = \frac{1}{2}[Z_a - (1+\varepsilon)Z_r]\ . \tag{5.9}$$

In difference to the model without frequency difference, the WS theory can only be applied to each group separately, see Ref. [68]. Each group then has $N/2-3$ constants of motion and the full system is 6-dimensional, consisting of two coupled systems of WS equations.

5.3.1 Synchronous State

The simplest observable state is the synchronous state, where both groups fully synchronize. This state is trivially reached for $\varepsilon < -1$, as both groups are attractively coupled. For $\varepsilon > -1$, we define the fully synchronous state as a two cluster state, where $\varphi_j = \varphi$ and $\psi_j = \psi$ for all j. Note that this state does not need to be stationary, but only entrained $\dot{\varphi} = \dot{\psi} = \nu$ with the observed frequency ν. Both groups are fully synchronized and have a constant phase shift, i.e., $\varphi = \nu t$ and $\psi = \nu t + \psi_0$, so also the forcing has the same observed frequency ν as the oscillators, $\Phi = \nu t + \Phi_0$. Writing the real and imaginary part of Eq. (5.9), we obtain

$$\begin{aligned}h\cos(\Phi_0) =& \frac{1}{2} - \frac{1+\varepsilon}{2}\cos(\psi_0)\ ,\\ h\sin(\Phi_0) =& -\frac{1+\varepsilon}{2}\sin(\psi_0)\ .\end{aligned} \tag{5.10}$$

Condition of Existence Subtracting the two parts of Eq. (5.9) yields

$$\omega = h[\sin(\Phi_0) - \sin(\Phi_0 - \psi_0)]\ . \tag{5.11}$$

Expanding the second term to $\sin(\Phi_0)\cos(\psi_0) - \cos(\Phi_0)\sin(\psi_0)$ and replacing $h\sin(\Phi_0)$ and $h\cos(\Phi_0)$ with Eq. (5.10) results in

$$\sin(\psi_0) = -\frac{2\omega}{\varepsilon}\ . \tag{5.12}$$

Clearly, there can be no synchrony for $\varepsilon = 0$. For $\varepsilon > 0$ the repulsion will be stronger than the attraction and an increase in repulsion can not lead to a stronger synchronization, so there will be no synchronous state for $\varepsilon > 0$. For

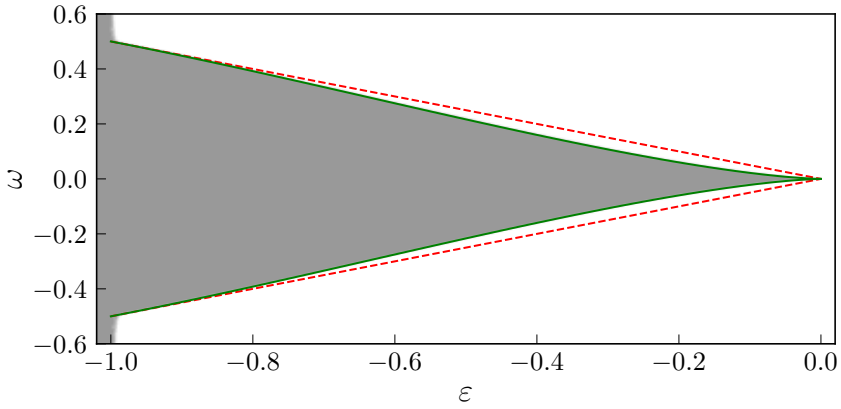

FIGURE 5.3: Full synchrony for the Eq. (5.7). The region of numerical observation of the state is shaded gray, while all other states are white. The dashed red line shows the calculated region of existence in Eq. (5.13), and the solid green line the analytical boundary for the stability in Eq. (5.21).

$\varepsilon < 0$ the region of existence is given by

$$|\omega| \leq -\frac{\varepsilon}{2} \,. \tag{5.13}$$

The observed frequency ν can be calculated by using the second part of Eq. (5.8), Eq. (5.10), and Eq. (5.12)

$$\begin{aligned}
\nu =& \omega + h\sin(\Phi_0 - \psi_0) \\
=& \omega + h\sin(\Phi_0)\cos(\psi_0) - h\cos(\Phi_0)\sin(\psi_0) \\
=& \omega - \frac{1+\varepsilon}{2}\sin(\psi_0)\cos(\psi_0) - \left[\frac{1}{2} - \frac{1+\varepsilon}{2}\sin(\psi_0)\right]\sin(\psi_0) \\
=& \omega - \frac{1}{2}\sin(\psi_0) \\
=& \omega + \frac{1}{2}\frac{2\omega}{\varepsilon} \,,
\end{aligned}$$

to

$$\nu = \frac{1+\varepsilon}{\varepsilon}\omega \,. \tag{5.14}$$

Since $-1 < \varepsilon < 0$, the observed frequency will have a different sign than ω. In this regime, the attraction of the first group is stronger than the second group, so it will dominate the dynamics and pull the system in the opposite direction to the repulsive group. Numerical observations in Fig. 5.3 show that the state is not observed in the whole region of existence.

Condition of Stability The clusters are perturbed to check the stability of the synchronous state. First, consider a symmetric perturbation of the repulsive cluster [74] as $\psi_\pm = \nu t + \psi_0 \pm \gamma$ with $\gamma \ll 1$. In this case, the mean-field Z_r

will not be changed in the first-order in γ. Stability is then determined by a decrease in $|\gamma|$ over time. The perturbed oscillators follow

$$\begin{aligned}\dot{\psi}_\pm =&\omega + h\sin(\Phi_0 - \psi_0 \mp \gamma) \,, &(5.15)\\ \nu \pm \dot{\gamma} =&\omega + h\sin(\Phi_0 - \psi_0)\cos(\gamma) \mp h\cos(\Phi_0 - \psi_0)\sin(\gamma)\\ =&\omega + h\sin(\Phi_0 - \psi_0) \mp h\cos(\Phi_0 - \psi_0)\gamma + \mathcal{O}(\gamma^2) \,. &(5.16)\end{aligned}$$

In the first-order in γ, the perturbation evolves with

$$\dot{\gamma} = -\gamma h\cos(\Phi_0 - \psi_0) \,. \tag{5.17}$$

The repulsive cluster is linearly stable for $h\cos(\Phi_0 - \psi_)) > 0$. Multiplying the first part of Eq. (5.10) with $\cos(\psi_0)$ and the second with $\sin(\psi_0)$ and adding the two yields

$$h\cos(\Phi_0 - \psi_0) = \frac{1}{2}\cos(\psi_0) - \frac{1+\varepsilon}{2} \,. \tag{5.18}$$

The condition Eq. (5.17) is then

$$\cos\psi_0 - (1+\varepsilon) > 0 \,. \tag{5.19}$$

The border of stability is, accordingly, $\cos\psi_0 = 1 + \varepsilon$. With Eq. (5.12) the border of stability for the repulsive group is

$$\begin{aligned}\cos^2\psi_0 + \sin^2\psi_0 =&(1+\varepsilon)^2 + \frac{4}{\varepsilon^2}\omega^2 \,, &(5.20)\\ 0 =&\omega^2 + \frac{\varepsilon^2(1+\varepsilon)^2}{4} - \frac{\varepsilon^2}{4} \,,\\ \omega =&\pm\sqrt{-\frac{\varepsilon^2 + 2\varepsilon^3 + \varepsilon^4}{4} + \frac{\varepsilon^2}{4}} \,,\\ \omega =&\pm\sqrt{-\frac{\varepsilon^3}{2} - \frac{\varepsilon^4}{4}} \,. &(5.21)\end{aligned}$$

The same approach applied to the attractive group gives its region of stability as

$$\cos\psi_0 < \frac{1}{1+\varepsilon} \,. \tag{5.22}$$

This condition is always fulfilled, as $\varepsilon < 0$ in the region of existence.

The last mode to consider is the phase shift between the clusters. Rewriting Eq. (5.7) for the synchronous case gives

$$\begin{aligned}\dot{\varphi} =&-\frac{1+\varepsilon}{2}\sin(\psi - \varphi) \,,\\ \dot{\psi} =&\omega + \frac{1}{2}\sin(\varphi - \psi) \,.\end{aligned} \tag{5.23}$$

With $\eta = \psi - \varphi$ this is

$$\dot{\eta} = \omega + \frac{\varepsilon}{2}\sin\eta \,, \tag{5.24}$$

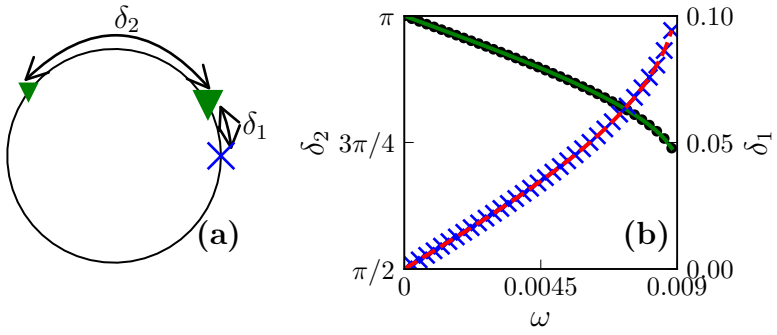

FIGURE 5.4: In (a), an illustration of the solitary state is shown. The blue crosses denote the attractive cluster, and the big (small) green triangles the repulsive cluster (solitary oscillator). The phase shifts for δ_1 and δ_2 are shown in (b), for a system of $N_a = N_r = 5$ and $\varepsilon = 0.212$. The blue crosses (black dots) mark the numerical observations for δ_1 (δ_2), and the red dashed line and the green solid line the analytical results from Eq. (5.35).

which is just a special case of the Adler equation Eq. (2.21). There exists a stable fixed point for $|\omega| < -\varepsilon/2$, so in the whole region of existence.

Thus, the final border of stability is given by the stability of the repulsive cluster in Eq. (5.21). This fits very well to the numerically observed region of stability in Fig. 5.3.

5.3.2 Solitary State

The main interest in researching this system lies in the solitary state. Like the solitary state found by Maistrenko et al., it is a rotating three cluster state, but the phase shifts between the clusters depend on the frequency difference ω. It can be written similarly to the synchronous state as $\varphi = \nu t$, $\psi_{1,\dots,N_r-1} = \nu t + \delta_1$, $\psi_{N_r} = \nu t + \delta_1 + \delta_2$, and $\Phi = \nu_t + \Phi_0$. This state is illustrated in Fig. 5.4(a).

Condition of Existence Inserting these conditions in Eqs. (5.8) and (5.9) yields

$$he^{i\Phi_0} = \frac{1}{2} - \frac{1+\varepsilon}{2N_r}\left[(N_r-1)e^{i\delta_1} + e^{i(\delta_1+\delta_2)}\right] , \tag{5.25}$$

$$\nu = h\mathrm{Im}\left[e^{i\Phi_0}\right] , \tag{5.26}$$

$$\nu = \omega + h\mathrm{Im}\left[e^{i(\Phi_0-\delta_1)}\right] , \tag{5.27}$$

$$\nu = \omega + h\mathrm{Im}\left[e^{i(\Phi_0-\delta_1-\delta_2)}\right] . \tag{5.28}$$

From the last two equations, it follows that $\mathrm{Im}\left[e^{i(\Phi_0-\delta_1)}\right] = \mathrm{Im}\left[e^{i(\Phi_0-\delta_1-\delta_2)}\right]$ and (assuming δ_2 is between 0 and 2π) $\mathrm{Re}\left[e^{i(\Phi_0-\delta_1)}\right] = -\mathrm{Re}\left[e^{i(\Phi_0-\delta_1-\delta_2)}\right]$. From there the phase shifts are connected via $2\delta_1 + \delta_2 = 2\Phi_0 - \pi$. Multiplying Eq. (5.25) with $e^{-i\Phi_0}$, taking the imaginary part and replacing $\Phi_0 - \delta_1 - \delta_2 =$

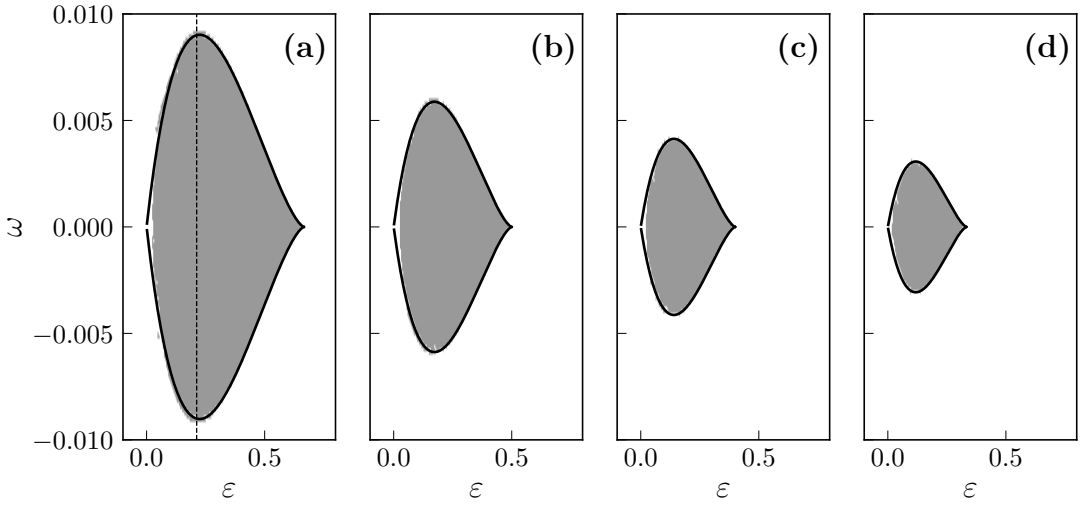

FIGURE 5.5: The solitary state for different system sizes $N_a = N_r = 5, 6, 7, 8$ from left to right. The solitary state is observed numerically in the gray region, while all other states are white. The analytical region of existence, as a solution of Eq. (5.33) is shown by the black line. The dashed black line marks the approximate maximal width in ω for $N_a = N_r = 5$ at about $\varepsilon = 0.212$

$-(\Phi_0 - \delta_1) + \pi$ gives

$$\begin{aligned} 0 =& \frac{1}{2}\mathrm{Im}\left[e^{-i\Phi_0}\right] - \frac{1+\varepsilon}{2N_r}\left[(N_r-1)\mathrm{Im}\left[e^{-i(\Phi_0-\delta_1)}\right] + \mathrm{Im}\left[e^{-i(\Phi_0-\delta_1-\delta_2)}\right]\right] \\ =& \frac{1}{2}\mathrm{Im}\left[e^{-i\Phi_0}\right] - \frac{1+\varepsilon}{2N_r}\left[(N_r-1)\mathrm{Im}\left[e^{-i(\Phi_0-\delta_1)}\right] + \mathrm{Im}\left[e^{-i(\Phi_0-\delta_1)}\right]\right] . \end{aligned}$$

And finally

$$\mathrm{Im}\left[e^{-i(\Phi_0-\delta_1)}\right] = \frac{1}{1+\varepsilon}\mathrm{Im}\left[e^{i\Phi_0}\right] . \tag{5.29}$$

Using this relation and Eqs. (5.26) and (5.27) allows for the calculation of the observed frequency ν. It follows the same relation as for the synchronous state in Eq. (5.14) but now $\varepsilon > 0$, so ν is positive, and the state rotates in the same direction as ω. Multiplying Eq. (5.25) next by $e^{-i\Phi_0}$, taking the real part and making the same phase replacements

$$\begin{aligned} h =& \frac{1}{2}\mathrm{Re}\left[e^{-i\Phi_0}\right] - \frac{1+\varepsilon}{2N_r}\left[(N_r-1)\mathrm{Re}\left[e^{-i(\Phi_0-\delta_1)}\right] + \mathrm{Re}\left[e^{-i(\Phi_0-\delta_1-\delta_2)}\right]\right] \\ =& \frac{1}{2}\mathrm{Re}\left[e^{-i\Phi_0}\right] - \frac{1+\varepsilon}{2N_r}\left[(N_r-1)\mathrm{Re}\left[e^{-i(\Phi_0-\delta_1)}\right] - \mathrm{Re}\left[e^{-i(\Phi_0-\delta_1)}\right]\right] \\ =& \frac{1}{2}\mathrm{Re}\left[e^{i\Phi_0}\right] - (1+\varepsilon)\frac{N_r-2}{2N_r}\mathrm{Re}\left[e^{i(\Phi_0-\delta_1)}\right] . \end{aligned}$$

Finally, replacing $\mathrm{Re}\left[e^{i\Phi_0}\right] = \sqrt{1 - \mathrm{Im}\left[e^{i\Phi_0}\right]^2}$

$$\begin{aligned} h =& \frac{1}{2}\sqrt{1 - \mathrm{Im}\left[e^{i\Phi_0}\right]^2} - (1+\varepsilon)\frac{N_r - 2}{2N_r}\sqrt{1 - \mathrm{Im}\left[e^{i(\Phi_0 - \delta_1)}\right]^2} \\ =& \frac{1}{2}\sqrt{1 - \mathrm{Im}\left[e^{i\Phi_0}\right]^2} - (1+\varepsilon)\frac{N_r - 2}{2N_r}\sqrt{1 - \frac{1}{(1+\varepsilon)^2}\mathrm{Im}\left[e^{i\Phi_0}\right]^2}\,, \end{aligned}$$

and moving $(1+\varepsilon)$ into the root

$$h = \frac{1}{2}\sqrt{1 - \mathrm{Im}\left[e^{i\Phi_0}\right]^2} - \frac{N_r - 2}{2N_r}\sqrt{(1+\varepsilon)^2 - \mathrm{Im}\left[e^{i\Phi_0}\right]^2}\,. \tag{5.30}$$

Replacing h with Eq. (5.25), the observed frequency with Eq. (5.14), and substituting $x = \mathrm{Im}\left[e^{i\Phi_0}\right]$ leads to

$$0 = x\sqrt{1 - x^2} - \frac{N_r - 2}{N_r}x\sqrt{(1+\varepsilon)^2 - x^2} - 2\frac{1+\varepsilon}{\varepsilon}\omega\,. \tag{5.31}$$

Finding the solitary state's region of existence is reduced to finding the range of ω so that this equation can be fulfilled for a given ε. First, it is important to note that Eq. (5.31) is invariant to the transformation $x \to -x$ and $\omega \to -\omega$. One branch is given by $x \in (0, 1]$, and the other, symmetric, branch can be inferred by $\omega \to -\omega$. To find the solution, consider the function f of the first two terms of Eq. (5.31)

$$f(x, N_r, \varepsilon) = x\sqrt{1 - x^2} - \frac{N_r - 2}{N_r}x\sqrt{(1+\varepsilon)^2 - x^2}\,. \tag{5.32}$$

The border of the region of existence is then the biggest possible value of w, where f can fulfill Eq. (5.31), i.e., $\omega = \frac{\varepsilon}{2(1+\varepsilon)}f_{max}(x, N_r, \varepsilon)$ (f_{max} denotes the maximum of $f(x)$). The derivative has to be calculated to find the maximum $\partial f/\partial x = 0$, i.e.,

$$(1 - 2x^2)N_r\sqrt{(1+\varepsilon)^2 - x^2} = [(1+\varepsilon^2) - 2x^2](N_r - 2)\sqrt{1 - x^2}\,. \tag{5.33}$$

Squaring this equation and ordering by powers of x yields a cubic equation for x^2, which can be solved analytically. The expressions for the roots are quite long, but the calculated ω are shown in Fig. 5.5 and fit very well to the numerical observations. Just as in the system of Maistrenko et al., the size of the region depends on the system size N, where an increase in N leads to a smaller region of existence.

Phase Shifts To calculate the phase shifts δ_1 and δ_2, first the second equation of Eq. (5.7) needs to be rewritten in terms of the phase shifts for the solitary

oscillator and the repulsive cluster,

$$\begin{aligned}
\nu + \dot{\delta}_1 =& \omega + \frac{1}{2}\sin(-\delta_1) - \frac{1+\varepsilon}{N}\sin\delta_2 \ , \\
\nu + \dot{\delta}_1 + \dot{\delta}_2 =& \omega + \frac{1}{2}\sin(-\delta_1 - \delta_2) - \frac{1+\varepsilon}{N}(N_r - 1)\sin(-\delta_2) \ , \\
\dot{\delta}_2 =& \nu + \dot{\delta}_1 + \dot{\delta}_2 - \nu - \dot{\delta}_1 \\
=& -\frac{1}{2}\sin(\delta_1 + \delta_2) + \frac{(1+\varepsilon)(N_r - 1)}{N}\sin\delta_2 + \frac{1}{2}\sin\delta_1 + \frac{1+\varepsilon}{N}\sin\delta_2 \\
=& \frac{1}{2}\left[\sin\delta_2\left((1+\varepsilon) - \cos\delta_1\right) - \cos\delta_2\sin\delta_1 + \sin\delta_1\right] \ .
\end{aligned}$$

Rewriting this, similarly to Ref. [24], yields

$$\dot{\delta}_2 = A[\sin(\delta_2 - \delta_2^*) + \sin\delta_2^*] \ , \tag{5.34}$$

where $\tan\delta_2^* = \sin\delta_1/((1+\varepsilon) - \cos\delta_1)$ and $A = \sin\delta_1/(2\sin\delta_2^*)$. A stable state has either the solution $\delta_2 = 0$ or $\delta_2 = 2\delta_2^* + \pi$, with the first solution being the two-cluster state and the second solution being the solitary state. With the earlier relation of the phase shifts of $2\Phi_0 - \pi = 2\delta_1 + \delta_2$, it follows that $\Phi_0 = \delta_1 + \delta_2^*$. Using Eq. (5.29), the relation between δ_2^* and Φ_0 can be written as

$$\sin\delta_2^* = \frac{1}{1+\varepsilon}\sin\Phi_0, \tag{5.35}$$

which allows for the calculation of δ_2^* and δ_1 from Φ_0. The phase of the forcing Φ_0 can be calculated numerically from Eq. (5.31). The resulting phase shifts are plotted in Fig. 5.4 and coincide with the numerical observations.

Condition of Stability Using the same perturbation on the cluster as for the synchronous state

$$\dot{\delta}_{2,\pm} = \dot{\delta}_2 \pm \dot{\gamma} = A[\sin(\delta_2 - \delta_2^* \pm \gamma) + \sin\delta_2^*] \ . \tag{5.36}$$

In the first-order in γ, this yields $\dot{\gamma} = -A\cos\delta_2^*\gamma$ and the condition for the stability becomes $A\cos\delta_2^* > 0$. With the definition of A, this can be written as

$$\frac{\sin\delta_1}{2\tan\delta_2^*} > 0 \ . \tag{5.37}$$

Using then the definition of $\tan\delta_2^*$ the condition of stability for δ_2 becomes

$$1 + \varepsilon - \cos\delta_1 > 0 \ , \tag{5.38}$$

which is always fulfilled, since the solitary state exists for $\varepsilon > 0$. Finding the stability of δ_1 is not as simple, as the equation for $\dot{\delta}_1$ has the form

$$\dot{\delta}_1 = \sin\delta_1\left[-\frac{1}{2} + \frac{1+\varepsilon}{N}\left((N_r - 1) + \cos\delta_2\right)\right] + \cos\delta_1\frac{1+\varepsilon}{N}\sin_2 + \omega - \frac{1+\varepsilon}{N}\sin\delta_2$$

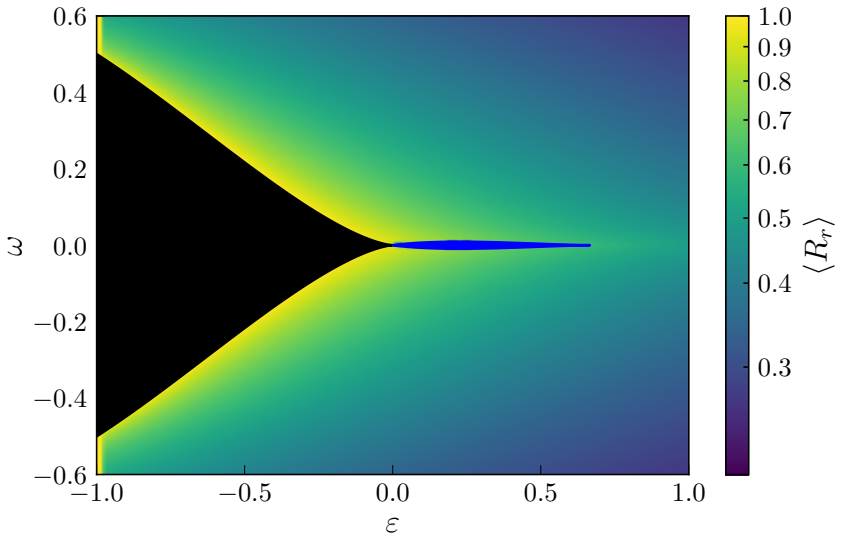

FIGURE 5.6: The average order parameter $\langle R_r \rangle$ as an overview of the states for $N_a = N_r = 5$. The black region shows the domain of full synchrnoy from Eq. (5.21). The blue region shows the domain of the solitary state as a solution of Eq. (5.31).

and cannot be reduced to the same form as in Eq. (5.34). Instead a direct substitution of $\delta_1 \pm \gamma$ yields in the first-order

$$\dot{\gamma} = \gamma \left[\cos\delta_1 \left(-\frac{1}{2} + \frac{1+\varepsilon}{N} \left((N_r - 1) + \cos\delta_2 \right) \right) - \sin\delta_1 \frac{1+\varepsilon}{N} \sin\delta_2 \right] . \quad (5.39)$$

Numerical evaluations of this equation using the computed values of δ_1 and δ_2 shows that δ_1 is also stable in the whole stability region of δ_2.

The biggest difference in the solitary state between this model and the model by Maistrenko et al. is in the basin of attraction. In the case of $\omega = 0$, the solitary state does not have full measure, as it allows states with $h = 0$. The numerical results for the state with $\omega \neq 0$ indicate that this is not possible here. The state with $h = 0$ and $R_a, R_r \neq 0$ is not a valid solution, as can be quickly checked by using Eq. (5.8), and numerical studies indicate that the asynchronous case $R_a = R_r = h = 0$ is unstable. Consequently, the solitary state is the only attractor in its region of existence.

One may assume that, aside from the fully synchronous and the solitary state, there may exist more clustered states, but this is forbidden by the WS theory [97], as already noted by Maistrenko et al.

5.3.3 Self-Consistent Partial Synchronization

Numerical Analysis

Outside of full synchrony and the solitary state, there exists a partial synchronous state, with $0 < R_r < 1$. Numerical studies indicate that the attractive

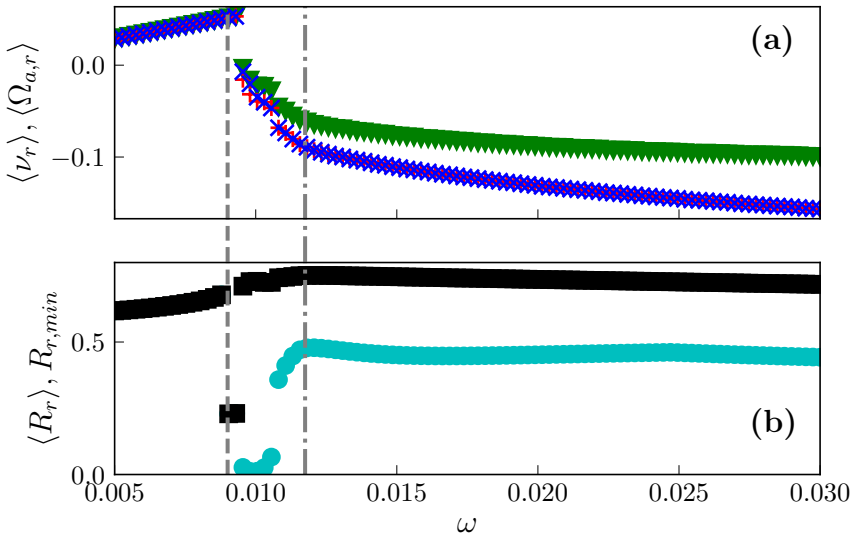

FIGURE 5.7: The average frequencies (a) and order parameters (b) at the border of the solitary state for $N_a = N_r = 5$ and $\varepsilon = 0.212$. The green triangles in (a) show the average frequency of the repulsive oscillators $\langle\nu_r\rangle$ and the blue crosses (red pluses) the average mean-field frequency $\langle\Omega_r\rangle$ ($\langle\Omega_a\rangle$). In (b), the average order parameter $\langle R_r\rangle$ is shown by black squares, and the minimum order parameter $R_{r,min} = \min_t R_r(t)$ by cyan circles. The dashed line marks the analytical boundary of the solitary state from Eq. (5.21). Left of it, all values coincide, while on the right of it, the minimum order parameter falls off quickly. Because of this, the phase is not well defined. This leads to some discrepancies between $\langle\Omega_r\rangle$ and $\langle\Omega_a\rangle$. The right border of this region is (arbitrarily) shown by a dashed-dotted line. On the right side of it, $\langle\Omega_r\rangle = \langle\Omega_a\rangle$.

group always fully synchronizes, regardless of ε. This has been tested for values up to $\varepsilon = 10$. Analytically, the stability of the attractive cluster can be extended from Eq. (5.22) in the case of full synchrony to a state with $R_r \leq 1$ as $R_r \cos(\Theta_r - \Theta_a) < (1+\varepsilon)^{-1}$. This expression cannot be treated analytically, as the dynamics of the mean-field are unknown. But the numerics indicates that this is always fulfilled. Even in the case of very weakly non-identical oscillators, sampled from a normal distribution with a standard deviation of 10^{-3}, the attractive group fully synchronizes. This is a very strong indication that the synchronization is not a numerical artifact. An overview of the average repulsive order parameter $\langle R_r\rangle$ can be found in Fig. 5.6, where the regions of stability of the solitary state and the fully synchronous state are marked separately.

The observed partial synchronous state can be seen as self-consistent partial synchrony, SCPS (or a self-organized quasiperiodic state, SOQ) [55,77,98]. This type of partial synchrony is characterized by a difference between the average frequency of the repulsive mean-field $\langle\Omega_r\rangle$ and the average frequency of the single oscillators $\langle\nu_r\rangle$. Numerically, not only the average frequencies but also

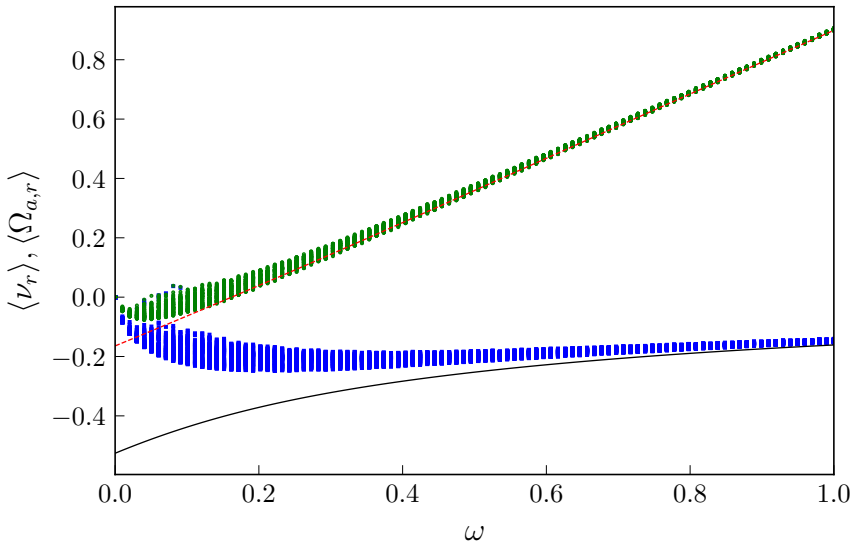

FIGURE 5.8: Observed frequencies for 100 random initial conditions per ω for $N_a = N_r = 5$ and $\varepsilon = 0.5$. The blue squares denote the average frequency of the repulsive mean-field $\langle \Omega_r \rangle$ and the green dots the average frequency of the oscillators $\langle \nu_r \rangle$. The dashed red line is the solution of Eq. (5.43), and the solid black line the solution of Eqs. (5.41) and (5.42).

the instantaneous frequencies differ nearly all the time. On the macroscopic scale, both mean-field frequencies coincide $\langle \Omega_a \rangle = \langle \Omega_r \rangle$ (see Fig. 5.7). This explains the difference between $\langle \Omega_r \rangle$ and $\langle \nu_r \rangle$, which increases with ω. Close to the border of the solitary state, the order parameter reaches values approaching 0. This leads to the frequencies not being well-defined in this region. The transient in the border region become very long, and the identification of the dynamical states there may be an interesting problem to solve in the future.

Similar results but for a wider range of ω are shown in Fig. 5.8. First of all, the increase in $\langle \Omega_r \rangle - \langle \nu_r \rangle$ with ω can be seen very clearly. But also the multistability of the system. In this figure, 100 different initial conditions are chosen per value of ω and, especially for small ω, lead to different average frequencies. The whole range of the SCPS is multistable, as can also be seen in Fig. 5.11. For all parameters and initial conditions, the mean fields of both populations remains synchronized, and their phases are well defined.

The observed frequency ν changes direction between the fully synchronous state and the solitary state. A similar change of the direction of rotation happens at the transition from the solitary state to the partial synchronous state. Before the transition, the observed frequency ν is positive, while immediately after the transition, all frequencies become negative, as can be seen in Fig. 5.7. With a bigger ω, the frequency of the oscillators $\langle \nu_r \rangle$ becomes positive until it finally tends to ω. For large ω, the distribution of the phases is nearly uniform with a slight perturbation caused by the attractive cluster.

One particular partial synchronous state is illustrated in Fig. 5.9. It appears for intermediate values of about $\omega = 0.1$. First, there exists a loose cluster of all

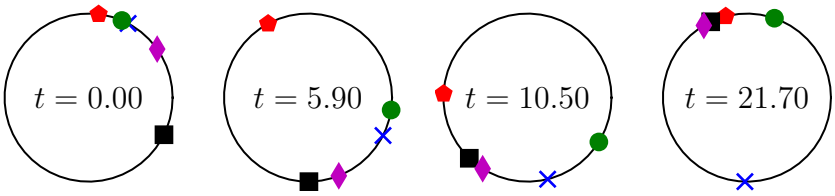

FIGURE 5.9: One specific type of partial synchronous state for intermediate values of ω around the solitary state. The figure shows four snapshots of the repulsive oscillators in a system with $N_r = N_a = 5$, $\varepsilon = 0.2$ and $\omega = 0.1$. Every oscillator is marked by a different color and symbol. At times $t = 5.9$ and $t = 21.7$, a single oscillator leaves the fuzzy cluster.

repulsive oscillators. Then, a single oscillator accelerates and leaves this cluster, stays in antiphase for a short time, and then rejoins the group as the last one. The cluster dissolves again and leaves a single oscillator. This oscillator was the third oscillator in the original cluster. It stays in antiphase for a short time and then rejoins the cluster. This can be seen as a transient solitary state, and only every second oscillator undergoes this state. These dynamics seem to be independent of the initial state and the exact system size. Like the solitary state, it appears only for small systems but is not restricted to odd or even numbers of oscillators N_r. This state somewhat resembles a state observed in an ensemble of attractive and repulsive active rotators in Ref. [99].

A final investigation of the multistability is shown in Fig. 5.10. A big system with $N_a = N_r = 1024$ is illustrated. The different distributions are the result of different initial conditions. In (a), a perturbed cluster is the initial condition, and in (b), a random initial condition is used. The distributions differ in their form and their dynamics. The distribution in (a) is bounded and bimodal. It is time-dependent and changes its width, resulting in a 'breathing' motion. The phase differences between the mean fields and the forcing vary over time. In (b), the distribution is unbounded and unimodal. It does not change significantly over time, and the phase differences between the mean fields and the forcing are nearly constant. The observed noise is probably caused by finite-size effects. The different distribution also lead to different average frequencies of $\langle \nu_r \rangle = 0.262$ and $\langle \Omega_r \rangle = -0.196$ in (a) and $\langle \nu_r \rangle = 0.264$ and $\langle \Omega_r \rangle = -0.181$ in (b).

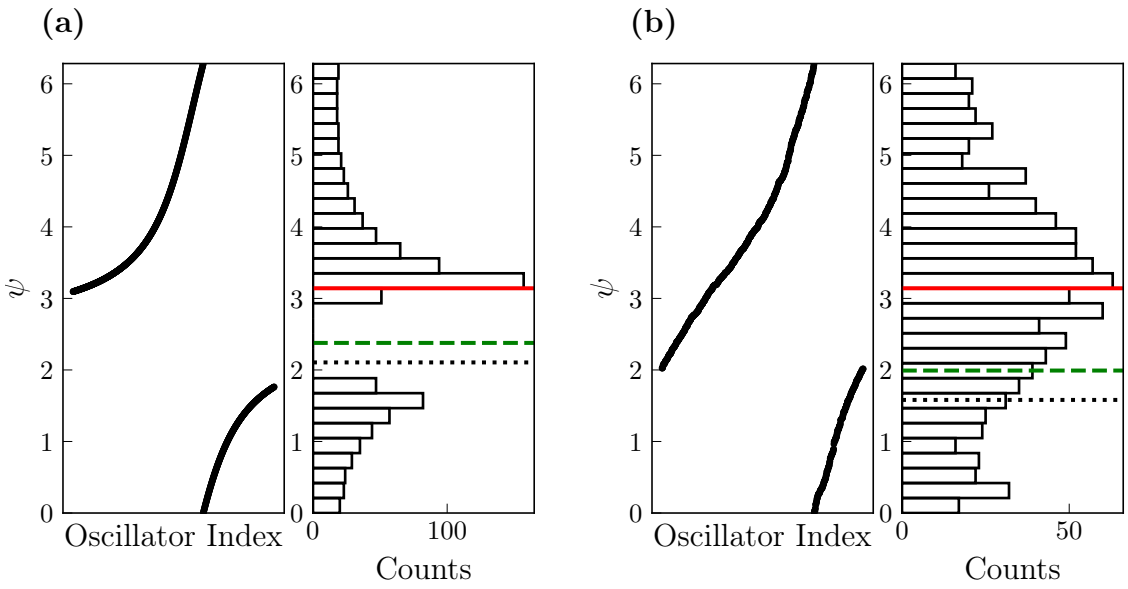

FIGURE 5.10: Phases of the repulsive group, and their histograms for $N_r = N_a = 1024$, $\omega = 0.75$, and $\varepsilon = 0.5$. In (a), a perturbed cluster was chosen as the initial condition, and in (b), a random initial condition was used. The solid red (dashed green) line is the phase of the repulsive (attractive) mean-field Θ_r (Θ_a) and the dotted black line the phase of the forcing. The distribution in (a) changes in time while the one in (b) is nearly stationary, except for some weak noise. Any motion is taken in reference to the repulsive mean field's phase.

Theoretical Analysis

The simplest case to consider when analyzing the system is $\omega = 0$. There, the repulsive order parameter is given by Eq. (5.4). The repulsive order parameter is $R_r = (1+\varepsilon)^{-1}$ since the attractive group always fully synchronizes. This is expected to also approximate small values of ω sufficiently well. It will also be the upper limit, as an increase in ω leads to a decrease in synchronization.

For the analysis of $\omega \gg 0$, the WS theory allows the reduction to six equations for the collective variables. For the analytical tractability, the OA manifold is considered (this corresponds to a uniform distribution of the constants of motion, as discussed earlier). Then the dynamics are further simplified to four equations for the mean-field variables $R_{a,r}$ and $\Theta_{a,r}$. Since $R_a = 1$ is always the case, this is reduced to a three-dimensional system from Eqs. (2.37). The mean-field dynamics then read [68]

$$\begin{aligned} \dot{R}_r =& \frac{1-R_r^2}{4}[\cos(\Theta_r - \Theta_a) - (1+\varepsilon)R_r] \,, \\ \dot{\Theta}_r =& \omega + \frac{1+R_r^2}{4R_r}\sin(\Theta_r - \Theta_a) \,, \\ \dot{\Theta}_a =& \frac{1+\varepsilon}{2} R_r \sin(\Theta_r - \Theta_a) \,. \end{aligned} \tag{5.40}$$

It is interesting to note here that only the phase shift $\eta = \Theta_r - \Theta_a$ is of importance. This leads to the two-dimensional system

$$\begin{aligned} \dot{R}_r =& \frac{1-R_r^2}{4}[\cos\eta - (1+\varepsilon)R_r] \,, \\ \dot{\eta} =& \omega - \frac{1+[1-2(1+\varepsilon)]R_r^2}{4R_r}\sin\eta \,. \end{aligned} \tag{5.41}$$

A caveat of this equation is the usage of the OA manifold, as it is only valid in the thermodynamic limit, which certainly does not describe small systems. Hence, this is only a crude approximation, and Eq. (5.41) is only an estimate and not an exact solution.

Stationary states are expected for a big difference in the frequencies. So the assumptions of $\dot{\eta} = 0$ and a stationary order parameter $\dot{R}_r = 0$ can be used. Inserting them into Eq. (5.41) and reordering leads to

$$\begin{aligned} \cos\eta =& (1+\varepsilon)\left\langle R_r \right\rangle \,, \\ \sin\eta =& \frac{4\omega \left\langle R_r \right\rangle}{1+(1-2(1+\varepsilon))\left\langle R_r \right\rangle^2} \,. \end{aligned} \tag{5.42}$$

Because the stationarity will not be perfect, these equations use the average order parameter $\langle R_r \rangle$. They can be solved easily by eliminating η and squaring. The result is a cubic equation in $\langle R_r \rangle^2$. The resulting expression for the roots is, again, too long to print here. A comparison of the different possible solutions is plotted in Fig. 5.11. There it can be seen that the $\omega = 0$ solution is a good approximation for small ω and the solution of Eq. (5.42) a good fit for large ω.

For a given $\langle R_r \rangle$, it is possible to calculate η from Eq. (5.42). This η can

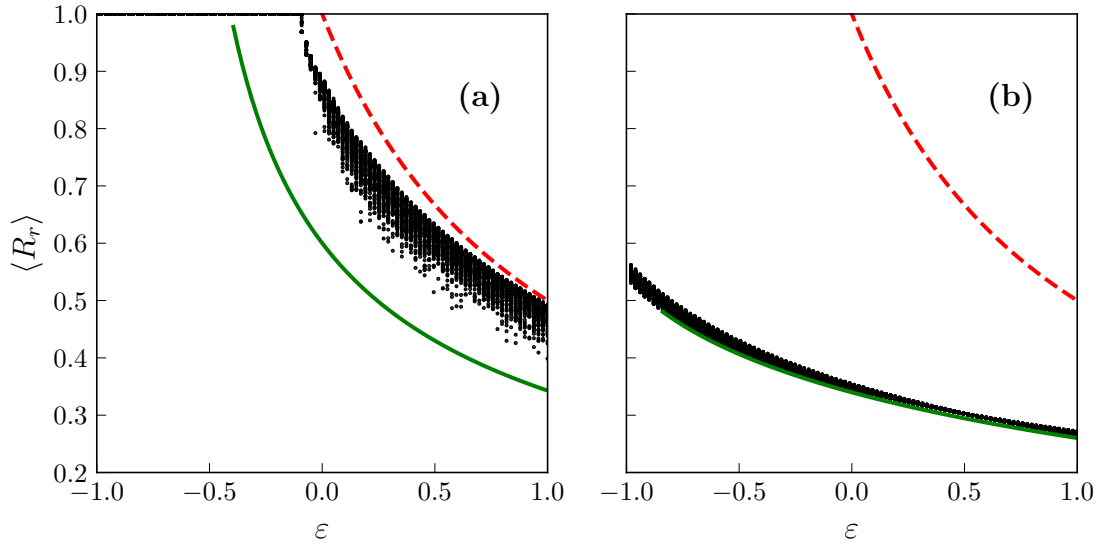

FIGURE 5.11: The average repulsive order parameter $\langle R_r \rangle$ (black dots) for 100 different initial conditions per ε with $N_a = N_r = 5$. The dashed red line shows $(1+\varepsilon)^{-1}$ and is the upper limit for small ω. The solid green line gives the solution of Eq. (5.42). In (a), $\omega = 0.02$, and the upper limit fits the data very well. In (b), $\omega = 0.6$.

then be used in the second equation of Eq. (5.40) to calculate $\langle \Omega_r \rangle$. For any known $\langle \Omega_r \rangle$, it is possible to calculate the average frequency of the oscillators in the WS theory, using Eq. (2.38). Expressing $\langle \nu_r \rangle$ via $\langle \Omega_r \rangle$ yields

$$\langle \nu_r \rangle = \langle \Omega_r \rangle - \frac{1 - R_r^2}{1 + R_r^2}(\langle \Omega_r \rangle - \omega) \; . \tag{5.43}$$

The estimates $\langle \nu_r \rangle$ and $\langle \Omega_r \rangle$ are shown in Fig. 5.8. The calculated $\langle \nu_r \rangle$ fit very well, even for intermediate ω. The $\langle \Omega_r \rangle$ are not as good for intermediate values but also fit well for big ω, where the stationarity conditions are better fulfilled.

5.4 Summary & Conclusion

Following the rather recent discovery of the solitary state, it has been observed in numerical, as well as experimental, setups. It appears in the transition between full and partial synchrony, but not much is known about it. In the original model of discovery, identical oscillators were split into two equally sized groups, one with attractive coupling and one with repulsive coupling. We have extended this model by allowing different dynamics of the oscillators, such that only oscillators in each group are identical. In this case, a fully synchronous two-cluster state can be observed, and its region of stability can be calculated analytically. The size of the synchronous region depends on the ratio between attractive and repulsive coupling and disappears when the repulsive coupling dominates or when the frequency difference between the groups becomes too big.

Outside of the fully synchronous state exists a partial synchronous regime, where the attractive cluster stays fully synchronized, but the repulsive cluster splits up. In this regime, the frequency of the repulsive mean-field differs from the one of the single oscillators but its stays entrained to the attractive mean-field. The order parameter of the repulsive group is between zero and one. Using the OA manifold and the WS theory, it is possible to find approximations for the frequency of the mean field as well as the order parameter that fit quite well for big frequency differences.

For small frequency differences, this transition happens via the solitary state, where a single repulsive oscillator leaves the repulsive cluster. The border of this state has been found analytically, as well as the phase shift between the oscillator and the clusters. It is important to note that, as in the original model, the region of the solitary state shrinks with the number of oscillators. In difference to the original model, the solitary state is stable and the only possible solution in its region of stability.

The solitary state is an interesting transition state, close to the border of synchrony and partial synchrony. We have shown that its stability depends strongly on the difference between the oscillatory units and hope that it can be useful for the study of neuronal populations of attractive and repulsive units.

Chapter 6

Conclusion & Outlook

Partial synchronization describes the states between trivial full synchrony, where all units of the system share the same dynamics, and asynchrony, where all oscillators are uniformly distributed. This wide range of partial synchronous states makes them an important topic to study in dynamical systems. The best way to investigate them lies in the usage of phase dynamics as their reduced dimensionality and regularity gives a more general and easier to handle abstraction of the studied system.

The usual first-order approximation of the phase dynamics is not enough to study all possible partial synchronous states. Higher-order phase approximations have also to be considered to reach more complex states. There are different methods to find these higher orders, but none has been developed yet to allow for a general and consistent calculation. We have developed a method in Chapter 3 based solely on the assumptions of the representation of the amplitude and the phase derivative as a power series in the coupling strength and known phase dynamics of the units. This method has been shown to give correct results in a simple model of Stuart-Landau oscillators, where modes up to the second order in the coupling strength were recovered. The proposed method is not restricted to just the second order, but the computational complexity increases with each additional order. To verify the analytical results, we also introduced a numerical way to calculate the phase derivative of a coupled system. Both the analytical and numerical results agree very well, and with the numerical method, it is even possible to find higher orders in the coupling strength, even for systems without a known phase dynamic, such as coupled Van der Pol oscillators. Again, the numerical method is not restricted to just the second order. Increasing the number of modes to consider also indirectly increases the possible order to reconstruct. However, as before, there is a great computational cost in increasing the order and increasing the system size.

Even in the second-order approximation, already important terms appear in the Stuart-Landau system that are necessary for the occurrence of some partial synchronous states. They include hyper-network-like connections between all units and pairwise coupling terms that do not appear in the coupling scheme. So, even though the higher-order terms are necessary for the study of partial synchronization, limited resources make it still advisable to use simpler phase models to study partial synchronization.

An interesting project to expand the phase dynamics method may lie in a programmatical application. The method itself is recursive and should be implementable in a computer algebra system. This would allow the easy calculation

of phase dynamics for moderate to small system sizes to higher orders.

When considering phase dynamics, the research of dynamical systems is usually restricted to one kind of interaction (in, e.g., the Kuramoto model). Either the coupling strength is constant or changes its magnitude in some predictable manner between each oscillator to model distances. What is seldom considered is the interaction of attractive and repulsive coupling. But this has been shown to lead to some interesting partial synchronous states, such as the solitary state or the Bellerophon state.

In an extension of the Kuramoto model, two groups with independent frequency distributions are considered. The oscillators in each group are coupled attractively and oscillators between groups repulsively. Systems of this type can also be represented as a Kuramoto model with a bimodal distribution and an additional bifurcation parameter. The model with two groups exhibits a rich partial synchronous transition. The critical coupling strengths for both groups are well described by a Kuramoto model with a double as wide frequency distribution. After the first groups' critical coupling strength, the narrower group forces the wider group and leads it to weakly synchronize. After the second group's critical coupling strength, clusters form at odd multiples of some fundamental frequency. Quasiperiodic regimes separate the clusters. Such a state is called a Bellerophon state and has been observed in similar systems. It is numerically observable for moderately sized systems but sensitive to noise in the frequencies. As the clusters are the main contributors to the order parameter, any reduction in their size leads to an immediate drop in the synchronization strength.

After a further increase to a strong coupling strength, the Bellerophon state begins to disappear, and the clusters contract. They asymptotically approach one big cluster, as expected for the Kuramoto model. Here, the synchronization behavior is better represented by a Kuramoto model with an equal width in the frequency distribution, i.e., for the same coupling strength, the groups are stronger synchronized than predicted before. These results show the enriching of dynamics by considering mixed-coupling.

In a simple model of identical Kuramoto oscillators, split into two groups, one attractive and repulsive, there appears an interesting solitary state, where all oscillators cluster at the same point, except for one single repulsive oscillator in anti-phase. We have extended this model to consider two groups of identical oscillators with a frequency difference. It has a fully synchronous two-cluster state, a solitary state, and a big partial synchronous region. The region of stability for both the fully synchronous state and the solitary state can be found analytically, directly from the dynamical equations. The self-consistent partial synchronous state, present outside of these two, is characterized by a difference in the frequencies of the repulsive mean-field and the repulsive oscillators. In this regime, the attractive cluster still fully synchronizes and entrains the repulsive mean-field. Using the Watanabe-Strogatz theory, the mean-fields of both groups and the average frequency of the oscillators can be approximated in the self-consistent partial synchronous state for big frequency differences and strong coupling. The observed solitary state is a bit different in that the solitary oscillator is not entirely in anti-phase, and the clusters of the groups do

not overlap in their phase. It is also the only stable state in its region of stability, in difference to the model without a frequency difference, and this region shrinks with an increase in the number of oscillators, like in the model without a frequency difference. This solitary state describes the transition between the fully synchronous state to the partial synchronous state for small frequency differences.

These results indicate the importance of the difference in coupling strength and the variety of units (in, e.g., their frequency) for rich partial synchronization to be observed. And more importance should be given to such setups in future research. In both cases that were considered here, only particular schemes of identical size were considered. They are the most straightforward expansion of the Kuramoto model to an attractive and repulsive setup. So researching a wider variety of the coupling strength may be an interesting future topic. On the experimental side, there were already a few observations of the solitary state and none of the Bellerophon state. Building a system that exhibits such a state may yield more information about the stability of the state in the presence of noise. And finally, a general problem of these types of problems is the absence of noise. Information about the stability of such 'exotic' partial synchronous states may help in explaining the transition to and from full synchrony.

Appendix A

Higher-Order Phase Reduction for Coupled Oscillators

A.1 Second Order Coupling Coefficients for the Stuart-Landau Oscillators

The coefficinets for the phase dynamics of the Stuart-Landau oscillators in Eq. (3.57) are given in Tabs. A.1 and A.1. As a shorthand, the following coefficients are used

$$C_{m,k} = \frac{1+\alpha^2}{2} \frac{2c_{m,k}}{4+(\omega_m-\omega_k)^2} \,, \tag{A.1}$$

$$D_{m,k} = \frac{1+\alpha^2}{2} \frac{(\omega_m-\omega_k)c_{m,k}}{4+(\omega_m-\omega_k)^2} \,. \tag{A.2}$$

The third oscillator has the same dynamics as the first oscillator, but with switched indices.

A.2 Higher Order Terms for the Coupled Stuart-Landau Oscillators

The terms beyond the second order are given in Tabs. A.3 and A.4.

A.3 Found Terms for the Coupled van der Pol Oscillators

For both oscillators there is only one constant mode, $\boldsymbol{l} = (0,0,0)$. All other fitted modes are given in Tab. A.5.

$a^{(2)}_{1;0,0,0}$	$c_{2,1}\Big(C_{1,2}\sin(\beta_{1,2}+\beta_{2,1})-D_{1,2}\cos(\beta_{1,2}+\beta_{2,1})-D_{2,1}\Big)$
$a^{(2)}_{1;-2,2,0}$	$c_{2,1}\Big(C_{1,2}\sin(\beta_{2,1}-\beta_{1,2})+D_{1,2}\cos(\beta_{2,1}-\beta_{1,2})$ $-C_{2,1}\sin 2\beta_{2,1}+D_{2,1}\cos 2\beta_{2,1}\Big)$
$b^{(2)}_{1;-2,2,0}$	$c_{2,1}\Big(C_{1,2}\cos(\beta_{2,1}-\beta_{1,2})-D_{1,2}\sin(\beta_{2,1}-\beta_{1,2})$ $-C_{2,1}\cos 2\beta_{2,1}-D_{2,1}\sin 2\beta_{2,1}\Big)$
$a^{(2)}_{1;-1,2,-1}$	$c_{2,1}\Big(C_{3,2}\sin(\beta_{2,1}-\beta_{3,2})+D_{3,2}\cos(\beta_{2,1}-\beta_{3,2})\Big)$
$b^{(2)}_{1;-1,2,-1}$	$c_{2,1}\Big(C_{3,2}\cos(\beta_{2,1}-\beta_{3,2})-D_{3,2}\sin(\beta_{2,1}-\beta_{3,2})\Big)$
$a^{(2)}_{1;-1,0,1}$	$c_{2,1}\Big(-D_{3,2}\cos(\beta_{2,1}+\beta_{3,2})+C_{3,2}\sin(\beta_{2,1}+\beta_{3,2})\Big)$
$b^{(2)}_{1;-1,0,1}$	$c_{2,1}\Big(D_{3,2}\sin(\beta_{2,1}+\beta_{3,2})+C_{3,2}\cos(\beta_{2,1}+\beta_{3,2})\Big)$

TABLE A.1: Coupling coefficients of the first Stuart-Landau oscillator.

$a^{(2)}_{2;0,0,0}$	$C_{2,1}c_{1,2}\sin(\beta_{2,1}+\beta_{1,2})-D_{2,1}c_{1,2}\cos(\beta_{2,1}+\beta_{1,2})-D_{1,2}c_{1,2}$ $+C_{2,3}c_{3,2}\sin(\beta_{3,2}+\beta_{2,3})-D_{3,2}c_{3,2}-D_{2,3}c_{3,2}\cos(\beta_{3,2}+\beta_{2,3})$
$a^{(2)}_{2;2,-2,0}$	$C_{2,1}c_{1,2}\sin(\beta_{1,2}-\beta_{2,1})+D_{2,1}c_{1,2}\cos(\beta_{1,2}-\beta_{2,1})$ $-C_{1,2}c_{1,2}\sin 2\beta_{1,2}+D_{1,2}c_{1,2}\cos 2\beta_{1,2}$
$b^{(2)}_{2;2,-2,0}$	$C_{2,1}c_{1,2}\cos(\beta_{1,2}-\beta_{2,1})-D_{2,1}c_{1,2}\sin(\beta_{1,2}-\beta_{2,1})$ $-C_{1,2}c_{1,2}\cos 2\beta_{1,2}-D_{1,2}c_{1,2}\sin 2\beta_{1,2}$
$a^{(2)}_{2;0,-2,2}$	$C_{2,3}c_{3,2}\sin(\beta_{3,2}-\beta_{2,3})+D_{2,3}c_{3,2}\cos(\beta_{3,2}-\beta_{2,3})$ $-C_{3,2}c_{3,2}\sin 2\beta_{3,2}+D_{3,2}c_{3,2}\cos 2\beta_{3,2}$
$b^{(2)}_{2;0,-2,2}$	$C_{2,3}c_{3,2}\cos(\beta_{3,2}-\beta_{2,3})-D_{2,3}c_{3,2}\sin(\beta_{3,2}-\beta_{2,3})$ $-C_{3,2}c_{3,2}\cos 2\beta_{3,2}-D_{3,2}c_{3,2}\sin 2\beta_{3,2}$
$a^{(2)}_{2;-1,2,-1}$	$D_{3,2}c_{1,2}\cos(\beta_{1,2}+\beta_{3,2})-C_{3,2}c_{1,2}\sin(\beta_{1,2}+\beta_{3,2})$ $-C_{1,2}c_{3,2}\sin(\beta_{3,2}+\beta_{1,2})+D_{1,2}c_{3,2}\cos(\beta_{3,2}+\beta_{1,2})$
$b^{(2)}_{2;-1,2,-1}$	$D_{3,2}c_{1,2}\sin(\beta_{1,2}+\beta_{3,2})+C_{3,2}c_{1,2}\cos(\beta_{1,2}+\beta_{3,2})$ $+C_{1,2}c_{3,2}\cos(\beta_{3,2}+\beta_{1,2})+D_{1,2}c_{3,2}\sin(\beta_{3,2}+\beta_{1,2})$
$a^{(2)}_{2;1,0,-1}$	$-D_{3,2}c_{1,2}\cos(\beta_{1,2}-\beta_{3,2})-C_{3,2}c_{1,2}\sin(\beta_{1,2}-\beta_{3,2})$ $-C_{1,2}c_{3,2}\sin(\beta_{3,2}-\beta_{1,2})-D_{1,2}c_{3,2}\cos(\beta_{3,2}-\beta_{1,2})$
$b^{(2)}_{2;1,0,-1}$	$(D_{3,2}c_{1,2}\sin(\beta_{1,2}-\beta_{3,2})-C_{3,2}c_{1,2}\cos(\beta_{1,2}-\beta_{3,2})$ $+C_{1,2}c_{3,2}\cos(\beta_{3,2}-\beta_{1,2})-D_{1,2}c_{3,2}\sin(\beta_{3,2}-\beta_{1,2})$

TABLE A.2: Coupling coefficients of the second Stuart-Landau oscillator.

$\boldsymbol{l}$	Asynchronous	Synchronous	Analytical
(0, 1, -1)	3	3	3
(0, 2, -2)	4	4	4
(0, 3, -3)	5	5	5
(0, 4, -4)	6	-	?
(1, -5, 4)	?	?	5
(1, -4, 3)	4	-	4
(1, -3, 2)	3	3	3
(1, 1, -2)	3	3	3
(1, 2, -3)	4	4	4
(1, 3, -4)	-	-	5
(2, -5, 3)	?	?	5
(2, -4, 2)	4	4	4
(2, -3, 1)	3	3	3
(2, -1, -1)	3	3	3
(2, 0, -2)	4	-	4
(2, 1, -3)	5	-	5
(2, 2, -4)	6	-	?
(3, -5, 2)	?	?	5
(3, -4, 1)	4	4	4
(3, -3, 0)	-	3	3
(3, -2, -1)	4	4	4
(3, -1, -2)	5	-	5
(4, -5, 1)	?	?	5
(4, -4, 0)	4	4	4
(4, -3, -1)	5	-	5
(4, -2, -2)	6	-	?
(5, -5, 0)	?	?	5

TABLE A.3: Fitted scaling for the higher order modes for the first oscillator for both the asynchrnous and synchrnous dynamics and the analytical modes up to the fifth order of the phase reduction. Missing modes are indicated by a '-'. Modes that are missing, because they could not be determines, i.e., with $m = 5$ for the numerical modes, or sixth-order modes of the analytical phase reduction, are marked by a '?'.

$\boldsymbol{l}$	Asynchronous	Synchronous	Analytical
(0, 3, -3)	3	3	3
(0, 4, -4)	4	4	4
(0, 5, -5)	?	?	5
(1, -5, 4)	?	?	5
(1, -4, 3)	4	4	4
(1, -3, 2)	3	3	3
(1, 1, -2)	3	3	3
(1, 2, -3)	4	4	4
(1, 3, -4)	-	-	5
(2, -5, 3)	?	?	4
(2, -4, 2)	4	4	4
(2, -3, 1)	3	3	3
(2, -1, -1)	3	3	3
(2, 0, -2)	4	4	4
(2, 1, -3)	5	5	-
(2, 2, -4)	6	-	?
(3, -5, 2)	?	?	4
(3, -4, 1)	4	4	4
(3, -3, 0)	5	3	3
(3, -2, -1)	4	4	4
(3, -1, -2)	5	-	5
(3, 0, -3)	6	-	?
(4, -5, 1)	?	?	5
(4, -4, 0)	4	4	4
(4, -3, -1)	5	-	5
(4, -2, -2)	6	-	?
(5, -5, 0)	?	?	5

TABLE A.4: Fitted scaling for the higher order modes for the second oscillator for both the asynchrnous and synchrnous dynamics and the analytical modes up to the fifth order of the phase reduction. Missing modes are indicated by a '-'. Modes that are missing, because they could not be determines, i.e., with $m = 5$ for the numerical modes, or sixth-order modes of the analytical phase reduction, are marked by a '?'.

	ε	ε^2
Oscillator 1	$(1,-3,0),(1,-1,0),(1,1,0),$ $(1,3,0),(3,-3,0),(3,-1,0),$ $(3,1,0),(3,3,0)$	$(0,2,0),(0,4,0),(1,-4,-1),$ $(1,-4,1),(1,-2,1-),(1,-2,1),$ $(1,0,-1),(1,0,1),(1,2,-3),$ $(1,2,-1),(1,2,1),(1,4,-1),$ $(1,4,1),(2,-4,0),(2,-2,0),$ $(2,0,0),(2,2,0),(2,4,0),$ $(3,-4,-1),(3,-4,1),(3,-2,-1),$ $(3,-2,1),(3,0,-1),(3,0,1),$ $(3,2,-1),(3,2,1),(4,-4,0),$ $(4,-2,0),(4,0,0),(4,2,0),\ (4,4,0)$
Oscillator 2	$(0,1,-3),(0,1,-1),(0,1,1),$ $(0,1,3),(0,3,-3),(0,3,-1),$ $(0,3,1),(0,3,3),(1,-3,0),$ $(1,-1,0),(1,1,0),(1,3,0),$ $(3,-3,0),(3,-1,0),(3,1,0),$ $(3,3,0)$	$(0,0,4),(0,2,-4),(0,2,-2),$ $(0,2,0),(0,2,4),(0,4,-2),$ $(0,4,0),(1,-4,1),(1,-2,-3),$ $(1,-2,-1),(1,-2,1),(1,0,-3),$ $(1,0,-1),(1,0,1),(1,2,-1),$ $(1,2,1),(1,4,-1),(1,4,1),$ $(2,-4,0),(2,-2,0),(2,0,0),$ $(2,2,0),(2,4,0),(3,-2,-1),$ $(3,-2,1),(3,0,-1),(3,2,-1),$ $(3,2,1),(4,-4,0),(4,-2,0),$ $(4,0,0),(4,2,0),(4,4,0)$

TABLE A.5: All the modes that were determined to be scaling with ε and ε^2 in the van der Pol system. In the first order there are 8 modes for the first oscillator and 16 modes for the second oscillator. In the second order there are 31 for the first oscillator and 34 for the second.

Bibliography

[1] M. Nixon, E. Ronen, A. A. Friesem, and N. Davidson, "Observing geometric frustration with thousands of coupled lasers," *Physical Review Letters*, vol. 110, may 2013.

[2] M. H. Matheny, M. Grau, L. G. Villanueva, R. B. Karabalin, M. Cross, and M. L. Roukes, "Phase synchronization of two anharmonic nanomechanical oscillators," *Physical Review Letters*, vol. 112, jan 2014.

[3] B. van der Pol and J. van der Mark, "The heartbeat considered as a relaxation oscillation, and an electrical model of the heart," *The London, Edinburgh, and Dublin Philosophical Magazine and Journal of Science*, vol. 6, no. 38, pp. 763–775, 1928.

[4] I. Ashraf, R. Godoy-Diana, J. Halloy, B. Collignon, and B. Thiria, "Synchronization and collective swimming patterns in fish (hemigrammus bleheri)," *Journal of The Royal Society Interface*, vol. 13, p. 20160734, oct 2016.

[5] S. H. Strogatz, D. M. Abrams, A. McRobie, B. Eckhardt, and E. Ott, "Theoretical mechanics: Crowd synchrony on the Millennium Bridge," *Nature*, vol. 438, no. 7064, pp. 43–44, 2005.

[6] E. Kaempfer, *The history of Japan: together with a description of the kingdom of Siam, 1690-92*, vol. 3. AMS Press, 1906.

[7] A. B. Cawthorne, P. Barbara, S. V. Shitov, C. J. Lobb, K. Wiesenfeld, and A. Zangwill, "Synchronized oscillations in josephson junction arrays: The role of distributed coupling," *Physical Review B*, vol. 60, pp. 7575–7578, sep 1999.

[8] A. E. Motter, S. A. Myers, M. Anghel, and T. Nishikawa, "Spontaneous synchrony in power-grid networks," *Nature Physics*, vol. 9, pp. 191–197, feb 2013.

[9] P. Uhlhaas, "Neural synchrony in cortical networks: history, concept and current status," *Frontiers in Integrative Neuroscience*, vol. 3, 2009.

[10] L. Glass, "Synchronization and rhythmic processes in physiology," *Nature*, vol. 410, pp. 277–284, mar 2001.

[11] A. Pikovsky, M. Rosenblum, and J. Kurths, *Synchronization: a universal concept in nonlinear sciences*, vol. 12. Cambridge university press, 2003.

[12] Y. Kuramoto and D. Battogtokh, "Coexistence of coherence and incoherence in nonlocally coupled phase oscillators.," *Nonlinear Phenomena in Complex Systems*, vol. 5, no. 4, pp. 380–385, 2002.

[13] Y. Kuramoto, *Chemical oscillations, turbulence and waves*. Springer, Berlin, 1984.

[14] E. Montbrió, J. Kurths, and B. Blasius, "Synchronization of two interacting populations of oscillators," *Phys. Rev. E*, vol. 70, p. 056125, Nov 2004.

[15] D. M. Abrams, R. Mirollo, S. H. Strogatz, and D. A. Wiley, "Solvable model for chimera states of coupled oscillators," *Physical review letters*, vol. 101, no. 8, p. 084103, 2008.

[16] E. Barreto, B. Hunt, E. Ott, and P. So, "Synchronization in networks of networks: The onset of coherent collective behavior in systems of interacting populations of heterogeneous oscillators," *Phys. Rev. E*, vol. 77, p. 036107, Mar 2008.

[17] C. Van Vreeswijk, L. F. Abbott, and G. Bard Ermentrout, "When inhibition not excitation synchronizes neural firing," *Journal of Computational Neuroscience*, vol. 1, no. 4, pp. 313–321, 1994.

[18] L. S. Tsimring, N. F. Rulkov, M. L. Larsen, and M. Gabbay, "Repulsive synchronization in an array of phase oscillators," *Phys. Rev. Lett.*, vol. 95, p. 014101, Jun 2005.

[19] A. V. Pimenova, D. S. Goldobin, M. Rosenblum, and A. Pikovsky, "Interplay of coupling and common noise at the transition to synchrony in oscillator populations," *Scientific Reports*, vol. 6, Dec. 2016.

[20] H. Hong and S. H. Strogatz, "Kuramoto model of coupled oscillators with positive and negative coupling parameters: An example of conformist and contrarian oscillators," *Phys. Rev. Lett.*, vol. 106, p. 054102, Feb 2011.

[21] H. Hong and S. H. Strogatz, "Conformists and contrarians in a Kuramoto model with identical natural frequencies," *Phys. Rev. E*, vol. 84, p. 046202, Oct 2011.

[22] D. Anderson, A. Tenzer, G. Barlev, M. Girvan, T. M. Antonsen, and E. Ott, "Multiscale dynamics in communities of phase oscillators," *Chaos: An Interdisciplinary Journal of Nonlinear Science*, vol. 22, no. 1, p. 013102, 2012.

[23] D. Iatsenko, S. Petkoski, P. V. E. McClintock, and A. Stefanovska, "Stationary and traveling wave states of the Kuramoto model with an arbitrary distribution of frequencies and coupling strengths," *Physical Review Letters*, vol. 110, feb 2013.

[24] Y. Maistrenko, B. Penkovsky, and M. Rosenblum, "Solitary state at the edge of synchrony in ensembles with attractive and repulsive interactions," *Phys. Rev. E*, vol. 89, p. 060901, Jun 2014.

[25] V. Vlasov, E. E. N. Macau, and A. Pikovsky, "Synchronization of oscillators in a Kuramoto-type model with generic coupling," *Chaos: An Interdisciplinary Journal of Nonlinear Science*, vol. 24, p. 023120, jun 2014.

[26] T. Qiu, S. Boccaletti, I. Bonamassa, Y. Zou, J. Zhou, Z. Liu, and S. Guan, "Synchronization and bellerophon states in conformist and contrarian oscillators," *Scientific reports*, vol. 6, 2016.

[27] H. R. Wilson and J. D. Cowan, "Excitatory and inhibitory interactions in localized populations of model neurons," *Biophysical Journal*, vol. 12, no. 1, pp. 1 – 24, 1972.

[28] C. Van Vreeswijk and H. Sompolinsky, "Chaos in neuronal networks with balanced excitatory and inhibitory activity," *Science*, vol. 274, no. 5293, pp. 1724–1726, 1996.

[29] A. Peyrache, N. Dehghani, E. N. Eskandar, J. R. Madsen, W. S. Anderson, J. A. Donoghue, L. R. Hochberg, E. Halgren, S. S. Cash, and A. Destexhe, "Spatiotemporal dynamics of neocortical excitation and inhibition during human sleep," *Proceedings of the National Academy of Sciences*, vol. 109, no. 5, pp. 1731–1736, 2012.

[30] N. Dehghani, A. Peyrache, B. Telenczuk, M. L. V. Quyen, E. Halgren, S. S. Cash, N. G. Hatsopoulos, and A. Destexhe, "Dynamic balance of excitation and inhibition in human and monkey neocortex," *Scientific Reports*, vol. 6, mar 2016.

[31] H. Nakao, "Phase reduction approach to synchronisation of nonlinear oscillators," *Contemporary Physics*, vol. 57, pp. 188–214, oct 2015.

[32] B. Pietras and A. Daffertshofer, "Network dynamics of coupled oscillators and phase reduction techniques," *Physics Reports*, vol. 819, pp. 1–105, jul 2019.

[33] H. Sakaguchi and Y. Kuramoto, "A soluble active rotater model showing phase transitions via mutual entertainment," *Progress of Theoretical Physics*, vol. 76, pp. 576–581, 09 1986.

[34] S. Watanabe and S. H. Strogatz, "Constants of motion for superconducting Josephson arrays," *Physica D: Nonlinear Phenomena*, vol. 74, no. 3, pp. 197 – 253, 1994.

[35] S. Watanabe and S. H. Strogatz, "Integrability of a globally coupled oscillator array," *Phys. Rev. Lett.*, vol. 70, pp. 2391–2394, Apr 1993.

[36] E. Ott and T. M. Antonsen, "Long time evolution of phase oscillator systems," *Chaos: An Interdisciplinary Journal of Nonlinear Science*, vol. 19, no. 2, p. 023117, 2009.

[37] E. Ott and T. M. Antonsen, "Low dimensional behavior of large systems of globally coupled oscillators," *Chaos: An Interdisciplinary Journal of Nonlinear Science*, vol. 18, p. 037113, Sept. 2008.

[38] I. León and D. Pazó, "Phase reduction beyond the first order: The case of the mean-field complex ginzburg-landau equation," *Physical Review E*, vol. 100, jul 2019.

[39] H. Daido, "Order function and macroscopic mutual entrainment in uniformly coupled limit-cycle oscillators," *Progress of Theoretical Physics*, vol. 88, pp. 1213–1218, dec 1992.

[40] W. Kurebayashi, S. Shirasaka, and H. Nakao, "Phase reduction method for strongly perturbed limit cycle oscillators," *Physical Review Letters*, vol. 111, nov 2013.

[41] K. Pyragas and V. Novičenko, "Phase reduction of a limit cycle oscillator perturbed by a strong amplitude-modulated high-frequency force," *Physical Review E*, vol. 92, jul 2015.

[42] D. Wilson and J. Moehlis, "Isostable reduction of periodic orbits," *Physical Review E*, vol. 94, nov 2016.

[43] B. Bezruchko, V. Ponomarenko, M. G. Rosenblum, and A. S. Pikovsky, "Characterizing direction of coupling from experimental observations," *Chaos: An Interdisciplinary Journal of Nonlinear Science*, vol. 13, pp. 179–184, mar 2003.

[44] I. T. Tokuda, S. Jain, I. Z. Kiss, and J. L. Hudson, "Inferring phase equations from multivariate time series," *Physical Review Letters*, vol. 99, aug 2007.

[45] K. A. Blaha, A. Pikovsky, M. Rosenblum, M. T. Clark, C. G. Rusin, and J. L. Hudson, "Reconstruction of two-dimensional phase dynamics from experiments on coupled oscillators," *Physical Review E*, vol. 84, oct 2011.

[46] B. Kralemann, M. Frühwirth, A. Pikovsky, M. Rosenblum, T. Kenner, J. Schaefer, and M. Moser, "In vivo cardiac phase response curve elucidates human respiratory heart rate variability," *Nature Communications*, vol. 4, sep 2013.

[47] Ç. Topçu, M. Frühwirth, M. Moser, M. Rosenblum, and A. Pikovsky, "Disentangling respiratory sinus arrhythmia in heart rate variability records," *Physiological Measurement*, vol. 39, p. 054002, may 2018.

[48] M. H. Matheny, J. Emenheiser, W. Fon, A. Chapman, A. Salova, M. Rohden, J. Li, M. H. de Badyn, M. Pósfai, L. Duenas-Osorio, M. Mesbahi, J. P. Crutchfield, M. C. Cross, R. M. D'Souza, and M. L. Roukes, "Exotic states in a simple network of nanoelectromechanical oscillators," *Science*, vol. 363, p. eaav7932, mar 2019.

[49] B. Kralemann, A. Pikovsky, and M. Rosenblum, "Reconstructing phase dynamics of oscillator networks," *Chaos: An Interdisciplinary Journal of Nonlinear Science*, vol. 21, no. 2, p. 025104, 2011.

[50] B. Kralemann, A. Pikovsky, and M. Rosenblum, "Reconstructing effective phase connectivity of oscillator networks from observations," *New Journal of Physics*, vol. 16, p. 085013, aug 2014.

[51] E. Teichmann and M. Rosenblum, "Solitary states and partial synchrony in oscillatory ensembles with attractive and repulsive interactions," *Chaos: An Interdisciplinary Journal of Nonlinear Science*, vol. 29, p. 093124, sep 2019.

[52] E. Gengel, E. Teichmann, M. Rosenblum, and A. S. Pikovsky, "High-order phase reduction for coupled oscillators," *Journal of Physics: Complexity*, oct 2020.

[53] E. Teichmann, "Using phase dynamics to study partial synchrony: Three examples," *European Physical Journal ST*, in press.

[54] E. Teichmann and R. Medrano-Torricos, "Partial synchronization in the kuramoto model with attractive and repulsive interactions via the bellerophon state," submitted.

[55] P. Clusella, A. Politi, and M. Rosenblum, "A minimal model of self-consistent partial synchrony," *New Journal of Physics*, vol. 18, no. 9, p. 093037, 2016.

[56] E. N. Lorenz, "Deterministic nonperiodic flow," *Journal of the Atmospheric Sciences*, vol. 20, pp. 130–141, mar 1963.

[57] S. Strogatz, *Nonlinear Dynamics and Chaos: With Applications to Physics, Biology, Chemistry, and Engineering.* Advanced book program, Westview Press, 1994.

[58] A. Wolf, J. B. Swift, H. L. Swinney, and J. A. Vastano, "Determining lyapunov exponents from a time series," *Physica D: Nonlinear Phenomena*, vol. 16, no. 3, pp. 285–317, 1985.

[59] A. Winfree, *The geometry of biological time.* Berlin New York: Springer-Verlag, 1980.

[60] P. Goel and B. Ermentrout, "Synchrony, stability, and firing patterns in pulse-coupled oscillators," *Physica D: Nonlinear Phenomena*, vol. 163, pp. 191–216, Mar. 2002.

[61] S. Achuthan and C. C. Canavier, "Phase-resetting curves determine synchronization, phase locking, and clustering in networks of neural oscillators," *Journal of Neuroscience*, vol. 29, no. 16, pp. 5218–5233, 2009.

[62] R. Cestnik and M. Rosenblum, "Reconstructing networks of pulse-coupled oscillators from spike trains," *Phys. Rev. E*, vol. 96, p. 012209, Jul 2017.

[63] R. Adler, "A study of locking phenomena in oscillators," *Proceedings of the IRE*, vol. 34, pp. 351–357, June 1946.

[64] J. A. Acebrón, L. L. Bonilla, C. J. P. Vicente, F. Ritort, and R. Spigler, "The Kuramoto model: A simple paradigm for synchronization phenomena," *Reviews of modern physics*, vol. 77, no. 1, p. 137, 2005.

[65] A. Pikovsky and M. Rosenblum, "Dynamics of globally coupled oscillators: Progress and perspectives," *Chaos: An Interdisciplinary Journal of Nonlinear Science*, vol. 25, no. 9, p. 097616, 2015.

[66] M. Breakspear, S. Heitmann, and A. Daffertshofer, "Generative models of cortical oscillations: Neurobiological implications of the Kuramoto model," *Frontiers in Human Neuroscience*, vol. 4, p. 190, 2010.

[67] F. Peter and A. Pikovsky, "Transition to collective oscillations in finite kuramoto ensembles," *Phys. Rev. E*, vol. 97, p. 032310, Mar 2018.

[68] A. Pikovsky and M. Rosenblum, "Partially integrable dynamics of hierarchical populations of coupled oscillators," *Phys. Rev. Lett.*, vol. 101, p. 264103, Dec 2008.

[69] Y. Baibolatov, M. Rosenblum, Z. Z. Zhanabaev, M. Kyzgarina, and A. Pikovsky, "Periodically forced ensemble of nonlinearly coupled oscillators: From partial to full synchrony," *Phys. Rev. E*, vol. 80, p. 046211, Oct 2009.

[70] A. Pikovsky and M. Rosenblum, "Dynamics of heterogeneous oscillator ensembles in terms of collective variables," *Physica D: Nonlinear Phenomena*, vol. 240, no. 9, pp. 872–881, 2011.

[71] R. E. Mirollo, "The asymptotic behavior of the order parameter for the infinite-n kuramoto model," *Chaos: An Interdisciplinary Journal of Nonlinear Science*, vol. 22, no. 4, p. 043118, 2012.

[72] Z. Levnajić and A. Pikovsky, "Phase resetting of collective rhythm in ensembles of oscillators," *Physical Review E*, vol. 82, p. 056202, Nov. 2010.

[73] D. Pazó and R. Gallego, "The winfree model with non-infinitesimal phase-response curve: Ott–antonsen theory," *Chaos: An Interdisciplinary Journal of Nonlinear Science*, vol. 30, p. 073139, jul 2020.

[74] A. Yeldesbay, A. Pikovsky, and M. Rosenblum, "Chimeralike states in an ensemble of globally coupled oscillators," *Phys. Rev. Lett.*, vol. 112, p. 144103, Apr 2014.

[75] J. Hizanidis, N. Lazarides, G. Neofotistos, and G. Tsironis, "Chimera states and synchronization in magnetically driven SQUID metamaterials," *The European Physical Journal Special Topics*, vol. 225, pp. 1231–1243, sep 2016.

[76] T. Chouzouris, I. Omelchenko, A. Zakharova, J. Hlinka, P. Jiruska, and E. Schöll, "Chimera states in brain networks: Empirical neural vs. modular fractal connectivity," *Chaos: An Interdisciplinary Journal of Nonlinear Science*, vol. 28, p. 045112, apr 2018.

[77] M. Rosenblum and A. Pikovsky, "Self-organized quasiperiodicity in oscillator ensembles with global nonlinear coupling," *Phys. Rev. Lett.*, vol. 98, p. 064101, Feb 2007.

[78] J. H. Sheeba, V. K. Chandrasekar, A. Stefanovska, and P. V. E. McClintock, "Routes to synchrony between asymmetrically interacting oscillator ensembles," *Physical Review E*, vol. 78, aug 2008.

[79] H. Hong and S. H. Strogatz, "Mean-field behavior in coupled oscillators with attractive and repulsive interactions," *Physical Review E*, vol. 85, may 2012.

[80] C. R. Laing, "Disorder-induced dynamics in a pair of coupled heterogeneous phase oscillator networks," *Chaos: An Interdisciplinary Journal of Nonlinear Science*, vol. 22, p. 043104, dec 2012.

[81] M. A. Lohe, "Conformist–contrarian interactions and amplitude dependence in the kuramoto model," *Physica Scripta*, vol. 89, p. 115202, oct 2014.

[82] B. Sonnenschein, T. K. D. Peron, F. A. Rodrigues, J. Kurths, and L. Schimansky-Geier, "Collective dynamics in two populations of noisy oscillators with asymmetric interactions," *Physical Review E*, vol. 91, jun 2015.

[83] B. Pietras, N. Deschle, and A. Daffertshofer, "Equivalence of coupled networks and networks with multimodal frequency distributions: Conditions for the bimodal and trimodal case," *Physical Review E*, vol. 94, nov 2016.

[84] T. Kotwal, X. Jiang, and D. M. Abrams, "Connecting the kuramoto model and the chimera state," *Physical Review Letters*, vol. 119, dec 2017.

[85] S. Achterhof and J. M. Meylahn, "Two-community noisy kuramoto model with general interaction strengths. i," *Chaos: An Interdisciplinary Journal of Nonlinear Science*, vol. 31, p. 033115, mar 2021.

[86] S. Achterhof and J. M. Meylahn, "Two-community noisy kuramoto model with general interaction strengths. II," *Chaos: An Interdisciplinary Journal of Nonlinear Science*, vol. 31, p. 033116, mar 2021.

[87] T. Kapitaniak, P. Kuzma, J. Wojewoda, K. Czolczynski, and Y. Maistrenko, "Imperfect chimera states for coupled pendula," *Scientific Reports*, vol. 4, sep 2014.

[88] I. A. Shepelev, G. I. Strelkova, and V. S. Anishchenko, "Chimera states and intermittency in an ensemble of nonlocally coupled Lorenz systems," *Chaos: An Interdisciplinary Journal of Nonlinear Science*, vol. 28, p. 063119, jun 2018.

[89] K. Sathiyadevi, V. K. Chandrasekar, D. V. Senthilkumar, and M. Lakshmanan, "Long-range interaction induced collective dynamical behaviors,"

Journal of Physics A: Mathematical and Theoretical, vol. 52, p. 184001, apr 2019.

[90] M. Mikhaylenko, L. Ramlow, S. Jalan, and A. Zakharova, "Weak multiplexing in neural networks: Switching between chimera and solitary states," *Chaos: An Interdisciplinary Journal of Nonlinear Science*, vol. 29, p. 023122, feb 2019.

[91] P. Jaros, S. Brezetsky, R. Levchenko, D. Dudkowski, T. Kapitaniak, and Y. Maistrenko, "Solitary states for coupled oscillators with inertia," *Chaos: An Interdisciplinary Journal of Nonlinear Science*, vol. 28, no. 1, p. 011103, 2018.

[92] E. Rybalova, N. Semenova, G. Strelkova, and V. Anishchenko, "Transition from complete synchronization to spatio-temporal chaos in coupled chaotic systems with nonhyperbolic and hyperbolic attractors," *The European Physical Journal Special Topics*, vol. 226, pp. 1857–1866, jun 2017.

[93] N. I. Semenova, E. V. Rybalova, G. I. Strelkova, and V. S. Anishchenko, "'Coherence–incoherence' transition in ensembles of nonlocally coupled chaotic oscillators with nonhyperbolic and hyperbolic attractors," *Regular and Chaotic Dynamics*, vol. 22, pp. 148–162, mar 2017.

[94] N. Semenova, T. Vadivasova, and V. Anishchenko, "Mechanism of solitary state appearance in an ensemble of nonlocally coupled Lozi maps," *The European Physical Journal Special Topics*, vol. 227, pp. 1173–1183, nov 2018.

[95] E. Rybalova, G. Strelkova, and V. Anishchenko, "Mechanism of realizing a solitary state chimera in a ring of nonlocally coupled chaotic maps," *Chaos, Solitons & Fractals*, vol. 115, pp. 300–305, oct 2018.

[96] S. Makovkin, A. Kumar, A. Zaikin, S. Jalan, and M. Ivanchenko, "Multiplexing topologies and time scales: The gains and losses of synchrony," *Physical Review E*, vol. 96, no. 5, p. 052214, 2017.

[97] J. R. Engelbrecht and R. Mirollo, "Classification of attractors for systems of identical coupled Kuramoto oscillators," *Chaos: An Interdisciplinary Journal of Nonlinear Science*, vol. 24, p. 013114, mar 2014.

[98] A. Pikovsky and M. Rosenblum, "Self-organized partially synchronous dynamics in populations of nonlinearly coupled oscillators," *Physica D: Nonlinear Phenomena*, vol. 238, no. 1, pp. 27 – 37, 2009.

[99] M. A. Zaks and P. Tomov, "Onset of time dependence in ensembles of excitable elements with global repulsive coupling," *Phys. Rev. E*, vol. 93, p. 020201, Feb 2016.